Pathways to Mitigate Chromium Poisoning in Electrolysis Devices

Muhammad Hanif, [1,*] and Mihalis N. Tsampas, [1,*]

1. Dutch Institute For Fundamental Energy Research (DIFFER), 5612AJ Eindhoven, The Netherlands

[*] corresponding authors:

B.H.: hanif@differ.nl; M.N.T: m.tsampas@differ.nl

Table of Content

Graphical Abstract

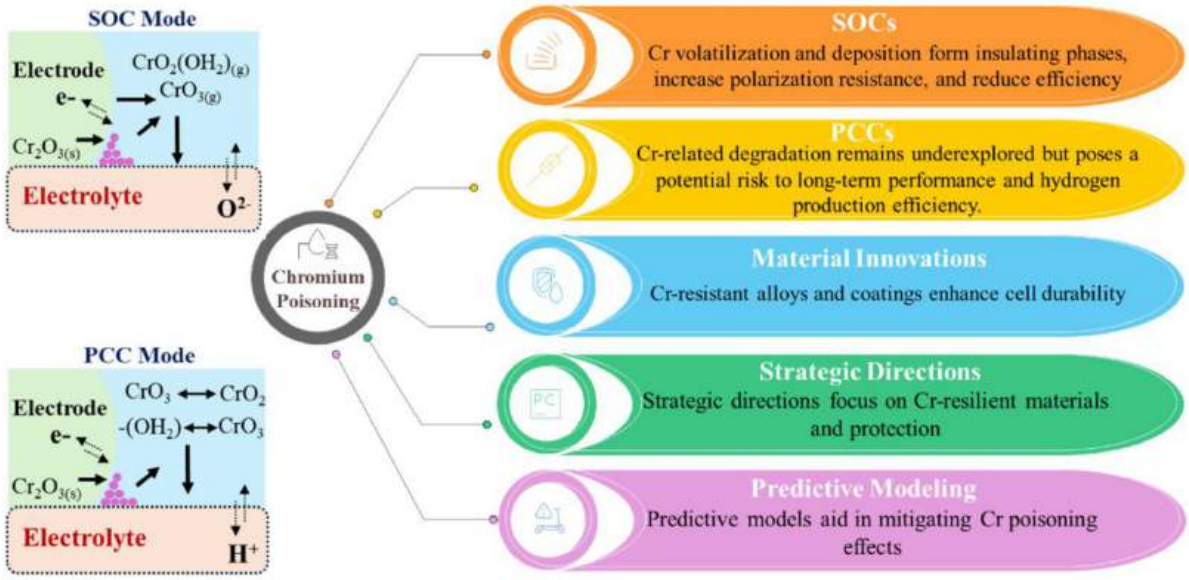

Abstract

Solid oxide (SOFC/SOEC) and protonic ceramic (PCFC/PCEC) electrochemical cells are key enabling technologies for the future energy transition. These high- and intermediate-temperature devices offer exceptional efficiency and fuel flexibility, positioning them as critical components in decarbonizing sectors where low-temperature systems fall short. Chromium (Cr) poisoning remains one of the most critical degradation mechanisms limiting the performance, durability, and commercial viability of these solid oxide and protonic ceramic electrochemical cells (SOCs and PCCs). Cr volatilization from ferritic stainless steel interconnects and subsequent deposition of volatile Cr species such as CrO_3 and $CrO_2(OH)_2$ at the oxygen electrode lead to the formation of electrically insulating phases, which compromise triple-phase boundary (TPB) activity, increase polarization resistance, and accelerate performance degradation. While Cr-related degradation has been extensively studied in SOCs, its impact on PCCs, which are promising candidates for efficient hydrogen production remains comparatively underexplored. This review critically analyzes Cr poisoning mechanisms across these electrochemical systems, highlighting the mechanistic differences arising from their distinct configurations, ion conduction modes, and operating environments. Advances in material innovations, including Cr-resistant alloys, protective coatings, and improved electrode formulations, are discussed with a focus on their cross-system applicability and effectiveness. The need for predictive modeling, long-term durability studies, and system-level validation under realistic conditions is emphasized as essential for advancing Cr mitigation strategies. By consolidating current understanding and identifying key research gaps, this review outlines strategic directions for the development of Cr-resilient materials, optimized getter integration, and tailored protection schemes for the unique challenges posed by PCECs. Ultimately, it underscores the urgency of developing robust, scalable solutions to enable the reliable deployment of next-generation high-temperature electrolysis technologies in sustainable energy systems.

Keywords: Chromium poisoning; Solid oxide cells; Proton ceramic cells; High- and intermediate-temperature electrolysis; Durability; Mitigation strategies

1. Introduction

Solid oxide cells (SOCs), which encompass both solid oxide fuel cells (SOFCs) and solid oxide electrolysis cells (SOECs), have emerged as transformative technologies in the landscape of sustainable energy [1,2]. Their ability to function efficiently in both fuel cell and electrolysis modes positions them as versatile candidates for next-generation energy systems. SOCs boast high operational efficiency, robust energy conversion capabilities, and adaptability to diverse applications ranging from power generation to hydrogen production [3,4]. As illustrated in **Figure. 1(a),** excess electricity from intermittent renewable sources like wind and solar can be stored by converting water into hydrogen using SOECs. This stored hydrogen can later be utilized in SOFCs to generate electricity when demand rises, making SOCs an integral component of a renewable energy cycle with near-zero emissions [5,6].

SOECs and proton ceramic electrolysis cells (PCECs) represent promising high-temperature electrolysis technologies for converting H_2O and CO_2 into value-added fuels and chemicals. While SOEC technology is comparatively more mature and primarily applied for syngas (CO, CO_2, and H_2) production, PCECs unlock access to the industrially appealing intermediate temperature window (350–600°C). This temperature range is conducive to coupling with catalytic synthesis, enabling the direct electrochemical generation of CH_4, higher hydrocarbons (C2, C3), and alcohols beyond just syngas. These emerging technologies hold significant potential for advancing power-to-X (P2X) applications and enabling chemical process electrification and intensification [7–9]. By leveraging proton conduction instead of oxygen ion conduction, PCECs also operate at lower temperatures while maintaining excellent hydrogen production rates, broadening the applicability of electrolysis technologies [10–13].

In addition to high efficiency and fuel flexibility, SOCs offer scalability, suitable for applications ranging from portable electronics to large-scale power plants. Theoretical studies suggest that by utilizing waste heat from SOFCs to support SOEC operation, the round-trip energy efficiency of this system could approach 98%, further reinforcing their viability for integrated energy systems [14,15]. Despite these advantages, one major challenge threatening the long-term durability of both SOCs and proton ceramic cells (PCCs) is chromium (Cr) poisoning, which stems from the volatilization of Cr species from metallic interconnects and severely degrades electrode performance [16–18]. Since SOC and PCC stacks are constructed using ferritic stainless steel (FSS) interconnects containing 17%–22% Cr due to their favorable cost and conductivity [19,20], exposure to high operating temperatures (600–800 °C) facilitates the formation and transport of gaseous Cr species, which react with oxygen electrodes and hinder electrochemical activity [21,22].

Cr poisoning undermines the durability and performance of oxygen electrodes by depositing volatile Cr species (e.g., CrO_3, $CrO_2(OH)_2$) onto active surfaces, where they block electrochemical reaction sites and impair catalytic activity [23–26]. This degradation mechanism, driven by Cr volatilization and deposition, alters oxygen exchange kinetics, degrades the electrode microstructure, and leads to severe performance losses [27–29]. The extent of this degradation depends on several factors, including electrode composition, current density, gas humidity, and partial pressures of oxygen and water [30,31]. At the core of this issue lies the complex interaction between Cr species and the electrode-electrolyte interface [32,33]. Once deposited, Cr compounds degrade electrode performance by disrupting ionic/electronic conduction pathways and altering surface morphology [34,35]. While mechanisms under SOFC conditions are relatively well-understood, Cr poisoning in SOEC and especially reversible operation remains less explored. High oxygen partial pressures and humidified atmospheres in SOECs exacerbate Cr volatilization, posing continued risks to cell stability [36,37]. Moreover, the distinct material properties of PCCs, particularly their reliance on proton-conducting ceramics add further complexity to understanding and mitigating Cr-induced degradation.

To address Cr poisoning, researchers have developed a variety of mitigation strategies [38–41]. These include protective coatings such as MnCo- spinels and perovskite-based films to limit Cr evaporation and migration [42], Cr-tolerant electrode materials like $La_2NiO_{4\pm\delta}$ and $SrTi_{1-x}Fe_xO_3$, and system-level approaches such as improved gas flow design and thermal management to reduce Cr transport to the electrode [43,44]. However, most of these strategies have been designed and validated for SOCs, and their transferability to PCCs remains uncertain due to the differing operating environments and degradation pathways [45–47].

The relatively early stage of PCC development means that much of the understanding of Cr poisoning in these systems is extrapolated from SOC studies, underscoring the need for dedicated research [48,49]. Durability testing over long operational periods is essential to evaluate the true efficacy of mitigation methods. Some protective coatings may delay Cr deposition, but their long-term performance and compatibility with PCC materials remain critical unknowns.

This review provides a comprehensive analysis of Cr poisoning in SOCs and PCCs, examining the degradation mechanisms, performance impacts, and current mitigation strategies. By comparing Cr behavior across these technologies, this work offers a unified perspective on how cell architecture, gas environments, and operational modes influence degradation. Particular focus is given to metallic interconnects and their role in Cr transport phenomena. We also assess protective coatings, Cr-tolerant electrodes, and system design optimizations, identifying gaps in knowledge and highlighting opportunities for transferring SOC-based strategies to PCC systems. Ultimately, this review aims to guide future research and innovation toward improving the stability and scalability of next-generation electrochemical energy conversion systems (**Figure 1(b)**).

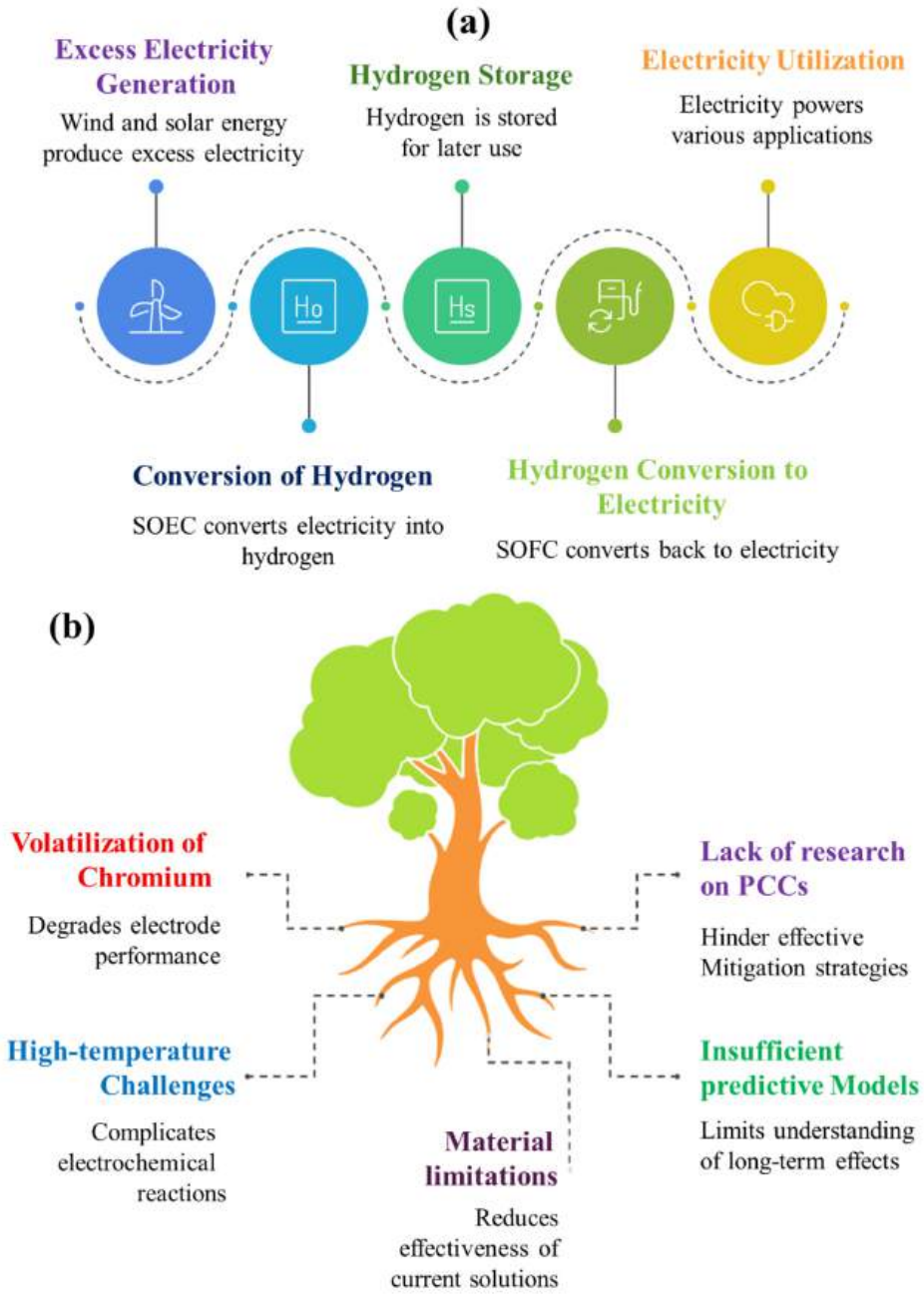

Figure. 1: Illustration of the role of SOC technology in a renewable energy-based sustainable system **(a);** Comparative overview of Cr poisoning in electrolysis devices. It highlights the need for tailored approaches to address Cr poisoning in PCCs, emphasizing gaps in research and opportunities for advancing electrolysis technologies **(b).**

2. Electrochemical Devices

2.1. Cell and Stack Design

SOCs and PCCs are typically constructed in planar or tubular configurations, with individual cells assembled into stacks to enhance power output. Each unit in the stack comprises a fuel electrode, electrolyte, air electrode, metallic interconnects, and gas flow channels (**Figure. 2**) [50,51].

A repeated stack unit generally follows a consistent arrangement: a metallic interconnect, air electrode, electrolyte, fuel electrode, and a second interconnect. This structure remains unchanged across fuel cell or electrolysis modes, with ionic and electronic currents flowing through different layers based on the operation. The design supports uniform current distribution, thermal management, and a compact footprint for system integration [53–55].

Planar stacks are especially favored for their high packing density and manufacturing scalability. In contrast, tubular cells offer better sealing and mechanical resilience but often exhibit lower power density [56].

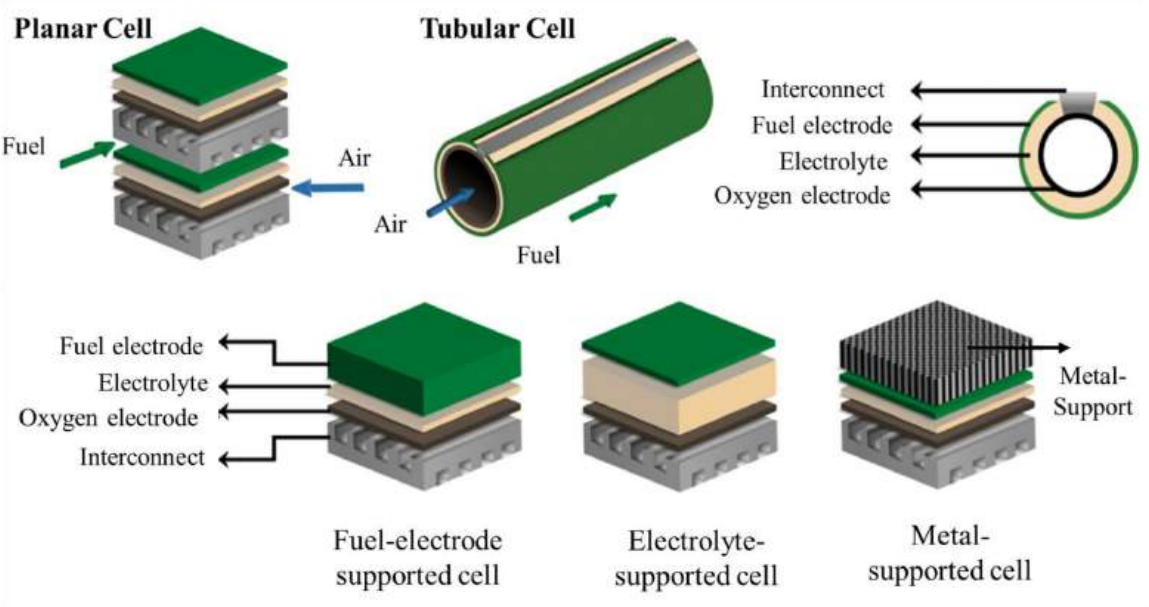

Figure. 2: Schematic representation of a solid oxide cell stack configuration, showing the repeating cell units and the integration of metallic interconnects with the electrode layers [52].

2.2. Metallic Interconnects: Composition and Function

Metallic interconnects are crucial in SOC and PCC stacks, serving as current collectors and gas separators between adjacent cells. Positioned at the interface of oxidizing and reducing atmospheres, they must retain electrical conductivity, mechanical strength, gas impermeability, and chemical stability over prolonged operation [57-59].

A critical requirement is their thermal expansion compatibility with neighboring components, generally between 10-13 $\times 10^{-6}$ K^{-1}, to prevent thermal mismatch and mechanical failure during start-up or cycling [60]. FSS, such as Crofer 22 APU and AISI 441, are widely adopted due to their cost-effectiveness, suitable thermal expansion coefficient (TEC), and fabrication ease. These alloys contain 17–22% Cr and offer a balance between mechanical robustness and electrochemical performance. However, under high-temperature conditions, Cr volatilization becomes problematic, as volatile Cr species can migrate to the air electrode and cause electrode poisoning [61].

To counter this, protective coatings and surface treatments are employed to suppress Cr evaporation and enhance oxidation resistance. These approaches help maintain the chemical integrity of interconnects and ensure long-term cell performance by limiting the deposition of Cr-containing compounds on the air electrode. The durability and compatibility of these coatings are especially important in PCCs, where operating environments differ from traditional SOC systems.

3. Chromium evaporation mechanisms

Cr poisoning remains a significant challenge in the long-term operation of SOCs, particularly due to the instability of Cr_2O_3 layers on chromia-forming alloys used in interconnects and other high-temperature components. This instability leads to the volatilization of Cr species, which subsequently migrate through the gas phase and deposit on electrode surfaces, causing severe performance degradation [29,62,63].

The volatilization of Cr_2O_3 occurs via a series of thermally activated reactions that are strongly influenced by the local oxygen and water vapor partial pressures. Under dry conditions, oxidation of

Cr_2O_3 primarily yields CrO_2 and CrO_3 as the dominant gaseous species through the following reactions [64,65]:

$$Cr_2O_3(S) + \frac{1}{2}O_2(g) \rightarrow 2CrO_2(g) \quad (1)$$

$$Cr_2O_3(S) + O_2(g) \rightarrow 2CrO_3(g) \quad (2)$$

However, under humid conditions typical of SOC operation, the presence of water vapor significantly alters the volatility pathway. Cr reacts with H_2O and O_2 to form chromium oxyhydroxide species, such as $CrO_2(OH)_2$ and $Cr(OH)_3$, through the following reactions.

$$Cr_2O_3(S) + H_2O(g) + O_2(g) \rightarrow 2CrO_2(OH)_2(g) \quad (3)$$

$$Cr_2O_3(S) + 2H_2O(g) + O_2(g) \rightarrow 2Cr(OH)_3(g) \quad (4)$$

Among the volatile Cr species generated during SOC operation, $CrO_2(OH)_2$ has been experimentally confirmed as the dominant and most persistent species, particularly in humid and oxidizing environments [66]. Opila et al. [66] demonstrated via equilibrium pressure measurements using the transpiration technique that $CrO_2(OH)_2$ forms readily at temperatures between 300–900°C, with significant volatility even at moderate humidity levels ($P(H_2O) \geq 0.001$ atm) and oxygen-rich environments. Under such conditions, CrO_3 contributes less than 1% to the total volatile Cr species and only becomes significant in dry atmospheres.

These findings are corroborated by Young and Pint [67], who modeled Cr evaporation fluxes for air with 10% H_2O and confirmed that $CrO_2(OH)_2$ dominates the gas phase up to ~800°C, with vapor pressure increasing with both temperature and gas flow rate. The mass loss observed from chromia-forming alloys could be quantitatively attributed to the evaporation of $CrO_2(OH)_2$.

Once in the gas phase, volatile Cr species especially $CrO_2(OH)_2$ are transported toward the air electrode, where they undergo heterogeneous decomposition and nucleation, resulting in the formation of insulating oxide deposits [66, 67]. The overall decomposition reaction of $CrO_2(OH)_2$ on the electrode surface can be expressed as:

$$2CrO_2(OH)_2(g) \leftrightharpoons Cr_2O_3(S) + 2H_2O(g) + \frac{3}{2}O_2(g) \quad (3)$$

According to the nucleation–growth theory, Cr deposition proceeds through three interconnected stages. i) Nucleation stage: Gaseous Cr species first adsorb onto reactive sites such as grain boundaries, pores, or segregated SrO on the electrode surface, leading to the formation of initial Cr–Sr–O nuclei. ii) Growth stage: These nuclei progressively enlarge through continued reaction with volatile Cr species, forming larger oxide clusters such as Cr_2O_3 and $SrCrO_4$ that extend across the electrode surface. iii) Saturation stage: As these deposits coalesce, they form a continuous and dense layer that restricts further diffusion of Cr species and significantly increases interfacial polarization resistance. The primary reactions involved in these stages can be represented as follows [95]:

$$SrO + CrO_3 \rightarrow Cr - Sr - O_x\ (nuclei) \quad (5)$$

$$Cr - Sr - O_x + CrO_3 \rightarrow Cr_2O_3 + CrO_y \quad (6)$$

$$Cr - Sr - O_x + CrO_3 + SrO \rightarrow SrCrO_4 \quad (7)$$

The formation of $SrCrO_4$ at the electrode surface is particularly detrimental, as it blocks oxygen reduction sites and increases polarization resistance. In contrast, Co- or Fe-based perovskite electrodes exhibit weaker chemical affinity toward Cr species, leading mainly to Cr_2O_3 nucleation rather than chromate formation [68,95].

To mitigate Cr-related degradation, thermodynamic analyses suggest operating at intermediate temperatures (~600 °C) and limiting water vapor content. These conditions can significantly suppress the formation of $CrO_2(OH)_2$ without greatly sacrificing electrochemical performance. Notably, the partial pressure of $CrO_2(OH)_2$ decreases gradually with temperature, whereas CrO_3 declines more steeply, highlighting the higher thermal persistence and volatility of $CrO_2(OH)_2$ under SOC-relevant conditions [66,68].

4. Cr poisoning effect in SOC: FC and EC

4.1. Main Effect in air Electrode

Among the various components in SOCs, the air electrode (also known as the oxygen electrode) is especially vulnerable to Cr poisoning, particularly under high-temperature operation. At elevated

temperatures (typically above 700 °C), these interconnects form volatile Cr oxides, mainly CrO_3 and $CrO_2(OH)_2$, which migrate through the cathode gas stream and reach the surface of the air electrode. Upon contact, these gaseous Cr species are electrochemically reduced and incorporated into the electrode structure, initiating surface reactions that degrade the cell's electrochemical performance [69–70].

The interaction between Cr species and the oxygen electrode results in several forms of degradation, including electrode delamination, increased polarization resistance, and loss of electrocatalytic activity. Cr-based interconnect oxidation also contributes to reduced electrical conductivity between the interconnect and electrode. While protective ceramic coatings are sometimes applied to reduce Cr volatilization and chromia evaporation, the delamination of the electrode caused by Cr interactions is more detrimental than mere loss of electronic contact, as it obstructs ionic transport within the electrolyte and leads to severe long-term degradation [71,72].

The most critical degradation pathway is the blockage of active oxygen reduction reaction (ORR) sites at the TPB. Cr has a strong chemical affinity for Sr-rich regions typically present in perovskite-type electrodes such as $La_{1-x}Sr_xMnO_{3-\delta}$ (LSM) and $La_{1-x}Sr_xCo_{1-Y}Fe_YO_{3-\delta}$ (LSCF) [71]. This leads to the formation of electrically insulating compounds like $SrCrO_4$ or Cr_2O_3, which hinder charge transfer and gas diffusion, thereby increasing polarization resistance and reducing ORR kinetics. Moreover, Cr deposition often enhances Sr surface segregation, which not only modifies the electrode surface chemistry but also accelerates further Cr incorporation and degradation, a phenomenon that is particularly pronounced in perovskite-based electrodes [71,73].

Several external and intrinsic factors modulate the severity of Cr poisoning. High humidity in the cathode gas stream favors the formation of more volatile Cr hydroxide species, thus promoting Cr transport. Higher operating temperatures also facilitate both volatilization and reaction kinetics. Under SOFC mode (cathodic polarization), the local environment at the air electrode becomes more reducing, enhancing the electrochemical reduction of gaseous Cr species and increasing their

likelihood of deposition [44]. Moreover, the proximity of interconnects to the electrode and the absence of protective barrier layers or coatings can significantly intensify Cr-related degradation.

The actual extent of degradation varies significantly depending on the electrode composition, as will be elaborated in Sections 4.3 (LSM-based electrodes) and 4.4 (LSCF-based electrodes). To further contextualize this variability, Table 1-3 summarizes key studies reporting Cr poisoning effects in commonly used air electrode materials under various SOC operation modes. These studies present a comparative view of how factors such as electrode composition, operating temperature, applied voltage/current density, and Cr source affect performance degradation typically manifested as increased polarization resistance (R_p), overpotentials (η), or total area-specific resistance (ASR). The data shows that while both LSM and LSCF-based cathodes experience performance losses, the degree of degradation is highly dependent on whether protective measures (e.g., Cr barrier layers or interconnect coatings) are implemented. Notably, LSCF-based electrodes exhibit more pronounced increases in R_p, attributed to their higher Sr content and greater susceptibility to Cr-induced Sr surface segregation. These findings serve as a precursor to the material-specific degradation mechanisms discussed in the following sections.

4.2. Any Effect in Fuel Electrode?

While Cr poisoning has been predominantly associated with the air electrode, emerging studies suggest that the fuel electrode (anode) may also experience minor but non-negligible Cr effects, particularly under aggressive or long-term operating conditions. The main pathways for Cr ingress to the fuel electrode include solid-state diffusion through the electrolyte, migration along interconnect pathways, or vapor-phase transport in configurations with thin electrolytes or high humidity. Though significantly less severe than in the air electrode, these effects raise concerns for the long-term integrity of anode-supported cells, especially in reversible SOCs.

Recent studies have provided experimental support for these mechanisms. For instance, Wei et al. [74] reported that under strong polarization conditions and elevated temperatures, trace Cr species can migrate through the electrolyte, especially when the electrolyte is ultra-thin (e.g., ~5 μm). Using

advanced characterization techniques such as STEM-EDS and SIMS, they identified low levels of Cr accumulation on Ni-based fuel electrodes after long-term testing. While the total Cr content was minimal and did not lead to substantial performance decline, the findings shows that Cr can cross the electrolyte barrier under high electrochemical driving forces, raising implications for electrolyte design and thickness in SOCs.

Similarly, Schrödl et al. [75] demonstrated that under extended operation (>1000 h) and at high current densities ($\geq$0.5 A cm^{-2}), trace Cr contamination could be detected on or near the anode side. This effect was particularly pronounced in electrode-supported cell configurations with reduced electrolyte thickness and in environments with high steam content. However, consistent with prior observations, the authors found no evidence of spinel or chromate formation at the fuel electrode and reported no significant impact on cell performance, reinforcing the notion that the fuel electrode is relatively resistant to Cr-induced degradation.

Thus, while the fuel electrode is not a primary target of Cr poisoning, certain modern SOC designs especially those featuring ultra-thin electrolytes, r-SOC, or compact stack geometries may increase susceptibility to trace Cr ingress. Although current data suggest limited electrochemical consequence, these findings emphasize the need for continued durability testing under realistic cycling conditions, such as SOFC–SOEC transitions, to fully understand the long-term implications of low-level Cr migration to the anode.

4.3. LSM based electrodes

$La_{1-x}Sr_xMnO_3$ (LSM) is a widely used Mn-based perovskite for high-temperature SOC air electrodes due to its excellent electronic conductivity, which stems from Sr^{2+} substitution at the A-site [76,77]. However, its low oxygen ion conductivity limits the ORR to the immediate electrode–electrolyte interface. To overcome this drawback, composite electrodes such as LSM/YSZ and LSM/GDC are commonly employed, which help extend the electrochemically active zone beyond the interface and thereby improve ORR performance [78,62].

A critical challenge associated with LSM cathodes is Cr poisoning, which arises from the migration of volatile Cr species from metallic interconnects. Studies have shown that the behavior of Cr poisoning varies significantly under different electrochemical conditions. Under open-circuit voltage (OCV) conditions, Cr species infiltrate the cathode and deposit as $(Mn, Cr)_3O_4$ spinel, but the amount of deposition remains relatively low during short-term exposure [79]. However, under constant current density conditions, Cr accumulates not only as $(Mn, Cr)_3O_4$ but also as Cr_2O_3 at the LSM/YSZ interface **(Figure. 3(a))**. The deposition rate and associated polarization resistance losses are significantly higher under polarization than under OCV [17,80]. Furthermore, as the applied current density increases, Cr accumulation at the three-phase boundary (TPB) intensifies, progressively diffusing into the cathode bulk. This phenomenon exacerbates polarization resistance and performance degradation, likely due to the accelerated decomposition of LSM at high temperatures under polarization conditions [81]. Interestingly, Konysheva et al. [82] noted that the extent of Cr poisoning does not exhibit a direct linear correlation with the amount of Cr deposited at the TPB and within the cathode bulk.

Temperature also plays a critical role in Cr poisoning, influencing both Cr volatility and LSM stability [83,84]. Higher temperatures accelerate Cr species volatilization and LSM decomposition, thereby increasing Cr infiltration into the cathode structure. Zhen et al. [85] observed that at elevated temperatures, Mn^{2+} diffusion from LSM to the YSZ surface is enhanced, promoting Cr accumulation at the interface. Similarly, Taniguchi et al. [86] investigated Cr deposition under a current load of 300 mA/cm^2 at different operating temperatures (850, 900, 1000, and 1100°C) and found that at lower temperatures (850°C and 900°C), Cr accumulation was confined to the LSM/YSZ interface. However, at 1000°C and 1100°C, Cr not only accumulated at the interface but also diffused deeper into the cathode bulk.

Interestingly, Krumpelt et al. [87] reported that while LSM decomposition and Cr deposition rates are higher at 800°C than at 700°C, the air electrode's electrochemical degradation under FC operation occurs more slowly at the higher temperature. One possible explanation is that at lower temperatures,

the effective TPB area decreases, leading to a proportionally greater loss of active sites, despite lower overall Cr deposition. Most studies assume Cr poisoning occurs primarily via gaseous-phase transport. However, when Cr-containing interconnects or coatings are in direct contact with the air electrode, solid-state surface diffusion of Cr species can also contribute to degradation. Experimental studies indicate that Cr deposition rates are significantly higher under direct contact conditions compared to gaseous-phase transport alone, although the final Cr compound phases remain unchanged.

Chen et al. [88] discussed the challenges of Cr poisoning in SOFCs, emphasizing the volatility of Cr species and their impact on cathode performance. At high temperatures, Cr_2O_3 volatilizes into $CrO_2(OH)_2$ in humid air and CrO_3 in dry air, with $CrO_2(OH)_2$ being more persistent under operating conditions, as shown in **Figure. 3(b)**. These species deposit on cathodes like LSM, forming resistive spinel phases $(Mn, Cr)_3O_4$ that hinder ORR and increase polarization resistance. The SEM images show significant Cr deposition on the YSZ electrolyte surface in contact with the LSM electrode after prolonged current passage at 900°C. Cr accumulation is notably higher in humidified air, as shown by the dense coverage of Cr-rich spinel phases, which obscure grain boundaries and increase interfacial resistance **(Figure. 3(c, d)).** The deposition pattern suggests that Cr poisoning is not directly correlated with the active TPBs but instead occurs across the entire surface, including areas between LSM contact rings. This highlights the severe impact of humidity on Cr poisoning. Mitigation strategies include protective coatings such as GDC or alumina, barrier layers to limit Cr migration, and optimizing interconnect alloy compositions. Despite these efforts, Cr poisoning remains a critical challenge, necessitating further research into advanced coatings and alternative cathode materials.

However, Horita et al. [89] further investigated the Cr deposition mechanism, emphasizing the role of cathode microstructure and reaction sites. In the setup shown in **Figure 3(e),** a porous LSM cathode on GDC is exposed to gaseous Cr from pre-oxidized Cr_2O_3, avoiding direct solid contact. Humidified air at 1073 K is used, with Pt counter and reference electrodes. This configuration shows that Cr preferentially deposits on the cathode surface rather than at the TPB, allowing precise assessment of deposition kinetics and distribution.

The time-dependent Cr deposition patterns, depicted in **Figure. 3(f)**, demonstrate that under polarization, Cr preferentially accumulates at the LSM/GDC interface, forming a concentrated layer within a micrometer-wide region. This localized deposition intensifies over time, contributing to electrode degradation. Meanwhile, **Figure. 3(g)** presents SIMS depth profiles that establish a direct correlation between Cr concentration and its accumulation in the porous LSM cathode, confirming that prolonged exposure leads to an increased presence of Cr-rich phases. These results highlight the severity of Cr poisoning in SOFCs, particularly in humid environments.

Table 1 showed a detailed summary of Cr poisoning test parameters at different temperatures (750–900°C) for various electrode materials. It includes key data points like resistance values (R_Ω and Rp), overpotential (η), current density, deposition area, and test conditions (temperature, time, applied potential). The data provides valuable insights into the performance degradation of these materials under Cr exposure, showing how factors such as temperature and material composition influence their resistance to Cr poisoning over time.

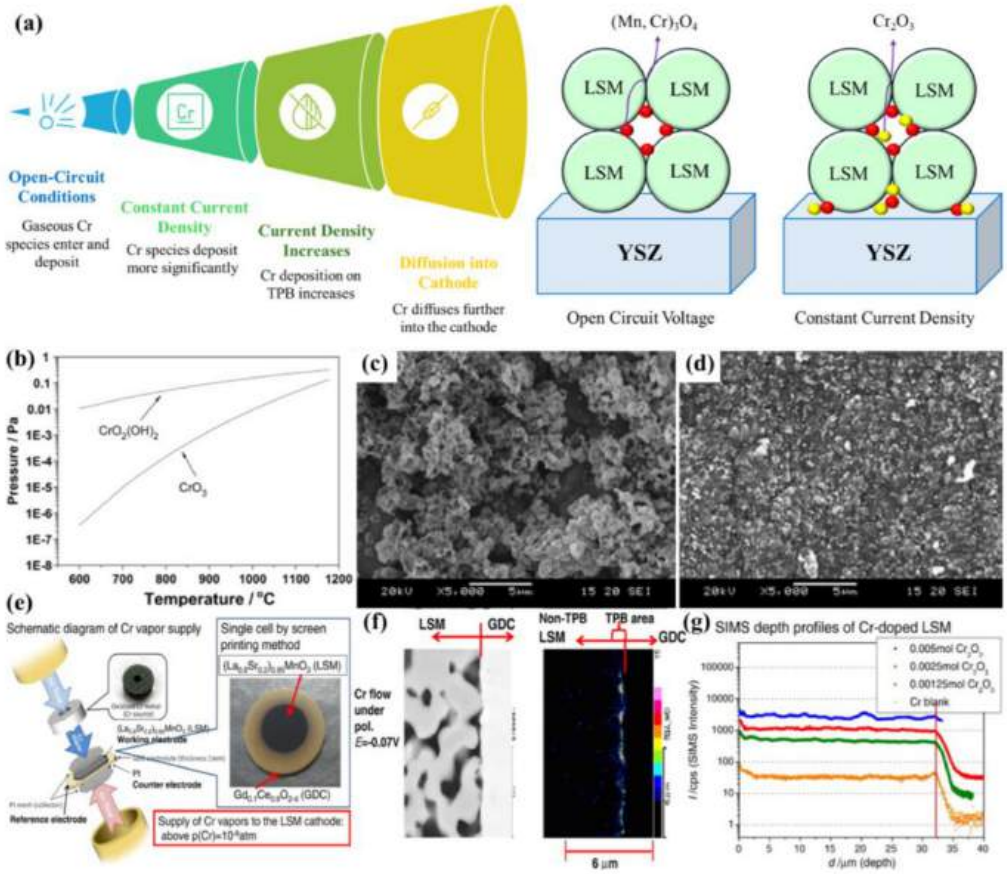

Figure 3: Schematic illustration of Cr poisoning in LSM-based cathodes. Under open-circuit conditions, Cr deposits as $(Mn, Cr)_3O_4$ with minimal accumulation **(a);** Partial pressure variations of $CrO_2(OH)_2$ in humid air (3 wt% H_2O) and CrO_3 in dry air over a chromia layer at different temperatures, highlighting the prolonged stability of $CrO_2(OH)_2$ under operational conditions, which intensifies Cr-induced degradation in SOFCs **(b);** SEM image of the YSZ electrolyte surface beneath the LSM electrode under the interconnect rib after 1200 minutes of current flow at 900°C in humid air, revealing substantial Cr accumulation and $(Mn, Cr)_3O_4$ spinel formation, which masks grain boundaries and increases polarization resistance **(c).** SEM micrograph of the YSZ electrolyte in contact with the LSM electrode under a 200 $mA.cm^{-2}$ current in humid air, depicting Cr deposition and its impact on the surface structure **(d)** Reprinted from ref. [88], copyright 2010, with permission from Elsevier. Schematic representation of the experimental setup for Cr-poisoning tests conducted at 1073 K **(e).** SEM/Wave Length Dispersive X-ray Spectroscopy (WDS) maps of Cr distribution at the LSM/GDC interface under different polarization conditions, showing localized deposition near the interface under applied voltage **(f).** SIMS depth profiles of Cr in porous LSM cathodes, demonstrating the increasing Cr concentration with prolonged exposure, which correlates with SOFC performance degradation **(g)** Reprinted from ref. [89], copyright 2012, with permission from Elsevier.

Tabe 1: Summary of Cr poisoning test parameters for various electrode materials at temperatures ranging from 750°C to 900°C under SOFC conditions.

Temp (°C)	**R_Ω (Ω)**	**R_p (Ω)**	**E (mV)**	**η (mV)**	**Current density (mA/cm^2) & Time**	**Deposition area**	**Cr poisoning test parameters**	**Ref**
750	1.10	34.8	1.20	0.75	400; 20 h	4.1 µm	LSM (1180 °C for 2 h); SUS430	[90]
800	2.00	33.0	1.20	0.12	800; 20 h	5.9 µm	LSM (1180 °C for 2 h); SUS430	[90]

800	---	---	---	---	800; 10 h	500 µm	LSM (1150 °C for 2 h); SS; Applied potential: -0.5 V,	[91]
900	---	---	---	---	200, 50-129 h	60-89 µm	LSM (1000 °C for 2 h); High Cr FSS	[92]
900	---	---	---	---	200; 50 h	89 µm	LSM (1150 °C for 2 h); Chromia-forming alloy	[93]
800	2.80	3.8	0.80	0.50	200; 20 h	2-3 µm	LSM (1150 °C for 2 h); Fe-Cr-Mn alloy (FeCM)	[94]
750	1.38	12.81	1.21	600	400; 20 h	0.2 µm	LSM (1180 °C for 2 h); SUS430	[21]

Chen et al. [95] studied the Cr-induced degradation and poisoning of LSM oxygen electrodes in SOECs and found that Cr deposition significantly affects the electrode's performance. Under anodic polarization conditions, SrO segregation from the bulk LSM electrode to the surface is promoted, as shown in **Figure 4(a)**. This surface segregation facilitates the interaction between SrO and gaseous Cr species, resulting in the formation of $SrCrO_4$, as observed in **Figure 4(c, d)**. **Figure 4(b)** illustrates the subsequent migration of SrO from the LSM surface to the YSZ electrolyte surface, where further Cr deposition and $SrCrO_4$ formation occur. This process, driven by the high polarization current and the presence of the Fe–Cr interconnect, accelerates Cr deposition, particularly at the electrode/electrolyte interface. The formation of $SrCrO_4$ in both the bulk of the electrode and at the electrode/electrolyte interface under SOEC conditions differs from the preferential Cr deposition observed under SOFC

conditions, where $(Cr, Mn)_3O_4$ spinels dominate. This distinct Cr deposition behavior can be explained by the enhanced Sr segregation under anodic polarization, which drives the formation of $SrCrO_4$, poisoning the electrocatalytic activity of the LSM electrodes.

Schrödl et al. [96] studied the long-term stability of $La_2NiO_{4+\delta}$ (LNO) in relation to its oxygen exchange kinetics and response to contaminants such as Cr and Si in dry and humidified atmospheres. Their findings highlighted that LNO exhibited excellent stability in dry conditions, with no significant degradation over the first 600 h of testing (**Figure 4(e)**). However, upon exposure to Cr and Si sources after 600 h under dry conditions, a slight reduction in oxygen exchange activity was observed. Following the introduction of humidified conditions (30% r.h. and higher), a significant decline in oxygen exchange activity occurred, which was attributed to the formation of secondary phases on the surface. SEM analysis shown the presence of fine crystallites and secondary phases on the degraded surface, particularly after exposure to humidified conditions, identified as Cr and Si-containing compounds. These observations further confirm the detrimental impact of Cr and Si contaminants on surface stability and reactivity, as shown in **Figure 4(f, g)**.

Similarly, Salari et al. [97] further investigated the effect of Cr contamination on LSM electrodes, particularly when enhanced by LNO infiltration. The study showed that Cr significantly disrupted the ORR process, as evidenced by an increase in the R_P of the LNO.P.LSM cathode from 1.05 to 1.70 Ω cm^2 within the first 30 mins (**Figure 4(h)**), followed by a decrease to 0.55 Ω cm^2 after 600 mins. This suggests that while LNO initially loses electrochemical activity, it can reactivate through surface reconstruction, possibly due to Cr-induced phase changes. The increase in R_P and $\eta_{cathodic}$ under cathodic polarization indicates that Cr interactions with LNO partially suppressed surface exchange reactions and enhanced oxygen vacancy formation. Despite these changes, the presence of Cr ultimately hindered the cathodic performance, demonstrating the complex interaction between Cr and LNO in the electrode structure (**Figure 4(i)**).

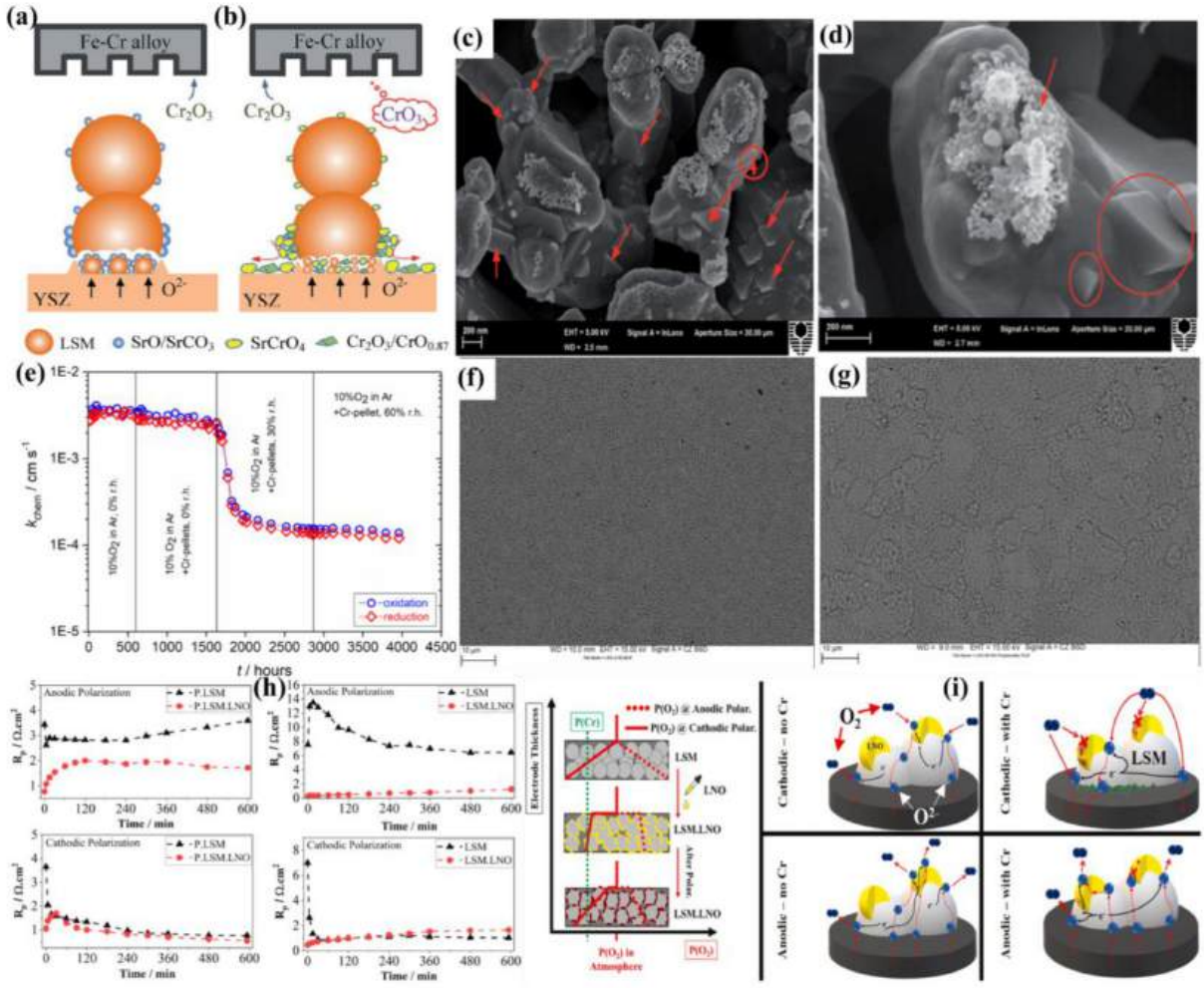

Figure. 4: Schematics illustrating the formation of LSM nanoparticles at the electrode-electrolyte interface and the accelerated segregation of SrO from the bulk to the surface under anodic polarization **(a);** Cr deposition and $SrCrO_4$ formation on the LSM surface **(b);** Surface morphology of the LSM inner surface in contact with the YSZ electrolyte **(c);** SEM micrograph showing the LSM inner surface with visible Cr-based deposits **(d)** This work is licensed under the terms of the Creative Commons Attribution 4.0 License © 2015 by the authors (CC BY, (https://creativecommons.org/licenses/by/4.0/)) [95]; Oxygen exchange activity of LNO under dry conditions over 600 h **(e);** SEM images of LNO after exposure to humidified O_2-Ar 1000 h at 30% RH **(f);** and 1000 h at 60% RH. **(g)** Reprinted from ref. [96], copyright 2018, with permission from Elsevier. Rp for LNO.LSM and LSM and with and without Cr species at 800°C **(h);** The schematic illustrates the Cr-induced degradation mechanism in the LNO.P.LSM electrode, showing the

formation of $LaCrO_3$ at the electrode/electrolyte interface and its impact on the cathodic performance **(i)** Reprinted from ref. [97], copyright 2024, with permission from Elsevier.

Table 2: Summary of Cr poisoning test parameters for various electrode materials at temperatures ranging from 750°C to 900°C under SOEC condition.

Temp (°C)	**R_Ω (Ω)**	**R_p (Ω)**	**η (mV)**	**Current density (mA/cm^2) & Time**	**Deposition area**	**Testing conditions**	**Ref**
800	8.20	8.20	---	500; 20 h	---	LSM (1150°C for 3 h); Without Fe–Cr Interconnect	[95]
800	11.00	9.50	---	500; 20 h	---	LSM (1150°C for 3 h); With Fe–Cr Interconnect	[95]
900	1.3	0.023	7	200; 20 h	---	LSM (1050 °C for 4 h); Without Fe–Cr Interconnect	[74]
900	1.3	0.413	127	200; 20 h	---	LSM (1050 °C for 4 h); With Fe–Cr Interconnect	[74]
800	---	0.37	7.55 to 6.47	±200; 0-600 min	0.5 cm^2	LSM (non-poisoned) 1100 °C for 2 h; 430 SS	[97]

800	---	0.37	3.44 to 3.60	±200; 0-600 min	0.5 cm^2	P.LSM (poisoned with Cr) 1100 °C for 2 h; 430 SS	[97]
800	---	0.24	0.53 to 1.67	±200; 0-600 min	0.5 cm^2	P.LSM.LNO (poisoned with Cr) 1100 °C for 2 h; 430 SS	[97]
900	---	0.15	12	200; 2 h	No Cr deposition	LSCF (1000 °C for 2 h); Without Fe–Cr Interconnect	[98]
900	---	0.21	21	200; 20 h	Under rib of interconnect (Cr deposition)	LSCF (1000 °C for 2 h); Without Fe–Cr Interconnect	[98]

4.4. LSCF based electrodes

LSCF is one of the most widely used cathode and oxygen electrode materials for SOFCs and SOECs due to its high mixed ionic–electronic conductivity and excellent oxygen surface exchange kinetics at intermediate to high temperatures. These properties make LSCF an attractive candidate for efficient oxygen reduction and evolution reactions. However, the long-term performance of LSCF electrodes is strongly affected by degradation phenomena, particularly under high-temperature anodic polarization in SOEC operation [71, 99].

A key degradation mechanism is Cr poisoning, which originates from chromia-forming ferritic steel interconnects. At high temperatures, volatile Cr species (e.g., CrO_3, $CrO_2(OH)_2$) are released

from the interconnect and migrate toward the cathode. On LSCF electrodes, Cr deposition occurs preferentially at the outer surface near the interconnect rather than at the electrode–electrolyte interface [23, 24].

The segregated SrO on the LSCF surface acts as a nucleation site, reacting with incoming Cr species to form electrically resistive $SrCrO_4$. This reaction leads to the accumulation of plate-like and octahedral deposits, increasing both polarization and ohmic resistances. Additionally, surface Sr enrichment causes Sr deficiency in the bulk and at the electrode–electrolyte interface, further deteriorating electrochemical activity. As a result, rapid increases in overpotential and polarization resistance are observed under SOEC operation, demonstrating the severe impact of Cr poisoning on the activity and durability of LSCF oxygen electrodes [25-27, 99].

To address these challenges, various mitigation strategies have been developed to improve the Cr tolerance of LSCF electrodes. Huang et al [100] investigated the impact of $BaCO_3$ nanoparticle infiltration on the electrocatalytic performance and Cr tolerance of LSCF cathodes used in SOFCs. The infiltration of $BaCO_3$ significantly improves the performance of LSCF cathodes, enhancing their peak power density to 1.30 $W \cdot cm^{-2}$ at 800°C, compared to the untreated LSCF cathodes. The polarization resistance of the $BaCO_3$ infiltrated LSCF cathode (0.28 $\Omega \cdot cm^2$) is lower than that of the untreated LSCF cathode (0.37 $\Omega \cdot cm^2$) (**Figure. 5(a, b)**). Additionally, $BaCO_3$ infiltration prevents Cr deposition and Sr segregation in the presence of gaseous CrO_3, while a $BaCrO_4$ surface layer forms, effectively mitigating Cr-induced degradation. This blocking effect of the $BaCrO_4$ layer, combined with the low reactivity between $BaCO_3$ nanoparticles and CrO_3 gas, plays a key role in the outstanding operating stability of the $BaCO_3$-modified LSCF cathodes under accelerated Cr poisoning conditions (**Figure. 5(c)**).

In a follow-up study, Huang et al. [101] explored the impact of a heterogeneous catalyst coating (CC-LSCF) on the electrocatalytic performance and Cr tolerance of LSCF cathodes for SOFCs. The catalyst coating, made from $BaCe_{0.8}Gd_{0.2}O_{3-\delta}$ (BCGO) and $BaCO_3$, enhanced the peak power density to 1.73 $W \cdot cm^{-2}$ at 750°C, significantly outperforming untreated LSCF cathodes, which showed only

0.83 $W \cdot cm^{-2}$ (**Figure. 5(d)**). This improvement was accompanied by a notable reduction in polarization resistance ((**Figure. 5(e)**)), indicating better electrochemical activity. Moreover, the catalyst coating greatly enhanced the Cr tolerance of the cathode, preventing degradation caused by Cr exposure. The formation of a $BaCrO_4$ layer on the surface blocked harmful interactions between Cr and Sr, thus stabilizing the cathode and maintaining performance (**Figure. 5(f)**).

Pei et al. [102] investigated the impact of $BaCoO_{3-x}$ (BCO) nanoparticle coating on the electrocatalytic performance and Cr tolerance of LSCF cathodes. The BCO coating significantly enhanced the peak power density of LSCF cathodes to 0.514 $W \cdot cm^{-2}$ at 700°C, outperforming the untreated LSCF cathodes, which exhibited a lower peak power density of 0.448 $W \cdot cm^{-2}$ (**Figure. 5(g)**). Furthermore, the BCO-coated LSCF cathodes demonstrated improved electrochemical stability, with a substantially lower polarization resistance of 0.05 $\Omega \cdot cm^2$ after 100 h of testing at 750°C, compared to the untreated LSCF's higher resistance (**Figure. 5(h)**). This enhanced performance is attributed to the BCO coating's ability to block Cr poisoning and improve the oxygen reduction reaction. The formation of a protective $BaCrO_4$ surface layer effectively mitigates the detrimental effects of Cr exposure, leading to the excellent durability and stability of the BCO-coated LSCF cathodes under Cr-poisoning conditions, ensuring their reliability for long-term operation in SOFCs (**Figure. 5(i)**).

Niu et al. [103] further investigated the impact of a multiphase catalyst (MP) coating, combining $Ba_{1-x}Co_{0.7}Fe_{0.2}Nb_{0.1}O_{3-\delta}$ (BCFN) and $BaCO_3$ on the performance and stability of LSCF cathodes. Their study showed significant improvements, with the MP catalyst-coated cathode achieving a peak power density of 1.40 $W \cdot cm^{-2}$ at 750°C, which is 2.1 times higher than the bare LSCF cathode (0.67 $W \cdot cm^{-2}$) (**Figure. 5(j)**). The mechanism behind this improvement is that while $BaCO_3$ remains inert to Cr species, forming a stable protective $BaCrO_4$ layer, BCFN also helps prevent Sr–O segregation and $SrCrO_4$ formation, which are detrimental to ORR. Thus, the MP catalyst coating effectively mitigates Cr-induced degradation, improving the long-term durability of the cathodes under harsh operational conditions (**Figure. 5(k)**).

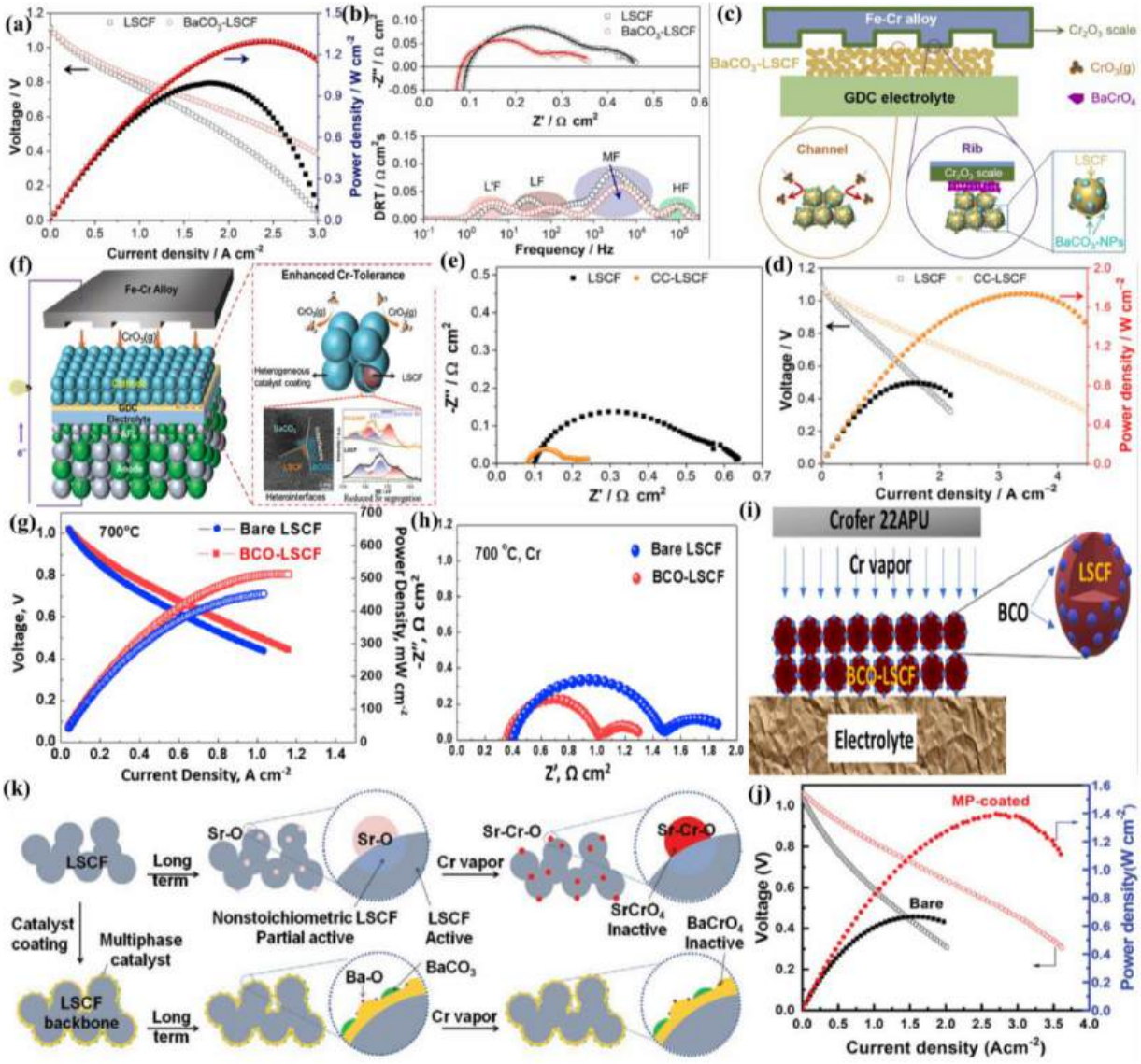

Figure. 5: Comparison of the peak power density and polarization resistance of $BaCO_3$ infiltrated LSCF cathodes Vs. untreated LSCF cathodes **(a, b);** Illustration of the blocking effect of the $BaCrO_4$ surface layer, formed by $BaCO_3$ infiltration, preventing Cr deposition and Sr segregation, which enhances Cr tolerance and operating stability under accelerated Cr poisoning conditions **(c)** Reprinted from ref. [100], copyright 2023, with permission from Elsevier; Peak power density comparison between CC-LSCF and untreated LSCF cathodes at 750°C **(d);** R_p measurements demonstrating a reduction in resistance for the CC-LSCF cathode, highlighting enhanced electrochemical activity **(e);** Formation of a $BaCrO_4$ layer on the surface of CC-LSCF, effectively preventing Cr-induced degradation and stabilizing the cathode by blocking harmful interactions between Cr and Sr **(f)**

Reprinted with permission from ref. [101], copyright 2024, John Wiley & Sons, Inc. Comparison of peak power density between BCO-coated and untreated LSCF cathodes at 700°C **(g);** R_p of BCO-coated and untreated LSCF cathodes after 100 h of testing at 750°C **(h);** The ORR activity and durability of the BCO-LSCF cathode were evaluated under direct contact with Cr in 3% H_2O humidified air **(i)** Reprinted from ref. [102], copyright 2020, with permission from Elsevier. Performance of MP catalyst-coated LSCF cathodes **(j);** Schematic illustration of the performance enhancement mechanism for BCFN-BCO-LSCF **(k)**, Reprinted with permission from ref. [103], copyright 2021, John Wiley & Sons, Inc.

Wang et al. [104] applied electroless Ag plating to LSCF cathodes. The silver-modified LSCF (LSCF-Ag) cathodes exhibited significantly improved resistance to Cr poisoning, with only a slight increase in polarization resistance (0.24 $\Omega \cdot cm^2$ to 0.26 $\Omega \cdot cm^2$) after 40 h of Cr exposure, compared to a more substantial rise in LSCF cathodes (0.26 $\Omega \cdot cm^2$ to 0.62 $\Omega \cdot cm^2$) at 700°C (**Figure. 6(a, b)**). This enhancement is attributed to the formation of $AgCrO_2$, which prevents the generation of $SrCrO_4$ and preserves the cathode's electrical conductivity, offering protection under Cr-poisoning conditions (**Figure. 6(c)**).

Chen et al. [105] used in-situ surface-enhanced Raman spectroscopy (SERS) to investigate Cr poisoning in LSCF cathodes, focusing on the role of Cr species like $SrCrO_4$. In **Figure. 6(d)**, they compared two LSCF thin-film electrodes, one in direct contact with a Cr-containing alloy and the other without demonstrating a more significant deposition of $SrCrO_4$ when in direct contact with the alloy. This deposition was predominantly observed at the LSCF-GDC boundary, as shown in **Figure. 6(e)**, and was attributed to surface segregation of SrO. The mechanism of Cr poisoning was explained through the sublimation of volatile Cr species from the alloy, which react with segregated SrO on the cathode surface to form $SrCrO_4$. This process effectively blocks active sites, thereby impairing the ORR at the TPB.

LSCF cathodes with the hybrid catalyst coating exhibited significantly improved performance under contamination conditions compared to bare LSCF electrodes. Specifically, cells with the hybrid

coating displayed a higher initial power density of 0.71 W/cm^2, in contrast to 0.46 W/cm^2 for the bare LSCF electrodes, when exposed to conditions involving 3% H_2O and direct Cr alloy contact (**Figure. 6(f)**). This enhancement in performance is attributed to the hybrid coating's ability to improve Cr tolerance and mitigate the detrimental effects of $SrCrO_4$ deposition, as indicated by the Raman analysis and its influence on ORR activity.

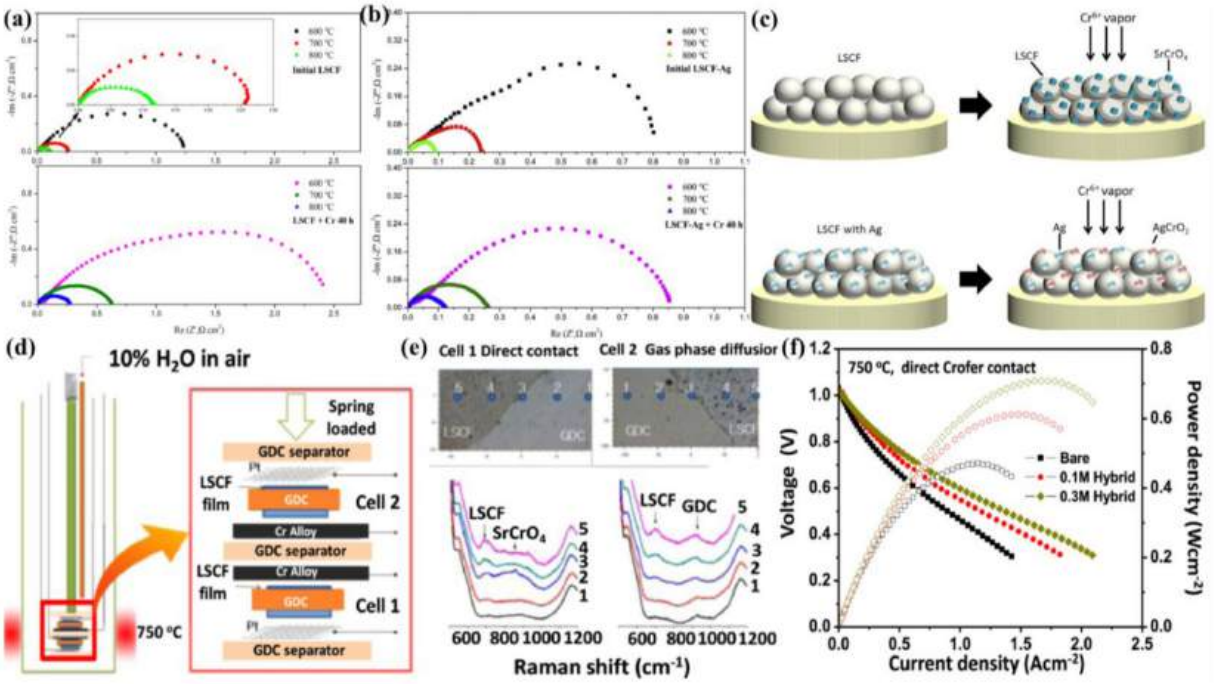

Figure. 6: R_p of LSCF and LSCF-Ag cathodes before and after exposure to Cr for 40 h at 700°C **(a, b);** Schematic representation of the mechanism of Cr tolerance in LSCF and LSCF-Ag cathodes **(c)** Reprinted from ref. [104], copyright 2022, with permission from Elsevier**;** Comparison of two LSCF thin-film electrodes, one in contact with a Cr-containing alloy and the other without, showing increased $SrCrO_4$ deposition in direct contact with the alloy. **(d);** Deposition of $SrCrO_4$ at the LSCF-GDC boundary due to surface segregation of SrO **(e);** IV Vs IP curves for bare and hybrid LSCF cathode **(f)** Reprinted from ref. [105], copyright 2018, with permission from Elsevier.

The study by Wei et al. [74] investigates the degradation of LSCF oxygen electrodes in SOECs due to Cr deposition from the Fe–Cr interconnect. Under high-temperature anodic polarization conditions (200 mA cm^{-2} at 900°C), Cr species from the interconnect react with SrO that segregates

on the LSCF surface, leading to the formation of $SrCrO_4$ and Cr_2O_3 deposits. This Cr poisoning significantly impairs the electrocatalytic performance of the LSCF electrodes, as evidenced by an increase in electrode polarization resistance and overpotential. **Figure. 7(a)** shows the stable electrochemical performance of LSCF oxygen electrodes without a Fe–Cr interconnect, with minimal increases in polarization resistance and overpotential after 20 h of anodic current passage. In contrast, **Figure. 7(b)** demonstrates significant degradation when the Fe–Cr interconnect is present, showing a rapid increase in overpotential and polarization resistance, indicating severe poisoning by Cr species. **Figure. 7(c)** shows distinct plate-like and octahedral Cr crystals formed on the electrode surface, particularly near the rib of the interconnect.

Jiang et al. [99] studied the electrochemical performance of LSCF electrodes under cathodic polarization at 200 mA cm^{-2} and 900°C, comparing conditions with and without the presence of a Fe–Cr interconnect. In the absence of the interconnect, the electrodes maintained high electrochemical activity with minimal increases in polarization resistance and overpotential. However, in the presence of the Fe–Cr interconnect, significant Cr deposition occurred, particularly under the rib of the interconnect, leading to a substantial increase in polarization resistance and overpotential, indicating the detrimental impact of Cr species on electrode performance.

In contrast to the Cr poisoning observed in LSCF electrodes due to Cr deposition from Fe–Cr interconnects, as reported by Wei et al. [74]. The study by Chen et al. [106] offers a different perspective on the role of Cr in perovskite electrodes (such as; $La_{0.75}Sr_{0.25}Cr_{0.9}Fe_{0.1}O_3$ (LSCrF)) under steam electrolysis conditions. The findings show that the role of Cr on the LSCrF electrode surface can be beneficial rather than harmful. Under high-temperature oxygen-rich environments, Cr undergoes partial oxidation and segregates to the surface, as shown in **Figure. 7(d, e)**. This surface segregation of Cr, along with Sr, leads to the formation of a stable $SrCrO_4$ compound, which improves the electrode's electrocatalytic performance. The Cr/Sr ratio, illustrated in **Figure. 7(e)**, clearly indicates a shift in surface composition, with a higher Cr concentration at the surface compared to the bulk material. Interestingly, the formation of Cr^{6+} species does not lead to poisoning but instead

promotes the electrochemical performance. **Figure. 7(f)** further illustrates this shift in surface composition, showing that, in oxygen-rich environments, Cr is not just a passive component but actively contributes to the electrode's function by forming beneficial surface phases like $SrCrO_4$. Therefore, while Cr deposition from Fe–Cr interconnects has a negative impact in other studies, in the case of LSCrF perovskite electrodes, Cr segregation and its oxidation to Cr^{6+} can act as a promoter for enhanced performance in steam electrolysis.

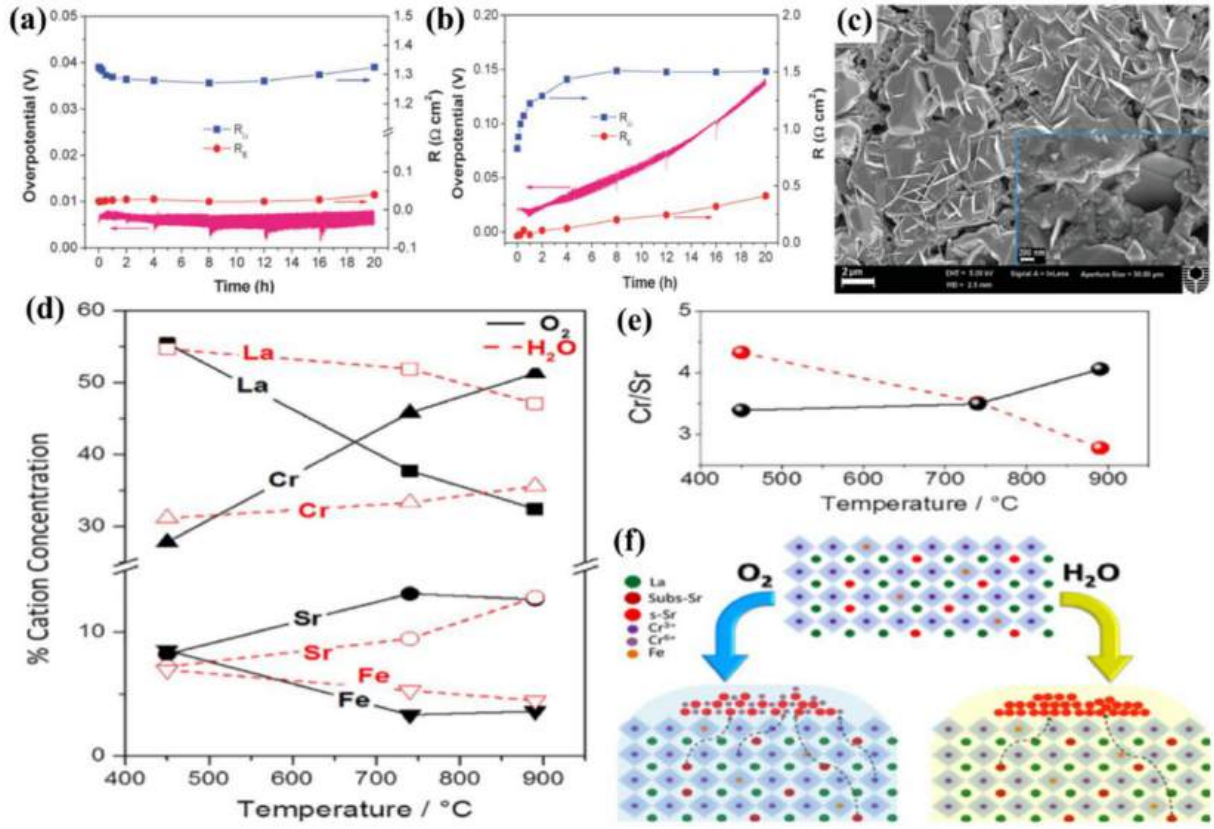

Figure. 7: Polarization curves of LSCF electrodes at 200 mA cm^{-2} for 20 h at 900°C: without a Fe–Cr interconnect **(a);** and with a Fe–Cr interconnect **(b);** SEM image of LSCF oxygen electrode surface after anodic polarization at 200 mA cm^{-2} and 900°C for 20 h **(c);** Reprinted from ref. [74], copyright 2015, with permission from the Royal Society of Chemistry; Evolution of the surface cationic composition of LSCrF electrodes under different atmospheric conditions (O_2 and H_2O) at varying temperatures **(d);** The Cr/Sr ratio at the surface of LSCrF electrodes under different annealing conditions **(e);** Schematic representation of the surface composition of LSCrF electrodes after

annealing in O_2, showing the segregation of Cr and its oxidation to form $SrCrO_4$ **(f)** Reprinted from ref. [106], copyright 2020, with permission from Elsevier.

Table. 3: Summary of Cr poisoning test parameters for various electrode materials at temperatures ranging from 750°C to 900°C.

Temp (°C)	R_Ω (Ω)	R_p (Ω)	E (mV)	η (mV)	Current density (mA/cm^2) & Time	Deposition area	Cr poisoning test parameters	Ref
800	---	---	---	---	750; 168 h	7.3	LSCF (1200 °C for 2 h); Crofer22APU	[33]
800	1.40	0.14	---	---	200; 40 h	---	LSCF (700 °C for 2 h); Fe–Cr alloy	[114]
900	1.37	0.25	70	---	400; 20 h	1.0	LSCF (1050 °C for 4 h); RA446 chromia-forming alloy	[115]
750	0.28	0.37	---	---	200; 100 h	121 ± 62 nm	LSCF-$BaCO_3$ (1000 °C for 42 h); Fe-Cr alloy	[104]
750	0.14	0.63	---	---	OCV; 100 h	---	LSCF (1080 °C for 2 h); Cr alloy	[105]
800	1.40	0.10	---	---	200; 100 h	---	LSCF (1000 °C for 2 h); Fe–Cr alloy	[114]
900	0.84	0.06	----	7	200; 20 h	----	LSCF (1050 °C for 4 h); RA446 Fe–Cr alloy	[74]

900	0.69	0.18	----	----	200; 20 h	~20 μm	LSCF (1050 °C for 2 h); RA446	[116]
900	0.74	1.49	----	----	200; 20 h	~20 μm	LSCF (1050 °C for 2 h); RA446	[116]
800	1.02	0.15	---	---	200; 40 h	---	LSCF-BaO (1000 °C for 2 h); Fe–Cr alloy	[114]
900	1.01	0.04	---	26	400; 20 h	~1 μm	LSCF (1050 °C for 4 h); RA446 chromia-forming alloy	[114]
750	0.35	0.16	---	---	200; 100 h	---	LSCF-CC (1000 °C for 2 h); Fe–Cr alloy	[101]
750	0.39	0.05	---	---	OCV; 100 h	---	LSCF-BCO (1000 °C for 2 h); Crofer 22APU	[102]
650	~0.24	0.04	---	---	250; 200 h	---	LSCF-BCFN-BCO (1080 °C for 2 h); Crofer 22 APU	[103]
900	0.10	0.08	---	16-160	200; 20 h	---	$(La_{0.6}Ba_{0.4})(Co_{0.2}Fe_{0.8})O_3$ (LBCF) (950 °C for 5 h); Fe–Cr alloy	[117]

700	---	0.64	---	---	200; 21 days	---	$(La_{0.2}Sr_{0.2}Pr_{0.2}Y_{0.2}Ba_{0.2})Co_{0.2}Fe_{0.8}O_{3-\delta}$ (LSPYB); (1300 °C for 4 h); 314 SS	[118]
700	---	0.71	---	---	200; 21 days	---	$(La_{0.2}Sr_{0.2}Pr_{0.2}Y_{0.2}Ba_{0.2})Co_{0.2}Fe_{0.8}O_{3-\delta}$ (LSPYB); (1300 °C for 4 h); 314 SS	[118]
700	---	0.24	---	---	OCV; 40 h	---	LSCF-Ag (1080 °C for 2 h); 314 SS	[104]
750	---	0.51	---	---	OCV; 200 h	2–3 μm	LSCF-GDC (1050 °C for 3 h); Crofer 22 APU	[119]

4.5. Beyond

As the limitations of traditional air electrode materials such as LSM and LSCF become more apparent under Cr-containing environments, attention has increasingly shifted toward emerging oxide systems, including double perovskites ($A_2BB'O_6$) and Ruddlesden–Popper (RP) structured materials. These advanced oxides are designed to address the trade-offs between electrochemical performance and chemical stability, especially under high-temperature operation and in the presence of volatile Cr species [107].

Double perovskites, such as $PrBaCo_2O_{5+\delta}$ (PBCO) and $PrBa_{0.5}Sr_{0.5}Co_{1.5}Fe_{0.5}O_{5+\delta}$ (PBSCF), feature ordered A- and B-site arrangements that enhance oxygen ion transport, surface exchange kinetics, and overall ORR activity. However, Wei et al. [108] demonstrated that even structurally advanced double perovskites, such as PBCO, are not entirely immune to Cr poisoning. To investigate

this, they employed a half-cell configuration (**Figure. 8(a)**) to expose the PBCO surface to volatile Cr species under controlled electrochemical conditions. Post-treatment analysis shows that heat treatment in high-purity oxygen atmospheres led to the formation of surface precipitates, as shown in **Figure. 8(b-d).** These precipitates became more pronounced and grew significantly in size as the annealing temperature increased from 800 °C to 1000 °C, with average particle sizes growing from ~0.21 μm to ~1.47 μm.

The mechanism of Cr deposition was schematically illustrated in **Figure. 8(e),** which shows that prolonged high-temperature exposure promotes Ba cation segregation to the surface. This segregation leads to the localized formation of Co_3O_4 and BaO phases. Cr vapors selectively react with the BaO-rich regions rather than with Co_3O_4 resulting in the nucleation of $BaCrO_4$, a highly resistive compound that deactivates ORR sites. Importantly, this process is chemically driven and initiated by surface restructuring rather than purely electrochemical degradation. The surface migration of Ba and the low-temperature threshold for segregation (~400°C) suggest that PBCO can become susceptible to Cr poisoning even within the intermediate temperature range (500–800°C), making it vulnerable in practical SOC applications.

This Cr-induced surface degradation was shown to severely impair the oxygen surface exchange and diffusion properties of the electrode, contributing to a marked increase in polarization resistance. These findings highlight the need for future strategies to suppress surface segregation and enhance the structural stability of double perovskite electrodes, particularly when exposed to Fe–Cr-based interconnects in SOCs. Tailoring the surface composition and introducing protective coatings or dopants may offer viable routes to improve the Cr tolerance of these promising but chemically sensitive materials.

Similarly Li et al. [109] investigated Cr poisoning behavior in structurally refined double perovskite PBSCF electrodes under realistic SOC operating conditions. In their study, a custom-designed test system (**Figure. 8(f)**) was used to perform Cr exposure tests under a cathodic current of

400 mA cm^{-2} at 750°C for 1200 minutes. The results shows a sharp increase in Rp), rising from 0.76 Ω·cm^2 to 2.58 Ω·cm^2 within just 20 hours, signifying severe electrochemical degradation.

Their findings also shed light on the Cr deposition mechanism unique to PBSCF. Unlike LSM, where Cr tends to accumulate at the cathode–electrolyte interface due to Mn^{2+}-induced nucleation, PBSCF resembles LSCF and BSCF systems in that Cr species deposit primarily on the cathode surface. This surface deposition is initiated by the segregation of Ba cations, which migrate to the surface at elevated temperatures and react with incoming Cr vapors to form intermediate nuclei. As schematically shown in **Figure 8(g),** the reaction proceeds through a sequence of steps: (1) formation of Ba–Cr–O nuclei via BaO and CrO_3 interaction, (2) growth of Cr_2O_3 from further CrO_3 exposure, and (3) final formation of $BaCrO_4$ through reaction with BaO and additional CrO_3. Over time, these BaCrO4 particles grow and accumulate on the PBSCF surface, obstructing oxygen reduction and transport pathways and leading to electrode decomposition and performance loss.

To mitigate this effect, Li et al. [109] introduced a $La_2NiO_{4-\delta}$ (LN) protective coating via an optimized infiltration method. As shown in **Figure 8(h),** the LN layer acts as a dense, continuous barrier that prevents direct interaction between Cr vapors and the PBSCF surface. In contrast to earlier GDC nanoparticle strategies, which left partial surface exposure, the LN film provided uniform protection. The LN-coated PBSCF retained its structural integrity and electrochemical stability in Cr-rich environments, demonstrating significantly improved resistance to Cr-induced degradation.

In parallel, RP-structured materials such as $La_4Ni_3O_{10}$, and $LaSr_3Fe_3O_{10}$ have attracted attention for their inherent Cr resistance. Their layered structures, low Sr content, and high oxygen mobility contribute to reduced surface reactivity with Cr vapors and limited A-site cation segregation. Moreover, their anisotropic conduction and structural flexibility under thermal cycling make them promising alternatives for long-term SOC operation.

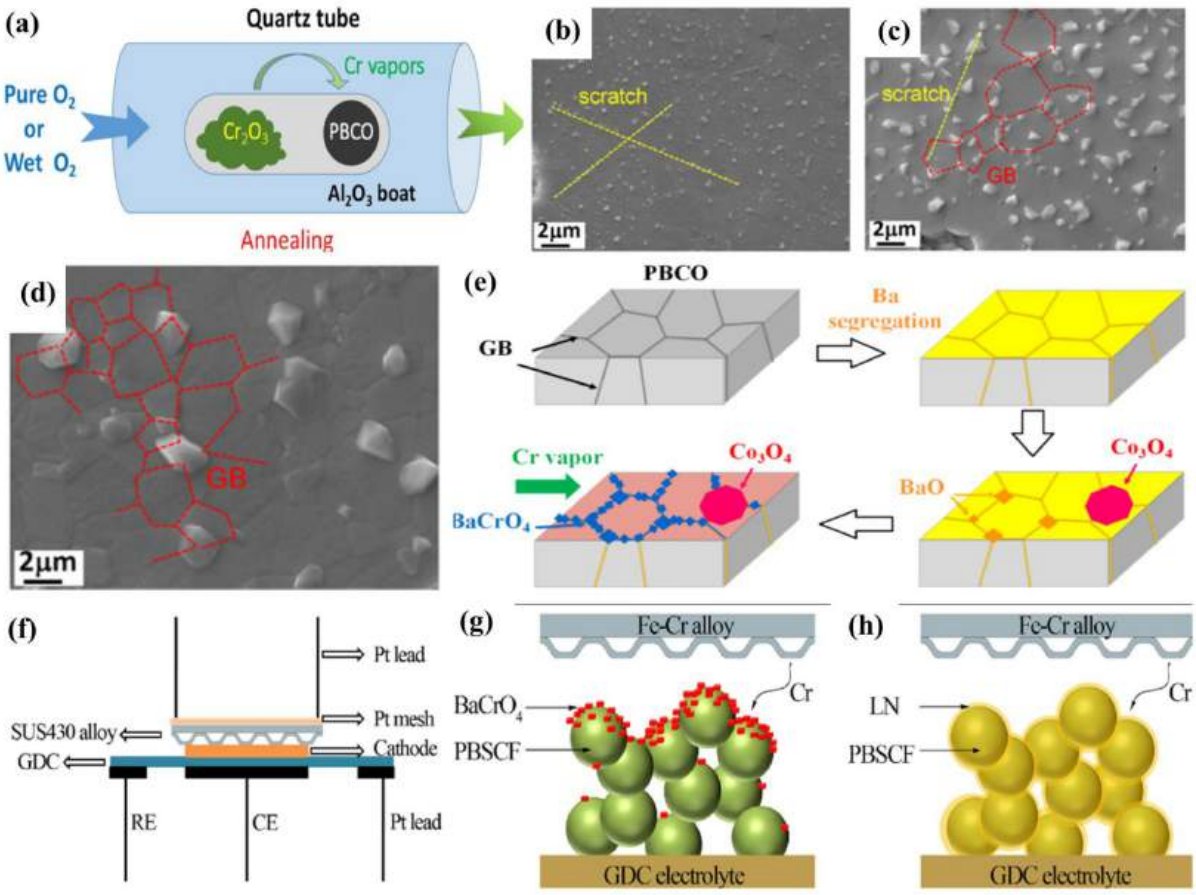

Figure. 8: Dual-atmosphere half-cell setup simulating Cr exposure from a metallic source to the PBCO electrode **(a);** SEM images of PBCO surfaces annealed in O_2 at 800°C **(b),** 900°C **(c),** and 1000 °C **(d);** Mechanism of Cr deposition on PBCO **(e)** Reprinted from ref. [108], copyright 2018, with permission from the American Chemical Society. Schematic of the test configuration used for Cr poisoning experiments, **(f);** Proposed mechanisms of Cr deposition: **(g);** On bare PBSCF **(h);** On LN-coated PBSCF, Reprinted from ref. [109], copyright 2018, with permission from Elsevier.

5. Mitigation Strategies in SOCs

Cr poisoning remains a persistent challenge in the advancement of SOCs, significantly impacting the stability and performance of the cathode [110]. At high operational temperatures, Cr-containing FSS used in interconnects and balance-of-plant components release volatile Cr species, such as CrO_3 and $CrO_2(OH)_2$, into the air stream [111,112]. These species migrate to the air electrode, where they react with the cathode material, forming resistive secondary phases and causing morphological

degradation. This interaction leads to increased polarization resistance and reduced electrochemical activity, compromising the overall efficiency and lifetime of the device.

To mitigate Cr-related degradation, several strategies have been explored. These include applying protective coatings to metallic interconnects, utilizing Cr-gettering layers that trap volatile species, designing Cr-tolerant electrode materials, and developing electrochemical regeneration protocols to recover lost performance. Each of these approaches contributes uniquely to enhancing SOC durability and reliability, as elaborated in the following subsections.

5.1. Protective coatings for interconnects

A widely adopted strategy to suppress Cr volatilization is the use of protective coatings on metallic interconnects. These interconnects, typically made from Cr-containing FSS, are essential in SOC stacks due to their excellent mechanical strength and thermal compatibility [20, 113].

However, at temperatures above 700 °C, FSS alloys oxidize and release volatile Cr species, which can migrate toward the oxygen electrode and degrade its electrochemical performance. Protective coatings function as diffusion barriers, blocking the outward migration of Cr and the inward penetration of oxygen, thereby minimizing the growth of chromia scales and preventing Cr-induced electrode poisoning [120–122].

Perovskite oxides with the general formula ABO_3, such as $La_{1-x}Sr_xCoO_3$ (LSC), $La_{1-x}Sr_xCo_{1-y}Fe_yO_3$ (LSCF), and $Ba_{0.5}Sr_{0.5}Co_{0.8}Fe_{0.2}O_{3-\delta}$ (BSCF) have demonstrated promising results as coatings due to their high electronic conductivity and compatibility with SOC cathodes [123,124]. In particular, BSCF coatings react preferentially with Cr vapors to form less resistive compounds like $BaCrO_4$ instead of $SrCrO_4$, preserving electrode performance while maintaining ASR below 0.01 $\Omega \cdot cm^2$ at 700–800 °C conditions favorable for long-term SOC operation [15,126].

Spinel oxides (AB_2O_4) have also garnered significant interest due to their thermal stability, electrical conductivity, and oxidation resistance [127, 128]. The efficacy of these coatings is strongly influenced by their microstructure and deposition method. Recent studies emphasize the importance of multilayer configurations and optimized fabrication techniques to enhance barrier properties. For

example, Mao et al. [129] developed a bilayer composite (Mn, $Co)_3O_4$ spinel coating deposited by magnetron sputtering to enhance oxidation resistance and minimize element diffusion in SOC interconnects. As illustrated in **Figure. 9**, the conventional single-layer Mn-Co coating (**Figure. 9(a)**) forms a dense but somewhat porous 2.4 μm film that thickens with void formation after annealing at 800 °C (**Figure. 9(b)**). In contrast, the bilayer composite coating (**Figure. 9(c)**) distinctly shows an inner (Mn, $Co)_3O_4$ layer (~0.8 μm) and an outer Mn-Co layer (~1.6 μm), which merge into a uniform, void-free spinel layer ~4.4 μm thick after annealing (**Figure. 9(d)**), indicating superior structural integrity. **Figure. 9(e, f)** further compares oxidation behaviors: the bilayer coating (**Figure. 9(e)**) effectively restricts inward oxygen and outward Cr diffusion, resulting in thinner thermally grown oxide and reaction layers which slow degradation and maintain low ASR. Conversely, the conventional coating (**Figure. 9(f)**) suffers from more severe diffusion, thicker oxide layers, and void formation, causing accelerated oxidation and higher ASR.

In a subsequent study, Mao et al. [**130**] employed reactive magnetron sputtering to fine-tune spinel phase formation by optimizing the Ar/O_2 gas flow ratio. This yielded a stable cubic $MnCo_2O_4$ phase after annealing at 800 °C, which significantly reduced oxidation rates over 1000 h at 650–750 °C and lowered ASR by up to 34%. The improved performance was attributed not only to suppressed oxygen ingress and Cr evaporation but also to the prevention of undesired elemental interdiffusion at the coating–substrate interface, thereby ensuring high compositional and structural stability under long-term SOFC conditions.

Molin et al. [131] investigated Mn-Co spinel coatings for SOFC interconnects were prepared using electrophoretic deposition (EPD), thermal co-evaporation, and RF magnetron sputtering, producing coatings with distinct thicknesses and microstructures that directly influence their protective behavior. **Figure. 9(g-j)** illustrates the cross-sectional microstructures of these coatings: the thick (~15 μm) EPD coating (**Figure. 9(g)**) features a dense inner layer adjacent to a chromium oxide reaction layer (~1.5 μm thick), while the thinner sputtered and co-evaporated coatings (1–1.5 μm) display more porosity and microcracks, especially when deposited at room temperature (**Figure. 9(h-j)**). These

structural differences impact Cr diffusion and oxide scale growth during prolonged exposure at 800°C, where thicker coatings better suppress chromium migration and maintain stability. This aligns with schematic mechanisms depicted in **Figure. 9(k-n)**, where bilayer or thicker coatings effectively reduce inward oxygen and outward Cr diffusion, limiting thick thermally grown oxide and reaction layer formation. In contrast, thinner single-layer coatings allow greater mutual diffusion, leading to thicker oxides and accelerated degradation (**Figure. 9(l-n)**).

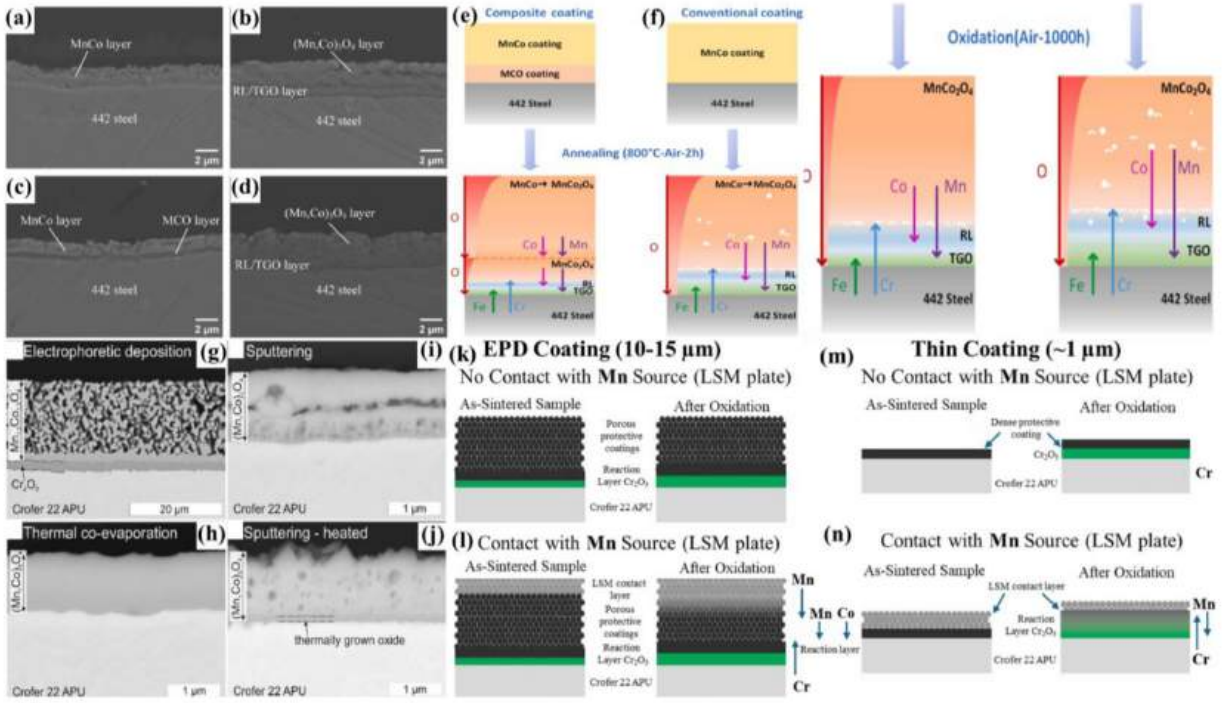

Figure. 9: Cross-sectional SEM images of coatings on FSS interconnects: **(a)** As-deposited single-layer Mn-Co coating; **(b)** Mn-Co coating after annealing at 800 °C for 2 h; **(c)** As-deposited bilayer composite coating layer; **(d)** Bilayer composite coating after annealing at 800 °C. Schematic of oxidation and diffusion after annealing in **(e)** the bilayer composite coatings, and **(f)** the conventional coating, Reprinted from ref. [129], copyright 2025, with permission from Elsevier. Cross-sectional SEM images of Mn-Co coatings prepared by different methods: **(g)** thick electrophoretic deposition coating with dense inner layer and porous outer part; **(h)** thermal co-evaporation coating; **(i)** sputtered coating at room temperature showing microcracks; **(j)** sputtered coating on heated substrate with denser microstructure. Schematic illustrations of oxidation and diffusion behaviors: **(k, m)** bilayer or

thick coatings suppressing oxygen and chromium diffusion, resulting in thin oxide and reaction layers; **(l, n)** conventional thin coatings with enhanced mutual diffusion and thicker oxide scale formation, Reprinted from ref. [131], copyright 2017, with permission from Elsevier.

Nouri et al. [132] demonstrated that a thermally grown $Cu_{1.3}Mn_{1.7}O_4$ spinel coating on AISI 430 stainless steel significantly mitigates Cr migration and reduces ASR by ~70% after 500 h at 750 °C. The oxidation process begins with rapid Mn oxidation to MnO and Mn_3O_4, followed by conversion to Mn_2O_3 and CuO, which then react to form a dense $CuMn_2O_4$ spinel layer. This spinel acts as an effective diffusion barrier, limiting Cr outward migration and oxygen ingress. As shown in **Figures. 10(a, b)**, the coating surface becomes progressively denser without cracking after 24 h and 100 h of oxidation, respectively, indicating stable growth. **Figures. 10(c)**, schematically illustrates the phase evolution and spinel formation mechanism, which underpins the coating's protective function and long-term stability.

To further understand performance, Zhu et al. [133] evaluated four spinel coatings, $CuNi_{0.2}Mn_{1.8}O_4$, $MnFe_{0.34}Co_{1.66}O_4$, $CuMn_2O_4$, and $MnCo_2O_4$ applied on SUS430 stainless steel interconnects for SOFCs. Their study show that Cu–Mn based spinels exhibit superior electrical conductivity compared to Mn–Co based counterparts, with $CuNi_{0.2}Mn_{1.8}O_4$ showing the highest conductivity due to the elimination of manganese oxide phases that impede charge transport. This high conductivity, combined with good sinterability and phase stability, makes $CuNi_{0.2}Mn_{1.8}O_4$ particularly promising for reducing ASR (**Figure. 10(d)**).

In contrast, Mn–Co based spinels, especially $MnFe_{0.34}Co_{1.66}O_4$, demonstrated excellent Cr gettering ability and thermal stability, efficiently limiting the growth of the thermally grown oxide layer by incorporating Cr into the spinel structure, thus suppressing Cr volatilization and interfacial degradation. Meanwhile, Cr solubility in the spinel matrix, shown in **Figure. 10(e),** indicates that $CuMn_2O_4$ and $CuNi_{0.2}Mn_{1.8}O_4$ can incorporate up to 2.4 mol of Cr per mol of spinel before secondary phases appear, while $MnFe_{0.34}Co_{1.66}O_4$ accommodates up to 3.4 mol of Cr, demonstrating its superior Cr-gettering ability despite having lower electrical conductivity.

Joshi et al. [134] reported that Ni substitution in $CuMn_2O_4$ spinels stabilizes the spinel phase at lower temperatures, prevents coating delamination, and promotes uniform, adherent coatings on UNS430 interconnects. Their conductivity isotherms (**Figure. 10(f)**) show that substituting Cu with Ni up to 40% slightly decreases conductivity from ~110 to ~95 S/cm at 800°C, while **Figure. 10(g)** shows Ni addition improves conductivity by stabilizing the spinel phase and preventing decomposition into non-conductive mixed oxides. Together, these studies emphasize the importance of balancing electrical conductivity, phase stability, and Cr-gettering in optimizing spinel coatings for SOFC interconnect protection.

These findings underscore that optimizing spinel coatings involves balancing Cr-gettering capability, phase stability, and electrical conductivity. Spinel coatings require careful control of stoichiometry and densification to minimize porosity and crack formation. Conversely, perovskite coatings while highly conductive may facilitate oxygen ion transport, which could accelerate Cr migration under certain conditions due to their mixed ionic–electronic conduction

Ultimately, the choice between spinel and perovskite coatings should be informed by application-specific needs, including operating temperature, thermal expansion compatibility, and desired electrical performance. Advanced coating architectures, such as multilayer or compositionally graded coatings, and scalable deposition techniques are key directions for future development to ensure long-term durability and commercial viability of SOC interconnects.

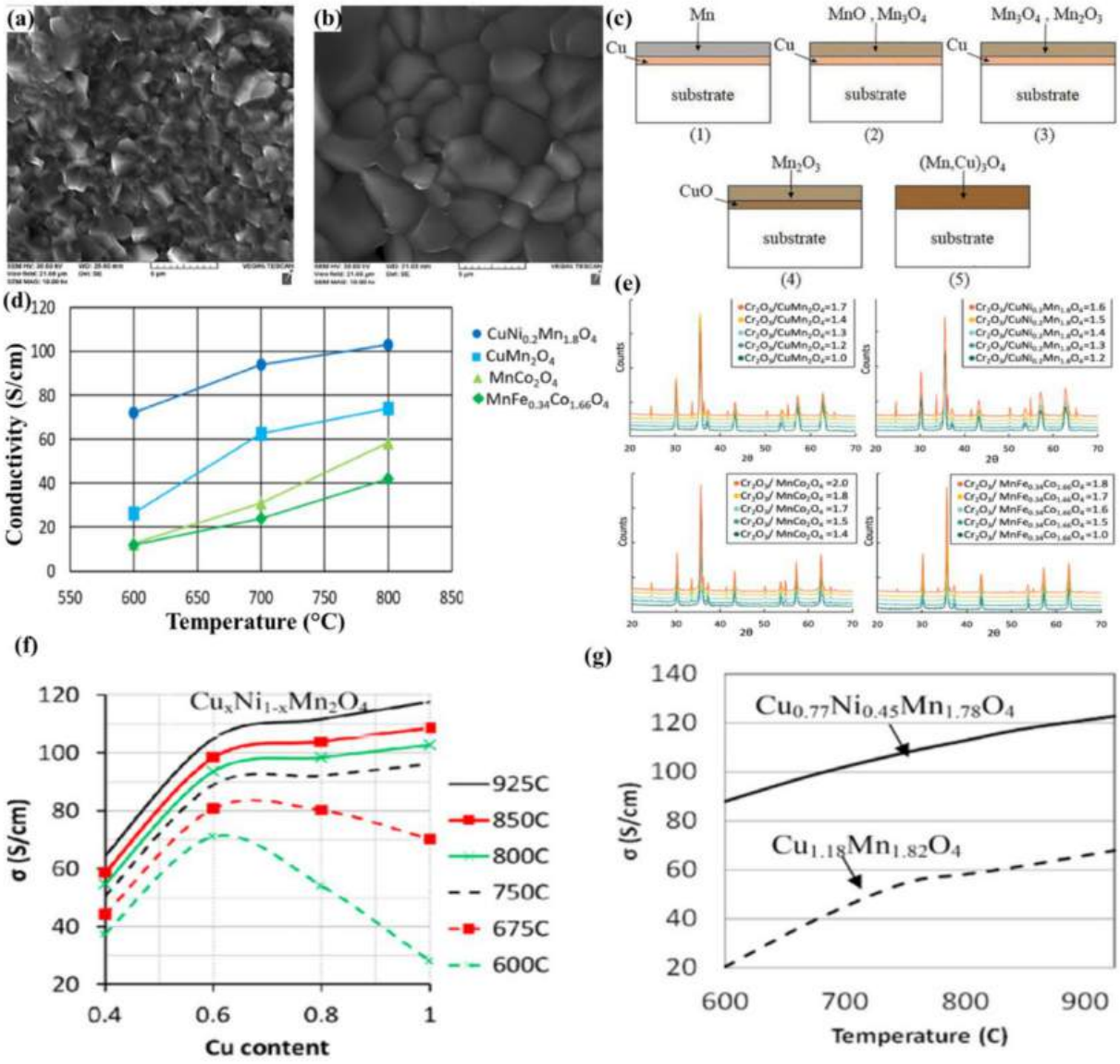

Figure. 10: Surface morphology of $Cu_{1.3}Mn_{1.7}O_4$ coated AISI 430 steel after oxidation at 750 °C for **(a)** 24 h and **(b)** 100 h. Schematic of oxidation and spinel formation in the Cu–Mn coating **(c)** Reprinted from ref. [132], copyright 2018, with permission from Elsevier. Electrical conductivities measured from 600–800 °C **(d);** along with the XRD patterns of of $CuNi_{0.2}Mn_{1.8}O_4$, $MnFe_{0.34}Co_{1.66}O_4$, $CuMn_2O_4$, and $MnCo_2O_4$ spinel structures sintered at 800 °C **(e)** Reprinted from ref. [133], copyright 2022, with permission from Elsevier. Electrical conductivity isotherms of $Cu_xNi_{1-x}Mn_2O_4$ spinels over the temperature range 600–925°C **(f);** along with the comparison of conductivity for $Cu_{0.77}Ni_{0.45}Mn_{1.78}O_4$ vs. $Cu_{1.18}Mn_{1.82}O_4$ spinels **(g)** Reprinted from ref. [134], copyright 2017, with permission from Elsevier.

5.2. Chromium Getters

Another promising solution is the development of Cr getters materials designed to capture and chemically stabilize volatile Cr species before they can reach the cathode. These getters work by reacting with Cr vapors to form stable solid compounds, such as $SrCrO_4$, which prevent the species from interacting with the cathode [135,136]. The effectiveness of a getter depends on several factors, including its material composition, porosity, and structural design. For instance, getters based on strontium-nickel oxides ($Sr_xNi_yO_z$; SNO), have demonstrated high efficiency in capturing Cr species under typical SOFC operating conditions. The formation of reaction products, however, reduces the porosity of the getter over time, which limits its capacity and underscores the importance of optimizing getter design for prolonged use.

Heo et al. [137] investigated Cr poisoning in LSM cathodes under intermediate temperatures (550–650°C) using humid air (3% H_2O) containing Cr vapors. They observed significant increases in polarization resistance and the formation of Cr_2O_3 and $(Mn,Cr)_3O_4$ at the LSM/YSZ interface. However, the use of a Sr-based getter material, specifically SNO, effectively captured Cr vapors, preventing deposition at the electrode interface and maintaining stable electrochemical performance over 100 h.

Uddin et al., [138] proposed a monolithic getter structure with a porous SNO coating to capture Cr vapors in SOFC environments. In their experimental setup (**Figure. 11(a)**), a getter pellet was exposed to Cr vapor from a chromia source under humidified air. Over time, a dense $SrCrO_4$ layer formed on the getter surface (**Figure. 11(b)**), acting as a diffusion barrier and enhancing Cr-trapping efficiency. The reaction pathway (**Figure. 11(c)**) showed Cr vapor reacting with the getter surface to form $SrCrO_4$ and NiO, with the porous structure accommodating reaction products and maintaining performance.

To address Cr vapor migration from interconnects to the cathode, Uddin et al. [139] proposed two getter configurations: spaced-apart (config-1) and direct-contact (config-2) (**Figure. 11(d, e)**). The config-1 maintained stable performance after 100 h of Cr exposure. Config-2's effectiveness varied

with composition; a 75 wt% LSCF–25 wt% SNO getter matched config-1's performance, whereas a 50 wt% LSCF–50 wt% SNO getter performed poorly. Cells without a getter suffered the most severe degradation, reinforcing the importance of effective Cr mitigation.

Aphale et al. [140] demonstrated the thermal stability of SNO-based getters, showing they remain stable up to 900°C. Above 950°C, decomposition into SrO and NiO occurs, leading to reactions with ambient air that cause volume expansion and structural degradation. Chou et al. [141] validated SNO getters in an SOFC stack environment, reducing degradation rates from 56% kh^{-1} (without getter) to 12.1% kh^{-1} (with getter) over 1000 h at 800°C. Post-mortem analyses confirmed that getters effectively prevented Cr migration to the cathode/electrolyte interface. Liang et al. [142] explored SNO-coated cordierite honeycomb structures under SOFC-like conditions. Tested at 850°C in humidified air (3% H_2O) for 500 h, these getters captured over 98% of Cr vapor (**Figure. 11(f)**). By intercepting Cr species, such as $CrO_2(OH)_2$, which degrade cathodes by forming resistive compounds like Cr_2O_3 and $SrCrO_4$ (**Figure. 11(g)**), the honeycomb getter effectively preserved cathode integrity, ensuring long-term SOFC durability.

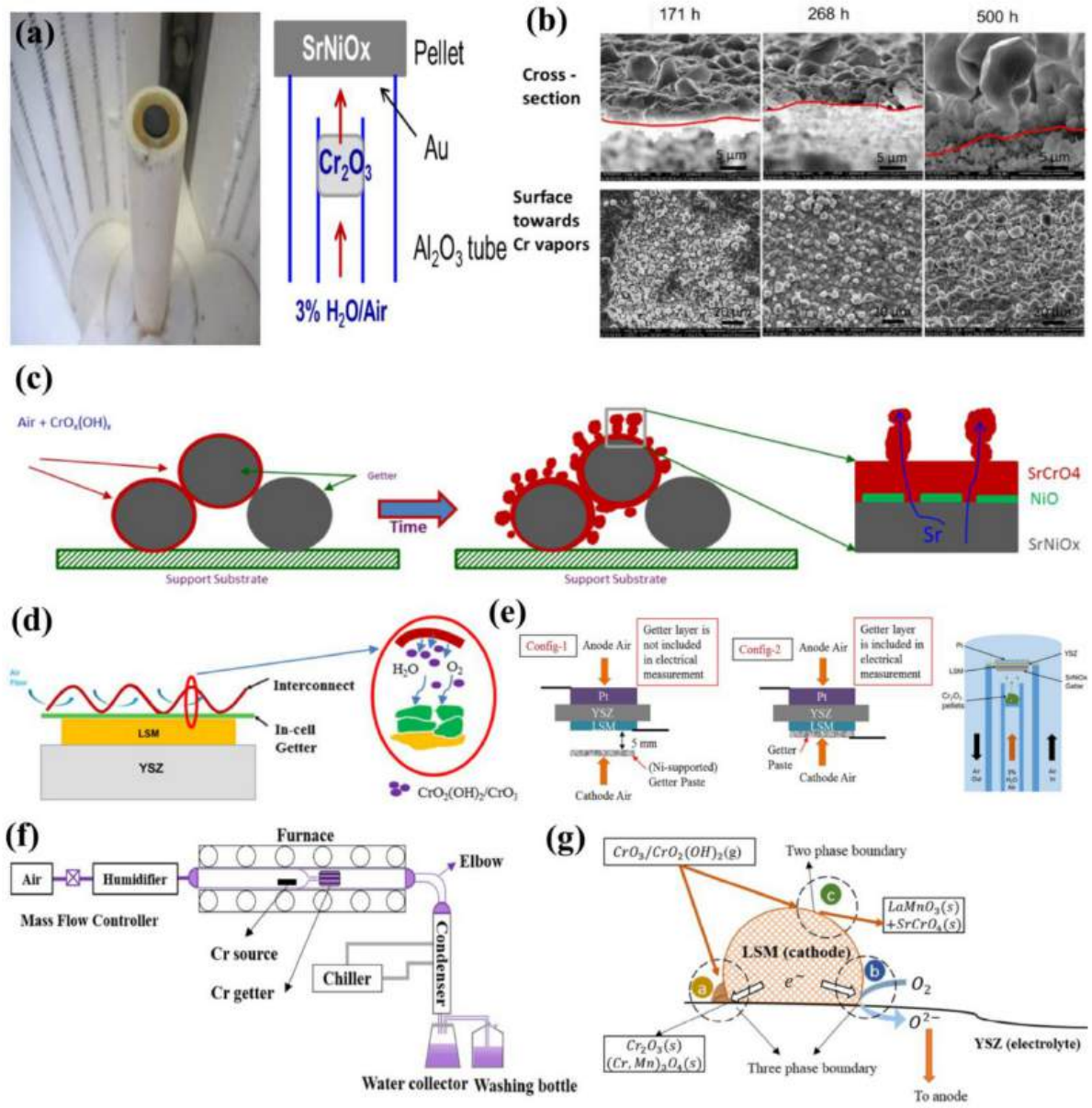

Figure. 11: Experimental setup for Cr diffusion tests, illustrating the placement of the $Sr_xNi_yO_z$ getter pellet and the Cr_2O_3 pellet as the Cr vapor source **(a);** Surface morphology of the getter pellet ($Sr_xNi_yO_z$) after prolonged exposure to Cr vapor **(b);** Schematic illustration of the Cr capture mechanism in the getter **(c)** Reprinted from ref. [138], copyright 2017, with permission from the Electrochemical Society (ECS). Schematic illustration of Cr vapor interaction with the getter layer and fuel cell components **(d);** Two getter configurations: config-1, where the getter is placed 5 mm away from the cathode (spaced-apart), and config-2, where the getter is in direct contact with the cathode **(e)** Reprinted from ref. [139], copyright 2017, with permission from the Electrochemical

Society (ECS).; Schematic of the experimental setup for Cr capture testing using $Sr_9Ni_7O_{21}$ coated cordierite under humidified air at 850°C **(f);** Illustration of Cr poisoning at the TPB **(g)** Reprinted from ref. [142], copyright 2017, with permission from the Electrochemical Society (ECS).

Hong et al. [143] presented an innovative approach to enhancing the stability and performance of Sr-Ni oxide-based Cr getters, particularly SNO, in humid environments where degradation is a common issue. Their study demonstrated that a protective $SrCO_3$ layer, formed through CO_2 treatment, mitigates both moisture-induced degradation and Cr vapor capture challenges. As shown in **Figure. 12(a),** Sr ions in the SNO structure experience significant compressive stress due to short Sr–O bond lengths (2.39–2.89 Å), promoting Sr segregation in humid conditions. **Figure. 12(b)** illustrates how the $SrCO_3$ layer prevents hydration-induced volume expansion and cracking, maintaining the structural integrity of SNO in such environments. Furthermore, **Figure. 12(c)** highlights the $SrCO_3$ layer's Cr-gettering efficiency, as exposure to Cr vapor at 650°C for 500 h led to the formation of a stable $SrCrO_4$ layer, confirmed via raman spectroscopy.

Expanding on this work, Hong et al. [144] developed a novel getter material, strontium manganese oxide ($SrMnO_3$), to capture both Cr and S contaminants. This material addresses the limitations of existing getters in high-temperature, humid conditions through its robust stability and dual functionality. **Figure. 12(d)** shows the SMO getter's 3D honeycomb structure, coated with ~5 μm thick SMO particles, designed for uniform airflow and efficient contaminant absorption. The architecture enhances gettering performance and supports prolonged SOFC operation by maintaining structural stability. Electrochemical tests (**Figure. 12(e)**) shows that SOFC cells equipped with the SMO getter sustained stable current density for 230 h, even when exposed to $CrO_2(OH)_2$ (1 ppb) and SO_2 (4 ppm), in contrast to rapid performance degradation in cells without the getter. This stability is attributed to the reactive Sr and Mn ions in the SMO structure.

Figure. 12(f) details the mechanisms of Cr and S absorption, showing the formation of $SrCrO_4$ nanowhiskers and $SrSO_4$ nanorods on the SMO surface. These reactions are driven by Sr ion diffusion and Mn_2O_9 dimers acting as catalytic sites. The resulting core-shell structure, with Mn-rich oxides at

the core and voids accommodating further reactions, ensures continuous contaminant absorption and prolonged getter effectiveness.

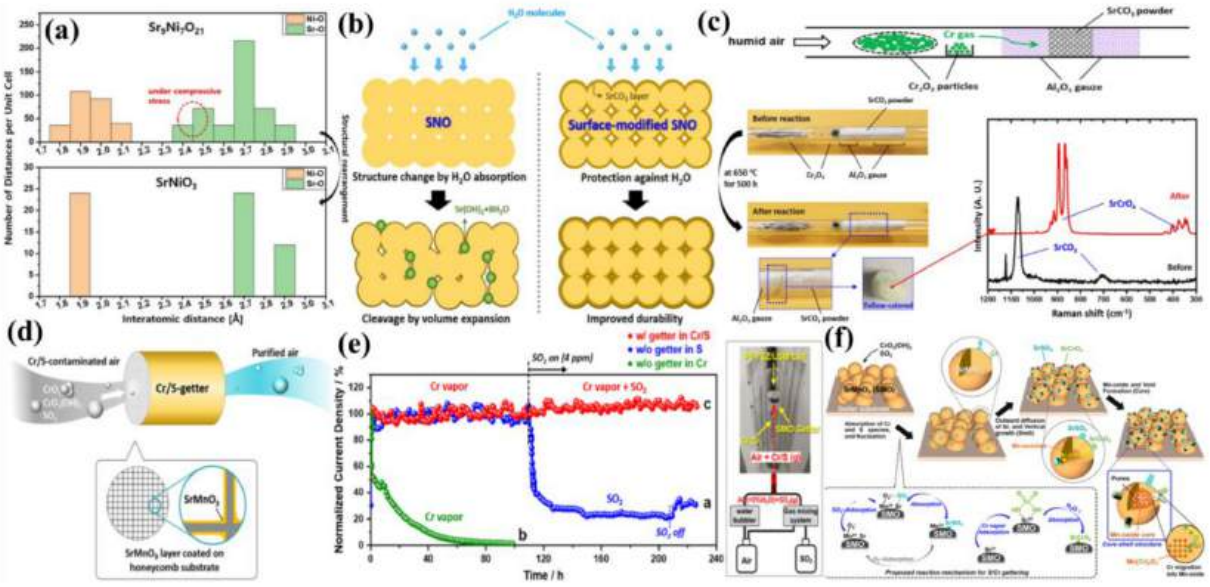

Figure. 12: Compressive stress in SNO **(a);** Protective role of the $SrCO_3$ layer, preventing hydration-induced volume expansion and cracking in SNO, ensuring structural integrity in humid environments **(b);** Cr-gettering capability of $SrCO_3$-coated SNO along with Raman spectroscopy **(c)** This work is licensed under the terms of the Creative Commons Attribution 4.0 License © 2019 by the authors (CC BY, (https://creativecommons.org/licenses/by/4.0/)) [143]; Schematic of the SMO honeycomb getter **(d);** Electrochemical performance comparison showing current density trends for SOFC cells exposed to Cr and S contaminants with and without the SMO getter **(e);** Mechanism of Cr and S absorption by SMO **(f)**, Reprinted from ref. [144], copyright 2019, with permission from the American Chemical Society.

5.3. Chromium-tolerant electrodes

While protective coatings and getters can reduce Cr volatilization, these approaches may not fully eliminate Cr-related degradation especially over prolonged operational periods. Therefore, another critical mitigation strategy is the development of Cr-tolerant electrodes that can maintain electrochemical performance even in Cr-contaminated environments [146].

Among conventional materials, LSCF and LSM have shown some degree of Cr tolerance. LSM, in particular, has long been favored for its chemical and thermal stability, though its limited catalytic activity at intermediate temperatures often necessitates additional modifications. LSCF offers higher catalytic performance but remains susceptible to Cr-induced deactivation, especially through $SrCrO_4$ formation at the electrode surface [147].

To address these limitations, Bang et al. [148] proposed an innovative heterostructured electrode architecture to mitigate Cr degradation. In Sr-doped perovskites, a common degradation pathway involves Sr segregation to the electrode surface, where it reacts with volatile Cr species to form Cr–Sr–O nuclei. These nuclei subsequently evolve into resistive phases such as $SrCrO_4$, which block TPBs, hinder oxygen exchange, and significantly reduce electrochemical performance. They also introduced a design strategy in which a Sr-free outer layer is applied over the Sr-containing perovskite. This heterostructure spatially separates the Sr-rich functional core from the Cr-sensitive surface, allowing the outer layer to serve as a protective barrier. Depending on its composition, the coating either chemically reacts with Cr species to form less detrimental compounds or physically impedes Cr penetration. This dual role effectively preserves the catalytic activity of the inner electrode by preventing Cr-induced degradation at the surface, thereby maintaining long-term stability under Cr-containing conditions.

In recent years, several studies have explored surface modifications and new material compositions to enhance Cr-tolerance in SOFC cathodes. Chen et al. [149] showed improved Cr resistance by coating LSCF electrodes with $PrNi_{0.5}Mn_{0.5}O_3$ and PrO_x catalysts, which maintained performance during prolonged operation. Huang et al. [150] demonstrated that impregnating LSCF with $BaCO_3$ forms a $BaCrO_4$ layer that effectively mitigates Cr poisoning. Additionally, Co-based materials such as $BaCoO_{3-\delta}$ have been reported to offer good Cr tolerance, although they face challenges related to high thermal expansion and cost. These studies indicate the potential of both surface treatments and new compositions to improve electrode durability in Cr-contaminated environments [151-153].

Following this line of innovation, Han et al. [146] introduced a Co-free A-site high-entropy oxide, $La_{0.2}Pr_{0.2}Nd_{0.2}Sm_{0.2}Gd_{0.2}BaFe_2O_{5+\delta}$ (LPNSGBF), to address the cost and thermal expansion issues of Co-based cathodes. The high configurational entropy from multiple rare-earth cations effectively suppressed Sr/Ba segregation and Cr-induced degradation. LPNSGBF achieved an impressive peak power density of 1020.69 $mW \cdot cm^{-2}$ at 800 °C and a low degradation rate of 0.17% h^{-1} over 100 h, significantly outperforming the reference PBF cathode.

5.4. Electrochemical recovery mechanism of Cr-poisoned cathodes

A novel electrochemical cleaning strategy was developed by Zhu et al. [145] to mitigate Cr poisoning in SOFCs, a prevalent degradation phenomenon resulting from the deposition of volatile Cr species on the cathode. By operating the cell in reverse as a SOEC, the direction of oxygen ion transport is reversed, and the air electrode functions as the anode, creating a locally oxidizing environment that promotes redox reactions at the electrode surface. This electrochemical shift enables the conversion of Cr-containing surface deposits into volatile species, which are subsequently removed by the air stream, thus cleansing the electrode surface.

The experimental configuration is illustrated in **Figure. 13(a),** featuring the cell mounted between alumina tubes, equipped with Ag and Ni mesh current collectors, precise gas flow control, and a Cr source positioned near the cathode to induce poisoning. **Figure. 13(b)** shows the surface of a Cr-poisoned cell, featuring dense accumulations of both large faceted (Cr, Mn) spinel particles and finer Cr_2O_3 clusters on the electrolyte. After cleaning, **Figure. 13(c)** shows a significantly reduced presence of Cr_2O_3, while the more stable spinel structures largely persist, indicating selective removal of the more reactive and resistive Cr phases. This partial but meaningful recovery reflects the method's ability to restore some cathodic activity by targeting harmful deposits.

The underlying mechanism of this recovery process aligns closely with findings from Liu et al. [154] where electrochemical operation in SOEC mode was shown to induce transformations in Cr-containing surface phases through electrochemical driving forces rather than changes in gas atmosphere alone. The anodic polarization at the air electrode establishes an oxidizing environment,

but local potential gradients and oxygen ion flux promote redox reactions at the electrode surface, facilitating the conversion of $SrCrO_4$ into $LaCrO_3$. This transformation involves the reduction of Cr^{6+} to Cr^{3+} within the solid phase, driven by interfacial electrochemical reactions. The effectiveness of this electrochemical cleaning was further validated on LSM-based cathodes through repeated poisoning–cleaning cycles, demonstrating that performance losses from Cr_2O_3 deposition could be consistently reversed without damaging the cell microstructure [155-157].

The detailed phase transformation process is schematically presented in **Figure. 13(d)** of Liu et al. [154] which outlines two stages: initial formation of $SrCrO_4$ from the reaction between $CrO_{3(g)}$ and SrO on the electrode surface, followed by its electrochemically driven conversion into $LaCrO_3$ during SOEC operation. This transformation is driven by interfacial electrochemical processes occurring under anodic polarization, rather than by the gas atmosphere alone, and is further supported by **Figure. 13(e),** which displays the SEM cross-section of the button cell used for electrochemical recovery experiments, and **Figure. 13(f),** which shows a notable restoration of peak power density from 0.505 to 0.630 W/cm^2 after recovery, representing a 39% improvement. These findings collectively indicate that SOEC-mode operation not only cleans the surface but also initiates in-situ redox-driven restructuring of the electrode, offering a self-healing mechanism that can partially reverse Cr-related performance losses and extend the operational life of the cell.

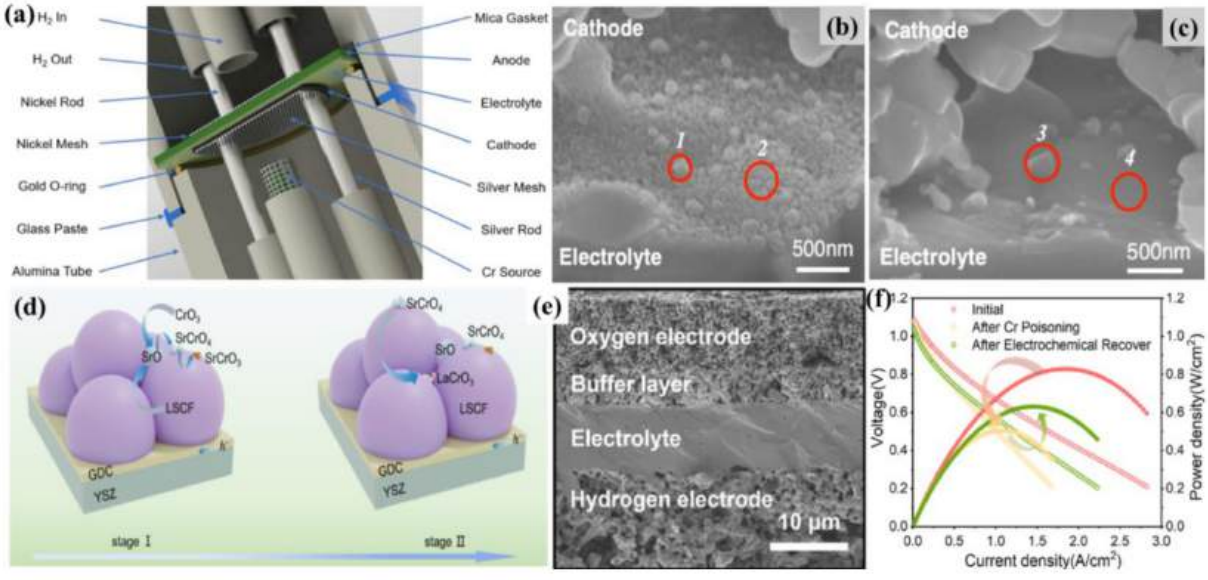

Figure. 13: Schematic of the experimental setup used for electrochemical cleaning **(a);** SEM image of the Cr-poisoned cell **(b);** SEM image of the cell after electrochemical cleaning **(c)** Reprinted from ref. [145], copyright 2020, with permission from Elsevier. Schematic diagram illustrating the two-stage transformation of Cr deposits on the LSCF cathode **(d);** Cross-sectional SEM image of the button cell used in electrochemical recovery tests **(e);** I-V curve of the cell before and after electrochemical recovery **(f)**, Reprinted from ref. [154], copyright 2024, with permission from the American Chemical Society.

6. Cr poisoning in PCCs: limited

Cr poisoning remains a well-known degradation mechanism in SOCs, but in PCCs including PCFCs and PCECs, the phenomenon remains less thoroughly explored yet potentially more severe. The intrinsic presence of water vapor at both electrodes in PCCs exacerbates Cr volatilization, migration, and deposition. This creates a more aggressive environment for Cr interactions, which can disrupt both oxygen evolution (OER) and ORR and compromise proton conduction pathways, ultimately resulting in performance degradation [36]. In PCFCs, Cr-induced surface phases such as $SrCrO_4$ or $BaCrO_4$ block oxygen adsorption sites and impede proton transfer, leading to reduced ORR kinetics and increased interfacial resistance [172].

6.1. Main effect in air Electrode

In PCCs, the air electrode remains the most vulnerable component to Cr poisoning, particularly under humid and high-temperature conditions. The oxidation of commonly used Cr-containing interconnects (e.g., SUS 430, Crofer 22 APU) in the presence of water vapor leads to the release of volatile Cr species such as $CrO_2(OH)_2$. These vapors condense on the cathode surface, forming either Cr_2O_3 or resistive phases like $SrCrO_4$. These deposits deactivate the TPBs, severely limiting oxygen exchange kinetics [158].

Unlike oxygen-ion-conducting SOCs, PCC cathodes experience intensified Cr-related degradation due to the higher humidity in their environment [159,160]. This humidity accelerates Cr volatilization and the formation of resistive secondary phases on cathode surfaces. For example, Sr-

doped perovskites like LSCF, when exposed to humid and CO_2-rich atmospheres around 600 °C, tend to form insulating compounds such as $SrCO_3$, which significantly hinder oxygen activation and surface diffusion processes [161]. Duan et al. [162] further studied the Cr tolerant materials $BaCo_{0.4}Fe_{0.4}Zr_{0.1}Y_{0.1}O_{3-\delta}$ (BCFZY), and observed that switching from pure air to 5% CO_2 under 1.0 $A \cdot cm^{-2}$ resulted in a voltage drop from 0.65 V to 0.58 V at 500°C, though the cell recovered upon returning to pure air.

Similarly, Lim et al. [56] investigated the degradation of a $PrBa_{0.5}Sr_{0.5}Co_{1.5}Fe_{0.5}O_{5+\delta}$ (PBSCF) air electrode under combined Cr- and CO_2-rich conditions. They observed rapid failure within 20 h, driven by the formation of $BaCrO_4$ and $BaCO_3$ at the air electrode–electrolyte interface, along with complete phase decomposition of the electrolyte. While the PBSCF cathode remained relatively stable, the degradation occurred primarily at the interfacial region. Notably, the application of a dense PBSCF protective layer between the air electrode and the electrolyte significantly improved stability, effectively shielding the electrolyte from corrosive species.

These findings collectively highlight the need for air electrode materials in PCCs that are not only resistant to Cr poisoning but also chemically stable in humid and CO_2-laden environments.

6.2. Any effect in Fuel electrode?

While Cr poisoning is predominantly associated with the air electrode due to direct exposure to oxidizing environments, its potential impact on the fuel electrode in PCCs particularly in PCECs cannot be entirely dismissed. In electrolysis mode, both electrodes are exposed to water vapor, which facilitates the formation of volatile chromium species such as $CrO_2(OH)_2$. These species may migrate through the electrolyte and potentially reach the anode side, raising concerns about long-term degradation under steam-rich conditions.

To date, however, there is no direct or systematic evidence confirming Cr-related degradation at the fuel electrode. Most available studies focus on cathode or electrolyte interfaces. For instance, Guo et al. [163] reported that Cr vapor can react with barium-containing electrolytes such as $BaZr_{0.1}Ce_{0.7}Y_{0.1}Yb_{0.1}O_{3-\delta}$ (BZCYYb), forming $BaCrO_4$ deposits that degrade proton conductivity and

disrupt grain structure. Although this interaction occurred at the electrolyte surface, it highlights the possibility of Cr transport across the cell and its interaction with critical internal components. Still, this does not directly confirm Cr accumulation or degradation at the fuel electrode itself.

Although current evidence does not substantiate a direct Cr-related degradation mechanism on the anode side, the possibility remains open especially under electrolysis conditions where steam exposure and Cr volatility are elevated. Therefore, while the primary focus of Cr poisoning research in PCCs rightfully remains on the air electrode, it is worthwhile to acknowledge this potential fuel-side effect. No dedicated studies have yet been conducted to investigate this aspect systematically, but future research could provide valuable insights into the long-term stability of fuel electrodes under Cr-rich and humid environments.

6.3. Effect on electrolyte?

Among the key components PCCs, the electrolyte plays a vital role in determining both ionic transport and overall durability [164,165]. While significant progress has been made in developing high-conductivity protonic ceramics such as $BaZr_{0.1}Ce_{0.7}Y_{0.2}O_{3-\delta}$ (BZCY) [166] and $BaZr_{0.1}Ce_{0.7}Y_{0.2}Yb_{0.2}O_{3-\delta}$ (BZCYYb) [163], their stability in the presence of Cr vapors remains a critical challenge that is still not thoroughly understood. Compared to SOCs, where Cr poisoning has been widely documented, studies focusing on Cr-related degradation in PCC electrolytes are scarce. Zhao et al. [166] addressed this gap by examining the effects of Cr_2O_3 vapor on BZCY electrolyte. In their study, BZCY samples were heat-treated at 600–800 °C in Cr-rich atmospheres, simulating long-term exposure to interconnect-sourced Cr species. Even at 600 °C, Cr began depositing onto the electrolyte surface, forming both physical layers of Cr_2O_3 and chemical compounds like $BaCrO_4$. The latter became dominant at higher temperatures (**Figure. 14(a-d)**). These deposits severely deteriorated the grain structure and disrupted the continuity of the proton conduction network. Proton conductivity measurements showed a sharp decline as Cr content increased, with surface layers effectively acting as insulating barriers that raised the electrolyte's ohmic resistance (**Figure. 14(e)**). These results

confirm that Cr poisoning in PCCs involves more than superficial contamination it also compromises the electrolyte's intrinsic transport and structural integrity.

To further explore these mechanisms under more realistic cell conditions, Guo et al. [163]. conducted a systematic investigation using BZCYYb1711 electrolytes in contact with a Fe–Cr alloy (SUS430) under humidified air, simulating realistic PCC conditions. They found that Cr deposition became progressively worse with increasing temperature. At 400 °C, the surface remained largely intact, but above 500 °C, Cr-containing particles began to form densely, particularly in areas where the alloy directly contacted the electrolyte. By 700 °C, the grain boundaries were almost completely masked by a thick Cr-rich layer, especially under the ribs, where solid-state diffusion dominates over gas-phase transport (**Figure. 14(f, g)**). This process was driven by barium segregation from the electrolyte surface, which reacted with infiltrating Cr vapors to form $BaCrO_4$ and CeO_2 secondary phases causing significant chemical imbalance and microstructural degradation.

Consequently, proton conductivity declined markedly (**Figure. 14(h)**), with reductions of nearly 30% at 700 °C and over 50% at 200 °C compared to pristine samples. Additionally, the activation energy for charge transport increased, indicating impaired proton mobility. The emergence of $BaCrO_4$ and CeO_2 phases (**Figure. 14(i)**) disrupted grain connectivity and introduced local non-stoichiometry, contributing to bulk phase decomposition rather than mere surface contamination. These findings highlight the susceptibility of Ba-rich proton-conducting perovskites like BZCYYb to Cr-induced structural and functional degradation. To maintain long-term performance, strategies such as protective interconnect coatings and designs that minimize Cr exposure are essential.

While this study provides crucial insight into degradation behavior in BZCYYb-based electrolytes, many gaps remain. To date, there has been no comprehensive evaluation of Cr tolerance across various BZCY based electrolytes. Future efforts should prioritize the development of electrolytes with lower Ba volatility, Cr-inert dopants, or integrated protective barrier layers. Advancing these approaches will be key to enhancing the chemical stability and operational longevity of PCCs in Cr-rich environments.

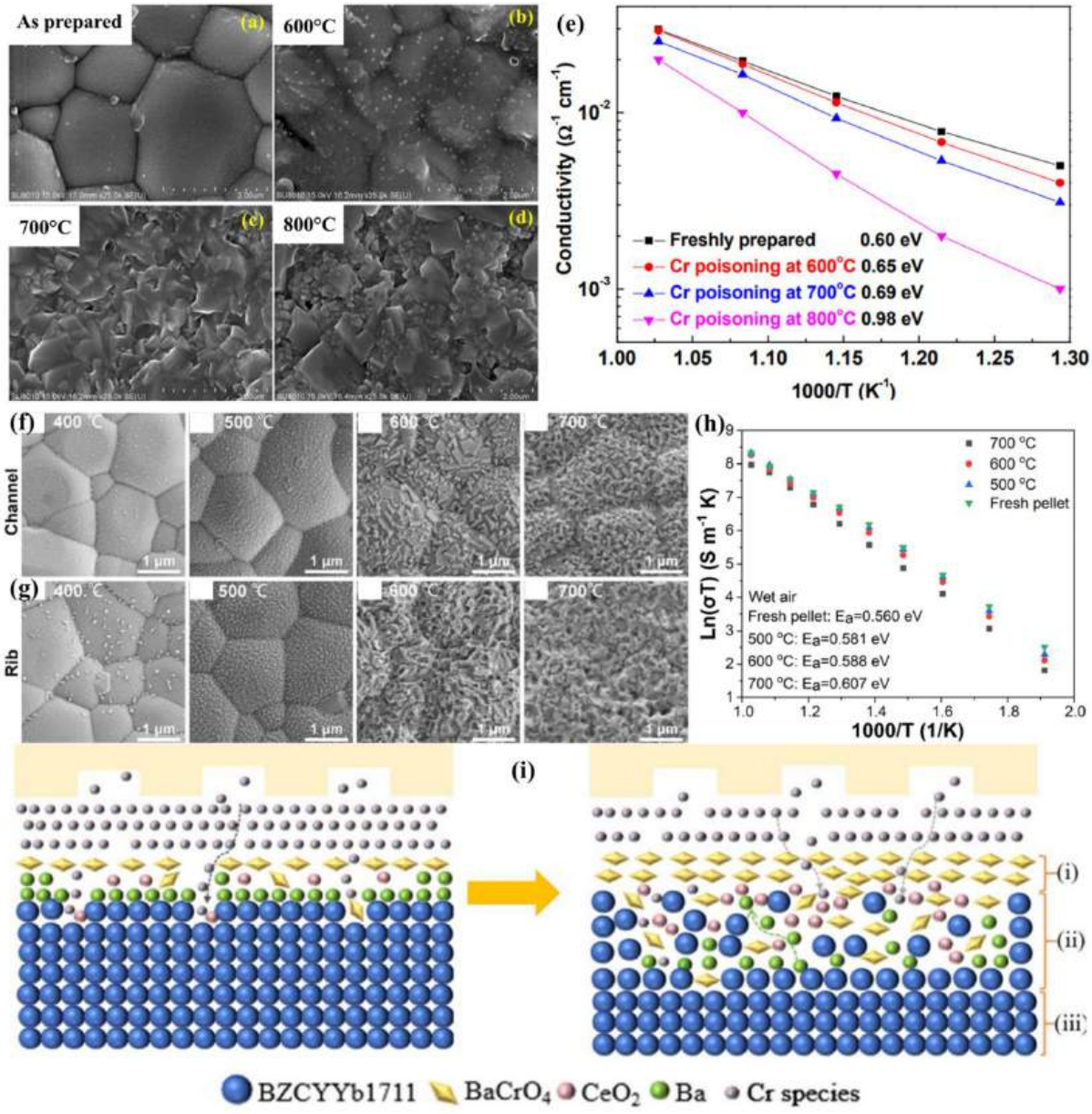

Figure 14: Surface SEM images of BZCY electrolytes before and after exposure to Cr vapor at 600-800°C for 50 h **(a-d)**; Temperature-dependent proton conductivity of BZCY measured in air before and after Cr deposition **(e)** Reprinted from ref. [166], copyright 2014, with permission from Elsevier. Surface morphology of BZCYYb1711 electrolytes after 20 h of exposure to Fe–Cr alloy (SUS430) under humidified air at 400–700 °C, observed beneath the ribs **(f);** and channels **(g)**; Proton conductivity of BZCYYb1711 before and after Cr exposure under various temperatures (200–700 °C) for 50 h **(h);** Schematic representation of the Cr poisoning mechanism in BZCYYb1711**(i),** Reproduced from ref. [163], copyright 2025, with permission from the Royal Society of Chemistry.

7. Mitigation Strategies in PCCs

Given the distinct operating environment of PCCs characterized by the presence of water vapor and proton-conducting electrodes developing effective mitigation strategies is crucial for ensuring long-term stability and commercial viability. This section reviews current mitigation efforts specific to PCCs, explores lessons learned from SOC research, and suggests advanced approaches to further enhance durability.

7.1. What has been done?

In the context of PCCs, recent studies have focused on understanding and mitigating oxidation and Cr poisoning phenomena that critically affect electrode longevity and performance. Wang et al. [167] carried out a comprehensive investigation on the oxidation behavior of common FSS, 430 SS, 441 SS, and Crofer 22 APU under PCEC and PCFC conditions. Their work demonstrated that oxidation rates and scale formation vary significantly depending on the steel type and operating environment. Notably, 430 SS exhibited the highest susceptibility to oxidation, primarily due to the formation of porous Fe_2O_3 layers that compromise protective barrier integrity. Conversely, oxidation was comparatively lower under PCEC conditions, although the long-term implications remain uncertain and require further investigation.

A key outcome of this study was the identification of effective protective coatings that substantially reduced Cr and Fe diffusion while limiting oxide scale growth. Coatings such as Ce-MC, Y_2O_3 (sol-gel), Ce/Co, and Cu-Mn, were applied to the stainless steels, with Cu-Mn and Ce-MC coatings showing superior performance on 441 SS and Crofer 22 APU substrates. These coatings contributed to the formation of stable Cr/Mn spinel phases that act as dense, effective barriers against oxygen and moisture ingress (**Figure 15(a-d)**). However, their effectiveness on 430 SS was limited by scale cracking, indicating that substrate microstructure and coating compatibility must be carefully optimized.

Beyond surface coatings, material doping strategies have emerged as promising routes to enhance CO_2 tolerance and structural stability of cathode materials in PCCs. For instance, Wei et al.

[168] demonstrated that La-doped $Ba_{0.95}La_{0.05}Fe_{0.8}Zr_{0.1}Y_{0.1}O_{3-\delta}$ (BLFZY) remained stable for 100 h in a 3% H_2O/3% CO_2 atmosphere at 600°C, with no secondary phase formation. Similarly, co-doping with Zr and Y in $SrCo_{0.4}Fe_{0.4}Zr_{0.1}Y_{0.1}O_{3-\delta}$ effectively suppressed $SrCO_3$ formation during extended exposure to CO_2 and water vapor, demonstrating the viability of doping to improve electrode durability [169].

Alternative cathode materials free of alkaline-earth elements, such as $PrNi_{0.5}Co_{0.5}O_{3-\delta}$ (PNC), have shown enhanced resistance to CO_2-induced degradation. Despite their promising phase stability, their electrochemical performance can be sensitive to electrolyte choice, as evidenced by increased polarization resistance in combination with certain electrolytes like BZCYYb4411 due to CO_2 adsorption effects [170]. Alkali-free spinel materials, like $Fe_{0.6}Mn_{0.6}Co_{0.6}Ni_{0.6}Cr_{0.6}O_4$, also demonstrate phase stability under harsh CO_2 environments, further broadening the material options for PCC electrodes [171].

These advancements underscore the multifaceted approach currently employed in PCC research, combining surface engineering, material doping, and novel compositions to address the unique challenges posed by the operating environment. However, the presence of proton-conducting electrolytes and continuous water vapor creates complex chemical interactions that differentiate PCCs from conventional SOCs, necessitating tailored strategies.

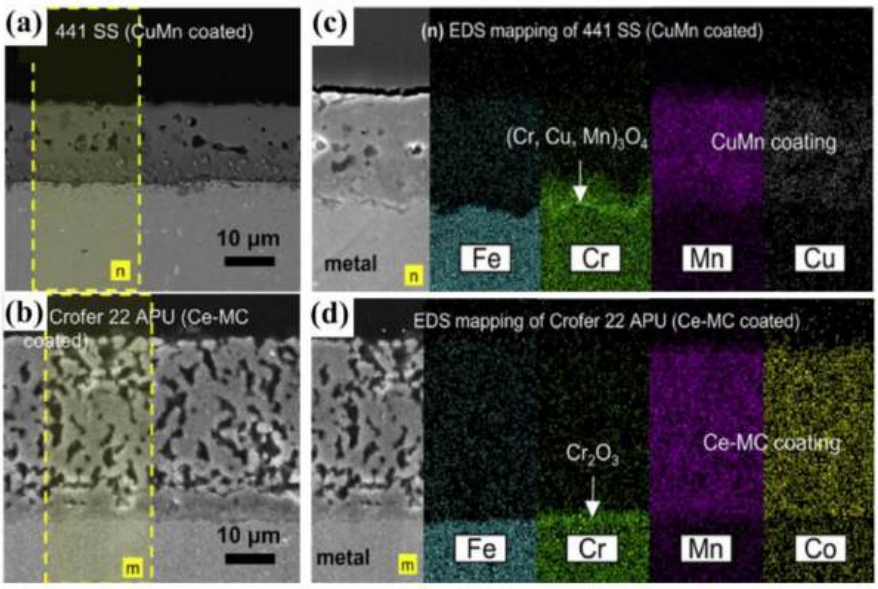

Figure 15: Cross-sectional SEM images **(a, b);** and EDS spectra **(c, d);** of Cu-Mn-coated Crofer 22 APU and Ce-MC-coated 441 SS, illustrating the formation of protective oxide layers, Reprinted from ref. [167], copyright 2019, with permission from Elsevier.

7.2. What we can be applied from SOC?

The extensive research on SOCs offers valuable insights and strategies that can be adapted and applied to PCCs to mitigate Cr poisoning and improve long-term stability. In SOCs, Cr volatilization and its subsequent deposition on cathode surfaces have been identified as major degradation mechanisms, prompting a wide range of preventive approaches that can be adapted for PCCs.

One of the key mitigation strategies developed in SOCs involves the use of Cr-resistant coatings on interconnects and electrodes, such as Mn-Co spinel or perovskite-type oxide layers. These coatings stabilize the Cr_2O_3 scale, minimizing Cr evaporation and subsequent contamination of the cathode. The success of such coatings in SOCs suggests similar approaches could be effective in PCCs, provided the coatings are compatible with the proton-conducting environment and can withstand the presence of water vapor.

Another strategy from SOC research is environmental control specifically, reducing humidity levels in the inlet air streams to limit the formation of volatile chromium oxyhydroxides. Although PCCs inherently operate in humid atmospheres, careful optimization of humidity and gas composition might reduce Cr volatility and prolong electrode life.

Additionally, SOC designs have incorporated interlayers or barrier layers between the interconnect and electrode to physically trap Cr species and prevent their migration to the active electrode sites. This physical separation can significantly reduce Cr poisoning and has proven effective in SOC stacks. Transferring this concept to PCCs would require evaluation of suitable interlayer materials compatible with proton conduction and intermediate -temperature stability.

Furthermore, doping and microstructural engineering strategies developed for SOC cathodes offer valuable guidance. For example, tailored perovskites with enhanced oxygen vacancy concentrations and improved resistance to CO_2 and moisture-induced degradation have proven effective in SOCs.

Such materials, when appropriately modified, may perform well in PCCs by providing both structural integrity and stable electrochemical performance in protonic environments.

These understandings from SOC development present a strong starting point for Cr mitigation in PCCs. However, direct implementation is not straightforward due to fundamental differences in operating conditions. PCCs operate in persistently humid environments and utilize proton-conducting materials such as barium zirconate, which interact differently with volatile Cr species. The long-term chemical stability and interface behavior between Cr species and these protonic materials are not yet fully understood.

Therefore, while the foundational principles of SOC-based strategies, such as protective coatings, environmental control, barrier layer design, and materials engineering are highly relevant, they require careful adaptation and validation within the specific electrochemical and environmental framework of PCCs. Targeted research in this direction is essential to develop robust and commercially viable mitigation approaches tailored to the demands of high-temperature electrolysis systems. The major Cr mitigation strategies developed for SOCs, their implementation, their demonstrated effectiveness, and challenges with applying each to PCC systems are shown in **Table 4**.

Table 4: Summary of mitigation strategies for Cr poisoning in SOCs and their transferability, effectiveness, and future research directions for PCC systems.

Mitigation Strategy	Description in SOCs	Effectiveness and Challenges in SOCs	Status, Applicability and Perspective in PCCs	Required Follow-up research for PCC implementation / optimization
Protective Coatings	Coatings (e.g. $MnCoO_x$, $MnCuO_x$) applied on metallic interconnects and electrodes to prevent Cr poisoning and interdiffusion.	High effectiveness for Cr and Fe suppression; enhances long-term stability. Possible mismatch in CTE; coating degradation under redox cycling.	Not yet widely tested in PCCs but conceptually applicable; lower operating temperature favors stability and effectiveness.	Test adhesion and long-term Cr transport under humid low-T conditions; evaluate chemical compatibility with protonic electrolytes.
Getters / Traps	Use of Mn-, Cu-, or Co-based getters to absorb volatile Cr species from interconnects.	Proven in SOCs; reduces Cr contamination but limited by finite capacity and replacement frequency.	Transferable to PCCs with expected higher efficiency due to lower Cr volatility.	Study getter regeneration and long-term trapping capacity under protonic and humid environments.
Electrode Doping	Tailored electrode design through compositional doping and microstructural optimization (particle size, porosity, and connectivity) to enhance oxygen vacancy concentration, maximize TPB area, improve gas diffusion, and suppress Sr segregation.	Highly effective in SOCs for enhancing oxygen reduction/evolution kinetics, improving long-term stability, and reducing SrO segregation. However, dopant volatility, trade-offs between conductivity and stability, and microstructural coarsening under redox and thermal cycling remain challenges.	Directly applicable to PCCs; lower operation temperature mitigates sintering but introduces new degradation from Ba or Ni migration in humid atmospheres. Doping can stabilize perovskite phases and improve tolerance to steam-induced surface reactions.	Develop processing techniques yielding stable doped Ni–BCZY or perovskite networks under humid H_2/H_2O atmospheres. Identify dopants that maintain electronic conductivity and suppress Ba/Ni migration; quantify how porosity and dopant concentration affect conductivity and durability.

Electrolyte Doping	Doping minimizes interdiffusion and chemical reactions that could otherwise promote Cr accumulation at the TPB.	Established approach in SOCs; improves redox stability and suppresses interdiffusion. Defect association, grain-boundary blocking, and phase instability can limit long-term performance	Already standard in PCCs; enhances proton conductivity and stability versus CO_2/H_2O.	Optimize dopant solubility limits and grain-boundary chemistry under steam electrolysis conditions.
Barrier layer	Thin dense layers (e.g., GDC, LSF) inserted between electrode and electrolyte to block Cr and Sr interdiffusion and enhance adhesion.	Highly effective in reducing Cr diffusion and reaction at the oxygen electrode/electrolyte interface. Interlayer delamination, added ohmic resistance, and microcrack formation under cycling can compromise durability.	Conceptually transferable; beneficial to prevent Ba or Ni migration in PCCs but must avoid proton-blocking effects.	Develop scalable thin-film fabrication routes compatible with protonic ceramics; evaluate thermal expansion and proton blocking effects.
Interface Engineering	Microstructural or compositional optimization (e.g., infiltration, graded composition) to reduce interfacial resistance and chemical instability.	Proven to improve electrochemical performance and durability in SOCs. Requires careful control of interfacial composition.	Directly applicable to PCCs; similar degradation mechanisms observed.	Adapt infiltration and gradient techniques for PCC electrodes; model long-term interfacial evolution under humidity.
Electrochemical Recovery	Application of controlled voltage/current pulses to regenerate electrode surfaces,	Allows partial recovery of electrochemical performance without full cell replacement. Requires precise control to avoid	Conceptually applicable to PCCs; proton conduction may support local redox recovery.	Determine safe operating potential/current limits for PCC materials; study transient redox

	remove contaminants (e.g., Cr, S), or reoxidize reduced phases	further degradation; effectiveness depends on degradation origin.		mechanisms under humid conditions.
Environmental Control	Gas purification and control of humidity or contaminants; protects oxygen electrode and electrolyte.	Effective in SOCs to reduce S, Si, and Cr poisoning; limited use for humidity control at oxygen side. Adds system complexity and operational cost; not effective for intrinsic degradation mechanisms.	Cannot fully applied in PCC due to the co-existence of steam and air, however, it can be used for degradation mechanism beyond Cr poisoning	Develop gas management and inlet humidity optimization strategies; assess effect on Ba-based phase stability.

7.3. Beyond e.g. electrolyte coating to avoid Cr diffusion

Going beyond established approaches, emerging strategies focus on innovative barrier layers and electrolyte modifications to prevent Cr diffusion and improve PCC durability. One promising direction is the application of protective coatings directly on the electrolyte or electrode-electrolyte interface to block Cr migration pathways. Such coatings, possibly based on dense oxide layers or spinel-type materials, can serve as physical and chemical barriers, limiting Cr transport from interconnects and steels to the reactive electrode surfaces.

Electrolyte coatings designed to be chemically compatible with proton conductors, such as barium zirconate-based electrolytes, could be engineered to resist Cr adsorption and incorporation. This approach not only prevents Cr poisoning but may also reduce the formation of secondary insulating phases that degrade electrode performance.

Moreover, composite or graded interlayers combining materials with high Cr affinity and stable proton conductivity could be developed to capture Cr species before they reach the electrode active sites, effectively serving as Cr traps. Such design enhancements would require careful control of microstructure and interfaces to maintain ionic conductivity while providing robust chemical protection.

In addition to physical coatings, novel materials with intrinsic Cr resistance and CO_2 tolerance, including alkali-free spinels and tailored perovskites, offer alternative pathways. Their integration into cell architectures either as electrode components or protective layers could provide synergistic benefits.

Finally, advanced environmental and operational strategies, such as optimizing gas compositions to minimize volatile Cr species formation and employing dynamic control of operating parameters, may complement material innovations. Combining multiple mitigation strategies, material design, coatings, interlayers, and environmental control will likely be necessary to overcome the complex degradation mechanisms in PCCs.

8. Perspectives

While substantial progress has been made in mitigating Cr-induced degradation in oxygen-ion-conducting SOCs, the transition to proton-conducting environments introduces new challenges. PCECs, operating under high water vapor partial pressures on both electrodes, are particularly vulnerable to Cr-related degradation due to enhanced volatilization of Cr species such as $CrO_2(OH)_2$. Moreover, proton-conducting materials are not only susceptible to surface poisoning but also bulk degradation through the formation of insulating compounds like $BaCrO_4$. These interactions can obstruct proton conduction pathways, destabilize the electrode microstructure, and accelerate performance decay.

A key challenge in advancing PCC technology lies in adapting mitigation strategies originally developed for SOCs to accommodate the unique chemical and electrochemical environment of protonic systems. Material doping and microstructural engineering proven effective in stabilizing SOC cathodes must be re-engineered for compatibility with humidified, alkaline earth-rich compositions. Similarly, while getter materials have demonstrated efficacy in intercepting volatile Cr species in SOFC and SOEC modes, heir application in PCCs demands chemical formulations and architectures with high thermal and chemical stability under dual-sided humidification.

Future efforts should focus on designing Cr-resistant proton-conducting materials, optimizing getter compositions, and developing robust coatings that maintain structural integrity under steam-rich, high-temperature conditions. Advanced modeling and in situ diagnostics can provide mechanistic insight into Cr transport and capture, guiding the rational design of protective strategies. Moreover, emerging electrochemical cleaning techniques such as reversal to SOEC mode for partial regeneration require deeper investigation to validate their applicability in proton-conducting systems without compromising long-term structural stability.

The synergistic degradation from Cr, H_2O, and CO_2 remains a significant hurdle. As PCECs are increasingly considered for grid-scale hydrogen production and other energy conversion applications, ensuring durability under practical operating environments is essential. Translating knowledge from

SOC development and adapting it to meet the chemical and operational challenges of PCECs will be crucial for enabling the transition from laboratory-scale prototypes to commercially viable systems.

9. Summary and Conclusions

This review summarized the current understanding of Cr poisoning in solid oxide electrochemical devices, focusing primarily on SOCs and their evolving counterpart, PCCs. The extensive work on SOCs has identified key mechanisms by which Cr volatilizes from interconnect materials and deposits on oxygen electrodes, causing degradation through the formation of insulating secondary phases. Numerous mitigation strategies in SOCs have been developed, including protective coatings on interconnects, environmental controls, and the use of Cr getters approaches that have proven effective in limiting Cr-induced degradation and extending device lifetimes.

Building upon this established SOC foundation, this review critically examined how these strategies might be adapted and implemented in PCC systems, which operate under more complex and chemically aggressive environments. These conditions present unique challenges that require tailored mitigation solutions. We highlighted recent advances in Cr-resistant materials, optimized getter compositions, and compatible interlayers specifically designed to function under high steam partial pressures, which are characteristic of PCC operation.

Importantly, this review bridges the knowledge gap between SOC and PCC research by providing insights into how well-established SOC mitigation strategies can inform next-generation PCC development. The understanding of Cr transport, interaction pathways, and mitigation mechanisms gained in SOC studies provides a valuable platform for accelerating progress in the PCC field. By adapting SOC-derived materials and strategies to the unique PCC electrochemical and thermal conditions, the field is poised to overcome the degradation pathways currently limiting PCC deployment.

Figure 16(a, b) presents a comparative overview of the critical short-term and long-term challenges associated with various Cr mitigation strategies in solid oxide cells. It also highlights the potential for translating these approaches to PCCs. Strategies including Cr-resistant coatings, humidity

control, and barrier interlayers for Cr capture are assessed for their effectiveness and limitations. This visual summary underscores the importance of transferring and modifying existing knowledge to accommodate the operational demands of emerging proton-conducting devices.

Furthermore, we emphasized the need for ongoing and integrated research targeting materials with intrinsic Cr resistance, as well as the development of stack-level strategies that address mechanical, thermal, and chemical stability simultaneously. The review advocates for a systems-level, multidisciplinary approach that merges material innovation with stack and operational engineering. This review consolidates the critical advancements made in understanding and mitigating Cr poisoning in SOCs and provides a roadmap for translating those insights into the PCC domain. By leveraging proven strategies from SOC research and refining them for PCC application, we offer a framework to guide the next generation of proton ceramic electrochemical devices toward improved durability, efficiency, and commercial viability. This work thus serves as both a synthesis of existing knowledge and a forward-looking perspective to inspire innovation in solid-state energy technologies.

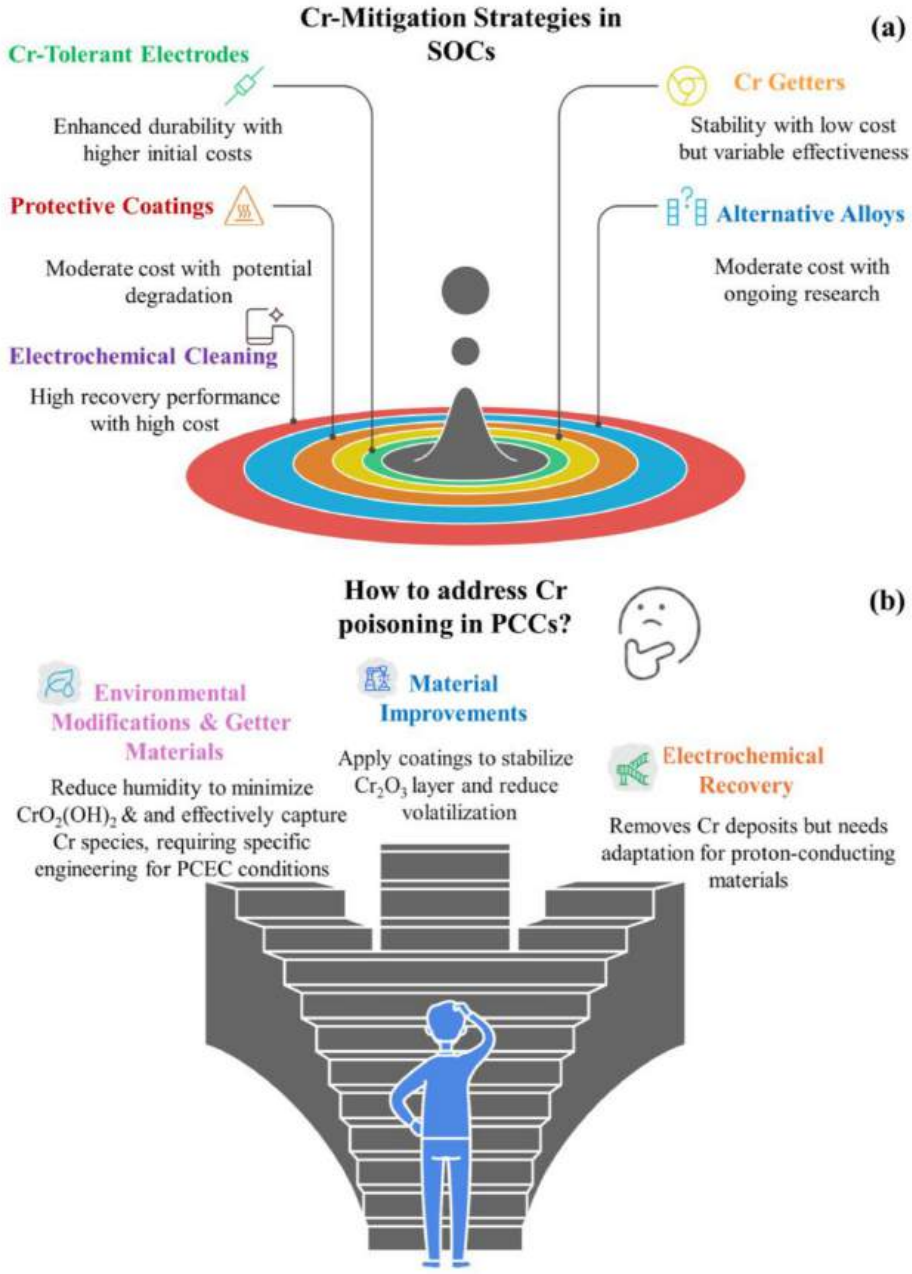

Figure 16: Comparative assessment of key short-term and long-term challenges associated with various Cr mitigation strategies in solid oxide cells **(a);** Strategies to mitigate Cr poisoning in PCCs **(b).**

Author contributions

Both authors contributed to the conception and structure of the review. MH conducted the literature analysis and drafted the manuscript. MNT provided critical revisions and supervision, funding acquisition. Both authors approved the final version of the manuscript.

Conflicts of interest

There are no conflicts to declare.

Data availability

This review is based on previously published data, which are cited throughout the manuscript. No new data were generated.

Acknowledgements

The authors are grateful for the financial support from the HyPRO project funded from GroenvermogenNL, under grant agreement NGF.1695.1695.012.

References

1 Lahrichi, A.; El Issmaeli, Y.; Kalanur, S. S.; Pollet, B. G. Advancements, Strategies, and Prospects of Solid Oxide Electrolysis Cells (SOECs): Towards Enhanced Performance and Large-Scale Sustainable Hydrogen Production. *J. Energy Chem.* **2024,** *94,* 688–715.

2 Hauch, A.; Küngas, R.; Blennow, P.; Hansen, A. B.; Hansen, J. B.; Mathiesen, B. V.; Mogensen, M. B. Recent Advances in Solid Oxide Cell Technology for Electrolysis. *Science* **2020,** *370* (6513), 6118.

3 Ur Rehman, H. S.; Coppola, N.; Singh, A.; Polverino, P.; Carapella, G.; Montinaro, D.; Maritato, L. Gadolinium-Doped Ceria Room-Temperature Sputtered Thin Barrier Layers in Large-Area Solid Oxide Fuel Cells: Influence of Their Thickness and Thickness Gradient on the Cathodic Processes. *ACS Appl. Energy Mater.* **2025,** *8* (7), 4281–4287.

4 Gulraiz, A.; Al Bastaki, A. J.; Magamal, K.; Subhi, M.; Hammad, A.; Allanjawi, A.; Said, Z. Energy Advancements and Integration Strategies in Hydrogen and Battery Storage for Renewable Energy Systems. *iScience* **2025,** *28* (3)

5 Li, T.; Wang, T.; Shi, C.; Chang, S.; Zhang, M.; Zhao, Y.; Dong, D. Efficient Reduction of Low-Concentration NO via Dendritically Channeled Solid Oxide Cells. *ACS Appl. Energy Mater.* **2021,** *4* (7), 6968–6974.

6 Ma, Q.; Balaguer, M.; Pérez-Coll, D.; de Haart, L. G.; Serra, J. M.; Mather, G. C.; Guillon, O. Characterization and Optimization of $La_{0.97}Ni_{0.5}Co_{0.5}O_{3-\delta}$-Based Air-Electrodes for Solid Oxide Cells. *ACS Appl. Energy Mater.* **2018,** *1* (6), 2784–2792.

7 Qiu, P.; Li, C.; Liu, B.; Yan, D.; Li, J.; Jia, L. Materials of Solid Oxide Electrolysis Cells for H_2O and CO_2 Electrolysis: A Review. *J. Adv. Ceram.* **2023,** *12* (8), 1463–1510.

8 Neagu, D.; Irvine, J. T.; Wang, J.; Yildiz, B.; Opitz, A. K.; Fleig, J.; Liu, G. Roadmap on Exsolution for Energy Applications. *J. Phys. Energy* **2023,** *5* (3), 031501.

9 Dossow, M.; Steinrücken, B.; Schmid, M.; Rosenfeld, D. C.; Fendt, S.; Kerscher, F.; Spliethoff, H. Technical Evaluation and Life-Cycle Assessment of Solid Oxide Co-Electrolysis Integration in Biomass-to-Liquid Processes for Sustainable Aviation Fuel Production. *Appl. Therm. Eng.* **2025,** *260,* 124882.

10 Medvedev, D. Trends in Research and Development of Protonic Ceramic Electrolysis Cells. *Int. J. Hydrogen Energy* **2019,** *44* (49), 26711–26740.

11 Wang, Y.; Ling, Y.; Wang, B.; Zhai, G.; Yang, G.; Shao, Z.; Li, T. A Review of Progress in Proton Ceramic Electrochemical Cells: Material and Structural Design, Coupled with Value-Added Chemical Production. *Energy Environ. Sci.* **2023,** *16* (12), 5721–5770.

12 Liu, F.; Diercks, D.; Kumar, P.; Seong, A.; Jabbar, M. H. A.; Gumeci, C.; Duan, C. Redesigning Protonic Ceramic Electrochemical Cells to Lower the Operating Temperature. *Sci. Adv.* **2025,** *11* (2), 2507.

13 Wang, J.; Chen, W.; Wang, Y.; Wei, J.; Zhang, W.; Sun, C.; Peng, S. Recent Advances in Proton-Conducting Solid Oxide Electrolysis Cells. *Mater. Sci. Eng., B* **2025,** *317,* 118188.

14 Walther, D. C.; Ahn, J. Advances and Challenges in the Development of Power-Generation Systems at Small Scales. *Prog. Energy Combust. Sci.* **2011,** *37* (5), 583–610.

15 Rogdakis, K.; Karakostas, N.; Kymakis, E. Up-Scalable Emerging Energy Conversion Technologies Enabled by 2D Materials: From Miniature Power Harvesters towards Grid-Connected Energy Systems. *Energy Environ. Sci.* **2021,** *14* (6), 3352–3392.

16 Zhu, Z.; Sugimoto, M.; Pal, U.; Gopalan, S.; Basu, S. Electrochemical Cleaning: An In-Situ Method to Reverse Chromium Poisoning in Solid Oxide Fuel Cell Cathodes. *J. Power Sources* **2020,** *471,* 228474.

17 Kornely, M.; Neumann, A.; Menzler, N. H.; Weber, A.; Ivers-Tiffée, E. Degradation of Solid Oxide Fuel Cell Performance by Cr-Poisoning. *ECS Trans.* **2011,** *35* (1), 2009.

18 Wolf, S. E.; Winterhalder, F. E.; Vibhu, V.; de Haart, L. B.; Guillon, O.; Eichel, R. A.; Menzler, N. H. Solid Oxide Electrolysis Cells–Current Material Development and Industrial Application. *J. Mater. Chem. A* **2023,** *11* (34), 17977–18028.

19 He, S.; Zou, Y.; Chen, K.; Jiang, S. P. A Critical Review of Key Materials and Issues in Solid Oxide Cells. *Interdiscip. Mater.* **2023,** *2* (1), 111–136.

20 Tan, K. H.; Rahman, H. A.; Taib, H. Coating Layer and Influence of Transition Metal for Ferritic Stainless Steel Interconnector Solid Oxide Fuel Cell: A Review. *Int. J. Hydrogen Energy* **2019,** *44* (58), 30591–30605.

21 Zhang, Y.; Yu, Z.; Tao, Y.; Lu, J.; Liu, Y.; Shao, J. Insight into the Electrochemical Processes of the Titanate Electrode with In Situ Ni Exsolution for Solid Oxide Cells. *ACS Appl. Energy Mater.* **2019,** *2* (6), 4033–4044.

22 Mao, J.; Wang, E.; Wang, H.; Ouyang, M.; Chen, Y.; Hu, H.; Liu, Y. Progress in Metal Corrosion Mechanism and Protective Coating Technology for Interconnect and Metal Support of Solid Oxide Cells. *Renew. Sust. Energy Rev.* **2023,** *185,* 113597.

23 Qiu, P.; Lin, J.; Lei, L.; Yuan, Z.; Jia, L.; Li, J.; Chen, F. Evaluation of Cr-Tolerance of the $Sr_2Fe_{1.5}Mo_{0.5}O_{6-\delta}$ Cathode for Solid Oxide Fuel Cells. *ACS Appl. Energy Mater.* **2019,** *2* (10), 7619–7627.

24 Jeong, H.; Roehrens, D.; Bram, M. Facile Route for Reactive Coating of $LaCrO_3$ on High-Chromium Steels as Protective Layer for Solid Oxide Fuel Cell Applications. *Mater. Lett.* **2020,** *258,* 126794.

25 Qiu, P.; Yang, X.; Zou, L.; Zhu, T.; Yuan, Z.; Jia, L.; Chen, F. $LaCrO_3$-Coated $La_{0.6}Sr_{0.4}Co_{0.2}Fe_{0.8}O_{3-\delta}$ Core–Shell Structured Cathode with Enhanced Cr Tolerance for Intermediate-Temperature Solid Oxide Fuel Cells. *ACS Appl. Mater. Interfaces* **2020,** *12* (26), 29133–29142.

26 Hong, J.; Aphale, A. N.; Heo, S. J.; Hu, B.; Reisert, M.; Belko, S.; Singh, P. Strontium Manganese Oxide Getter for Capturing Airborne Cr and S Contaminants in High-Temperature Electrochemical Systems. *ACS Appl. Mater. Interfaces* **2019,** *11* (38), 34878–34888.

27 Sugimoto, M. Chromium Poisoning Mitigation in Solid Oxide Fuel Cell Air Electrodes: Mechanisms for Cr Deposition and Removal. Ph.D. Dissertation, Boston University, Boston, MA, **2022**.

28 Liang, Q. New Gravitational Interactions in Cosmology From Effective Field Theory to Observation. Ph.D. Dissertation, University of Pennsylvania, Philadelphia, PA, **2023**.

29 Chen, S. Making Sense of the Doctoral Dissertation Defense: A Student-Experience-Based Perspective. In *Doctoral Education: Research-Based Strategies for Doctoral Students, Supervisors and Administrators*; Springer Netherlands: Dordrecht, **2011**; pp 97–114.

30 Fergus, J. W. Effect of Cathode and Electrolyte Transport Properties on Chromium Poisoning in Solid Oxide Fuel Cells. *Int. J. Hydrogen Energy* **2007**, *32* (16), 3664–3671.

31 Chen, X. Chromium deposition and poisoning of cathodes of solid oxide fuel cells–a review. *Int. J. Hydrogen Energy* **2014**, *39* (1), 505-531.

32 Harrison, C. A Study of Lanthanum Nickelate Cathodes for Employment in Solid Oxide Fuel Cells. Ph.D. Dissertation, University of Birmingham, Birmingham, UK, **2023**.

33 Barrio-Querol, E.; Almar, L.; Catalán-Martínez, D.; Leonard, K.; Serra, J. M.; Escolástico, S. Redox-Stable Electrodes for Ethane Dehydrogenation Based on Proton Ceramic Electrochemical Reactors. *ACS Appl. Energy Mater.* **2025,** *8* (7), 4345–4354.

34 Liu, H.; Yu, M.; Tong, X.; Wang, Q.; Chen, M. High Temperature Solid Oxide Electrolysis for Green Hydrogen Production. *Chem. Rev.* **2024,** *124* (18), 10509–10576.

35 Chasta, G.; Himanshu; Dhaka, M. S. A Review on Materials, Advantages, and Challenges in Thin Film Based Solid Oxide Fuel Cells. *Int. J. Energy Res.* **2022,** *46* (11), 14627–14658.

36 Wu, J.; Zhang, J.; Xiao, C. Focus on Factors Affecting pH, Flow of Cr and Transformation between Cr(VI) and Cr(III) in the Soil with Different Electrolytes. *Electrochim. Acta* **2016,** *211,* 652–662.

37 Wang, R.; Würth, M.; Pal, U. B.; Gopalan, S.; Basu, S. N. Roles of Humidity and Cathodic Current in Chromium Poisoning of Sr-Doped $LaMnO_3$-Based Cathodes in Solid Oxide Fuel Cells. *J. Power Sources* **2017,** *360,* 87–97.

38 Chen, X. Chromium Deposition and Poisoning of Cathodes of Solid Oxide Fuel Cells–A Review. *Int. J. Hydrogen Energy* **2014,** *39* (1), 505–531.

39 Schuler, J. A.; Yokokawa, H.; Calderone, C. F.; Jeangros, Q.; Wuillemin, Z.; Hessler-Wyser, A. Combined Cr and S Poisoning in Solid Oxide Fuel Cell Cathodes. *J. Power Sources* **2012,** *201,* 112–120.

40 Sugimoto, M.; Zhu, Z.; Gopalan, S.; Basu, S.; Pal, U. B. Chromium Poisoning Mitigation Strategy in Strontium-Doped Lanthanum Manganite-Based Air Electrodes in Solid Oxide Fuel Cells. *J. Electrochem. Energy Convers. Storage* **2024,** *21* (1), 011003.

41 Chen, K.; Jiang, S. P. Surface Segregation in Solid Oxide Cell Oxygen Electrodes: Phenomena, Mitigation Strategies and Electrochemical Properties. *Electrochem. Energy Rev.* **2020,** *3* (4), 730–765.

42 Hayes, J. The Performance of Mn-Co Spinel Cathode-Side Contact Layer and Interconnect Coating for Solid Oxide Fuel Cell Application. M.S. Thesis, Tennessee Technological University, Cookeville, TN, 2021.

43 Yang, C.; Gan, Y.; Lee, M.; Ren, C.; Xue, X. Electrochemical Kinetic Properties and Stability of A-Site Cation-Deficient Perovskite $Ba_{1-x}Co_{0.6}Fe_{0.2}Zr_{0.1}Y_{0.1}O_{3-\delta}$ (x = 0, 0.05) as

Cathode Materials for Low-Temperature SOFCs. *ACS Appl. Energy Mater.* **2025,** *8* (2), 1154–1166.

44 Salari, H.; Zare, A.; Babaei, A.; Abdoli, H.; Aslannejad, H. Elucidating the Role of $La_2NiO_{4\pm\delta}$ (LNO) Nanoparticles in Modulating Chromium Poisoning in LSM Air Electrodes of Solid Oxide Cells: A Study on Oxygen Reduction and Evolution Reactions. *J. Power Sources* **2024,** *594,* 234001.

45 Zvonareva, I. A.; Mineev, A. M.; Tarasova, N. A.; Fu, X. Z.; Medvedev, D. A. High-Temperature Transport Properties of $BaSn_{1-x}Sc_xO_{3-\delta}$ Ceramic Materials as Promising Electrolytes for Protonic Ceramic Fuel Cells. *J. Adv. Ceram.* **2022,** *11* (7), 1131–1143.

46 Liu, F.; Ding, D.; Duan, C. Protonic Ceramic Electrochemical Cells for Synthesizing Sustainable Chemicals and Fuels. *Adv. Sci.* **2023,** *10* (8), 2206478.

47 Chen, X.; Tan, Y.; Li, Z.; Liu, T.; Song, Y.; Zhai, S.; Ni, M. Advanced Air Electrodes for Reversible Protonic Ceramic Electrochemical Cells: A Comprehensive Review. *Adv. Mater.* **2025,** 2418620.

48 Hu, Q.; Tian, C.; Bao, D.; Zhong, H.; Zhang, X. Protonic Ceramic Electrochemical Cells: Opportunities and Challenges for Ammonia Synthesis. *Next Energy* **2024**, *4*, 100144.

49 Wang, Y.; Ling, Y.; Wang, B.; Zhai, G.; Yang, G.; Shao, Z.; Li, T. A Review of Progress in Proton Ceramic Electrochemical Cells: Material and Structural Design, Coupled with Value-Added Chemical Production. *Energy Environ. Sci.* **2023,** *16* (12), 5721–5770.

50 Unal, F. A.; Mat, M. D.; Demir, I.; Kaplan, Y.; Veziroglu, N. Application of a Coating Mixture for Solid Oxide Fuel Cell Interconnects. *Int. J. Hydrogen Energy* **2015,** *40* (24), 7689–7693.

51 Minh, N. Q. Solid Oxide Fuel Cell Technology—Features and Applications. *Solid State Ionics* **2004,** *174* (1–4), 271–277.

52 Wolf, S. E., Winterhalder, F. E., Vibhu, V., de Haart, L. B., Guillon, O., Eichel, R. A., & Menzler, N. H. Solid oxide electrolysis cells–current material development and industrial application. *J. Mater. Chem. A*, **2023,** *11* (34), 17977-18028.

53 Wu, J.; Liu, X. Recent Development of SOFC Metallic Interconnect. *J. Mater. Sci. Technol.* **2010,** *26* (4), 293–305.

54 Yeh, A. C.; Chen, Y. M.; Liu, C. K.; Shong, W. J. Development of an Advanced Bond Coat for Solid Oxide Fuel Cell Interconnector Applications. *J. Power Sources* **2015,** *296,* 426–432.

55 Zhu, H.; Li, J.; Zhang, J. Recent Advances in Spinel-Based Protective Coatings on Metallic Interconnects for Solid Oxide Fuel Cells from the Perspective of Coating Design. *Int. J. Hydrogen Energy* **2025,** *113,* 26–38.

56 Lim, Y.; Chong, J. H.; Guha, P.; Lee, W. J.; Cho, I.; Oh, S. H.; Yang, S. Failure of Protonic Ceramic Fuel Cells (PCFCs) under Gaseous Cr and CO_2 Exposure and the Introduction of a Protective Barrier Layer for Mitigation. *J. Mater. Chem. A* **2025,** *13* (23), 17709–17719.

57 Yang, Z. Recent Advances in Metallic Interconnects for Solid Oxide Fuel Cells. *Int. Mater. Rev.* **2008,** *53* (1), 39–54.

58 Liu, Z.; Zhang, L.; Zheng, C. J.; Zhang, Y.; Chen, B.; Shao, Z.; Ge, J. Advanced Electrode Materials for Efficient Hydrogen Production in Protonic Ceramic Electrolysis Cells. *Adv. Mater.* **2025,** 2503609.

59 Ekhlasiosgouei, O.; Bik, M.; Smeacetto, F.; Jasinski, P.; Molin, S. Electrophoretic Deposition of Novel Hybrid $MnCo_2O_4$: $Mn_{1.7}CuFe_{0.3}O_4$ Spinel Protective Coating on Stainless-Steel Metallic Interconnects for SOFCs Application. *Int. J. Hydrogen Energy* **2025,** *158,* 150569.

60 Fontana, S.; Amendola, R.; Chevalier, S.; Piccardo, P.; Caboche, G.; Viviani, M.; Sennour, M. Metallic Interconnects for SOFC: Characterisation of Corrosion Resistance and

Conductivity Evaluation at Operating Temperature of Differently Coated Alloys. *J. Power Sources* **2007,** *171* (2), 652–662.

61 Bongiorno, V.; Spotorno, R.; Paravidino, D.; Piccardo, P. On the High-Temperature Oxidation and Area Specific Resistance of New Commercial Ferritic Stainless Steels. *Metals* **2021,** *11* (3), 405.

62 Long, Q.; Sha, R.; Wang, R.; Xu, B.; Men, H.; Wang, Q.; Hou, J. Research Progress of Composite Cathode Materials for Solid Oxide Fuel Cells. *Prog. Nat. Sci.: Mater. Int.* **2023,** *33* (3), 267–278.

63 Yang, Z. Recent Advances in Metallic Interconnects for Solid Oxide Fuel Cells. *Int. Mater. Rev.* **2008,** *53* (1), 39–54.

64 Chamberland, B. L. The Chemical and Physical Properties of CrO_2 and Tetravalent Chromium Oxide Derivatives. *Crit. Rev. Solid State Mater. Sci.* **1977,** *7* (1), 1–31.

65 Chertihin, G. V.; Bare, W. D.; Andrews, L. Reactions of Laser-Ablated Chromium Atoms with Dioxygen. Infrared Spectra of CrO, OCrO, CrOO, CrO_3, $Cr(OO)_2$, Cr_2O_2, Cr_2O_3, and Cr_2O_4 in Solid Argon. *J. Chem. Phys.* **1997,** *107* (8), 2798–2806.

66 Opila, E. J.; Myers, D. L.; Jacobson, N. S.; Nielsen, I. M.; Johnson, D. F.; Olminsky, J. K.; Allendorf, M. D. Theoretical and Experimental Investigation of the Thermochemistry of $CrO_2(OH)_2$(g). *J. Phys. Chem. A* **2007,** *111* (10), 1971–1980.

67 Young, D. J.; Pint, B. A. Chromium Volatilization Rates from Cr_2O_3 Scales into Flowing Gases Containing Water Vapor. *Oxid. Met.* **2006**, *66* (3), 137–153.

68 Key, C.; Eziashi, J.; Froitzheim, J.; Amendola, R.; Smith, R.; Gannon, P. Methods to Quantify Reactive Chromium Vaporization from Solid Oxide Fuel Cell Interconnects. *J. Electrochem. Soc.* **2014**, *161* (9), C373–C379.

69 Tian, Y.; Wang, W.; Liu, Y.; Zhang, L.; Jia, L.; Yang, J.; Li, J. Cobalt-Free Perovskite Oxide $La_{0.6}Sr_{0.4}Fe_{0.8}Ni_{0.2}O_{3-\delta}$ as Active and Robust Oxygen Electrode for Reversible Solid Oxide Cells. *ACS Appl. Energy Mater.* **2019**, *2* (5), 3297–3305.

70 Peng, C.; Mabaleha, S. S.; Kwong, P.; Zheng, Y.; Xu, X. Recent Advances in Perovskite Air Electrode Materials for Protonic Solid Oxide Electrochemical Cells. *Energy Environ. Sci.* **2025**, *18*, 4555–4595.

71 Dang, X.; Lu, Y.; Fan, Z.; Jiang, Y.; Gao, Z. Strategies to Mitigate Sr Segregation of the LSCF Oxygen Electrode for Solid Oxide Cells. *J. Mater. Chem. A* **2025**, *13* (26), 20268–20288.

72 Sohal, M. S.; O'Brien, J. E.; Stoots, C. M.; Sharma, V. I.; Yildiz, B.; Virkar, A. Degradation Issues in Solid Oxide Cells During High-Temperature Electrolysis. *J. Fuel Cell Sci. Technol.* **2012**, *9* (1), 011017

73 Sirvent, J.; Kreka, K.; Sha, Z.; Fearn, S.; González-Rosillo, J. C.; Liedke, M. O.; Tarancón, A. Blocking Sr-Segregation in Perovskite Cathodes for Solid Oxide Cells by Mn Co doping. *ACS Appl. Energy Mater.* **2025**, *8* (4), 12345–12356.

74 Wei, B., Chen, K., Zhao, L., Lü, Z., & Jiang, S. P. Chromium deposition and poisoning at $La_{0.6}Sr_{0.4}Co_{0.2}Fe_{0.8}O_{3-\delta}$ oxygen electrodes of solid oxide electrolysis cells. *Phys. Chem. Chem. Phys.*, 2015, *17* (3), 1601-1609.

75 Schrödl, N.; Egger, A.; Lammer, J.; Hofer, F.; Sitte, W. Long-Term Stability of $Pr_2NiO_{4+\delta}$ Air Electrodes for Solid Oxide Cells against Chromium Poisoning. *J. Electrochem. Soc.* **2021**, *168* (1), 014509.

76 Jiang, S. P. Development of Lanthanum Strontium Manganite Perovskite Cathode Materials of Solid Oxide Fuel Cells: A Review. *J. Mater. Sci.* **2008**, *43* (21), 6799–6833.

77 Wu, T.; Yu, B.; Zhang, W.; Chen, J.; Zhao, S. Fabrication of a High-Performance Nano-Structured $Ln_{1-x}Sr_xMO_{3-\delta}$ (Ln = La, Sm; M = Mn, Co, Fe) SOC Electrode through Infiltration. *RSC Adv.* **2016**, *6* (72), 68379–68387.

78 Wu, L.; Jiang, Z.; Wang, S.; Xia, C. (La, Sr)MnO_3–(Y, Bi)$_2O_3$ Composite Cathodes for Intermediate-Temperature Solid Oxide Fuel Cells. *Int. J. Hydrogen Energy* **2013**, *38* (5), 2398–2406.

79 Gong, Y. Chromium Poisoning in Cathodes of Solid Oxide Fuel Cells: The Role of Current Density, Humidity, and Cathode Composition, and Strategies for Mitigation. Doctoral Dissertation, Boston University, Boston, MA, **2018**.

80 Gomez-Vidal, J. C.; Fernandez, A. G.; Tirawat, R.; Turchi, C.; Huddleston, W. Corrosion Resistance of Alumina-Forming Alloys against Molten Chlorides for Energy Production. I: Pre-Oxidation Treatment and Isothermal Corrosion Tests. *Sol. Energy Mater. Sol. Cells* **2017**, *166*, 222–233.

81 Badwal, S. P. S., Deller, R., Foger, K., Ramprakash, Y., & Zhang, J. P. Interaction between chromia forming alloy interconnects and air electrode of solid oxide fuel cells. *Solid State Ionics*, 1997, *99*(3-4), 297-310.

82 Konysheva, E.; Penkalla, H.; Wessel, E.; Mertens, J.; Seeling, U.; Singheiser, L.; Hilpert, K. Chromium Poisoning of Perovskite Cathodes by the ODS Alloy $Cr_5Fe_1Y_2O_3$ and the High Chromium Ferritic Steel Crofer 22 APU. *J. Electrochem. Soc.* **2006**, *153* (4), A765–A772.

83 Jin, T.; Lu, K. Chromium Deposition and Interfacial Interactions of an Electrolyte–Air Electrode–Interconnect Tri-Layer for Solid Oxide Fuel Cells. *J. Power Sources* **2012**, *202*, 143–148.

84 Wang, C. C.; Becker, T.; Chen, K.; Zhao, L.; Wei, B.; Jiang, S. P. Effect of Temperature on the Chromium Deposition and Poisoning of $La_{0.6}Sr_{0.4}Co_{0.2}Fe_{0.8}O_{3-\delta}$ Cathodes of Solid Oxide Fuel Cells. *Electrochim. Acta* **2014**, *139*, 173–179.

85 Zhen, Y. D.; Zhang, S.; Tan, V. Interaction between Metallic Interconnect and Constituent Oxides of (La, Sr)MnO_3 Coating of Solid Oxide Fuel Cells. *J. Eur. Ceram. Soc.* **2006**, *26* (15), 3253–3264.

86 Taniguchi, S.; Kadowaki, M.; Kawamura, H.; Yasuo, T.; Akiyama, Y.; Miyake, Y.; Saitoh, T. Degradation Phenomena in the Cathode of a Solid Oxide Fuel Cell with an Alloy Separator. *J. Power Sources* **1995**, *55* (1), 73–79.

87 Krumpelt, M.; Cruse, T. A.; Ingram, B. J.; Routbort, J. L.; Wang, S.; Salvador, P. A.; Chen, G. The Effect of Chromium Oxyhydroxide on Solid Oxide Fuel Cells. *J. Electrochem. Soc.* **2009**, *157* (2), B228–B234.

88 Chen, X.; Zhen, Y.; Li, J.; Jiang, S. P. Chromium Deposition and Poisoning in Dry and Humidified Air at $(La_{0.8}Sr_{0.2})_{0.9}MnO_{3+\delta}$ Cathodes of Solid Oxide Fuel Cells. *Int. J. Hydrogen Energy* **2010**, *35* (6), 2477–2485.

89 Horita, T.; Cho, D. H.; Wang, F.; Shimonosono, T.; Kishimoto, H.; Yamaji, K.; Yokokawa, H. Correlation between Degradation of Cathode Performance and Chromium Concentration in (La, Sr)MnO_3 Cathode. *Solid State Ionics* **2012**, *225*, 151–156.

90 Li, J.; Yan, D.; Pu, J.; Chi, B.; Jian, L. The Investigation of Cr Deposition and Poisoning Effect on Sr-Doped Lanthanum Manganite Cathode Induced by Cathodic Polarization for Intermediate Temperature Solid Oxide Fuel Cell. *Electrochim. Acta* **2017**, *255*, 31–40.

91 Paulson, S. C.; Birss, V. I. Chromium Poisoning of LSM-YSZ SOFC Cathodes: I. Detailed Study of the Distribution of Chromium Species at a Porous, Single-Phase Cathode. *J. Electrochem. Soc.* **2004**, *151* (11), A1961–A1970.

92 Jiang, S. P.; Zhang, J. P.; Apateanu, L.; Foger, K. Deposition of Chromium Species at Sr-Doped $LaMnO_3$ Electrodes in Solid Oxide Fuel Cells. I. Mechanism and Kinetics. *J. Electrochem. Soc.* **2000**, *147* (11), 4013–4020.

93 Jiang, S. P.; Zhang, J. P.; Foger, K. Deposition of Chromium Species at Sr-Doped $LaMnO_3$ Electrodes in Solid Oxide Fuel Cells: III. Effect of Air Flow. *J. Electrochem. Soc.* **2001**, *148* (7), C447–C454.

94 Xiong, C., Li, W., Duan, N., Pu, J., Chi, B., & Jian, L. The effect of molybdenum on chromium deposition at $(La_{0.8}Sr_{0.2})_{0.95}MnO_{3-\delta}$ cathode of solid oxide fuel cells. *Int. J. Hydrogen Energy, 2016, 41*(22), 9529-9537.

95 Chen, K.; Hyodo, J.; Dodd, A.; Ai, N.; Ishihara, T.; Jian, L.; Jiang, S. P. Chromium Deposition and Poisoning of $La_{0.8}Sr_{0.2}MnO_3$ Oxygen Electrodes of Solid Oxide Electrolysis Cells. *Faraday Discuss.* **2015**, *182*, 457–476.

96 Schrödl, N.; Egger, A.; Gspan, C.; Höschen, T.; Hofer, F.; Sitte, W. Phase Decomposition of $La_2NiO_{4+\delta}$ under Cr- and Si-Poisoning Conditions. *Solid State Ionics* **2018**, *322*, 44–53

97 Salari, H.; Zare, A.; Babaei, A.; Abdoli, H.; Aslannejad, H. Elucidating the Role of $La_2NiO_{4+\delta}$ (LNO) Nanoparticles in Modulating Chromium Poisoning in LSM Air Electrodes of Solid Oxide Cells: A Study on Oxygen Reduction and Evolution Reactions. *J. Power Sources* **2024**, *594*, 234001.

98 Zhang, S., & Zhen, Y. D. Deposition of Cr species at (La, Sr)(Co, Fe) O_3 cathodes of solid oxide fuel cells. *J. Electrochemist. Soc.,* 2005, *153* (1), A127.

99 Jiang, S. P. Solid-state electrochemistry and solid oxide fuel cells: status and future prospects. *Electrochem. Energy Rev.* **2022**, 5 (Suppl 1), 21.

100 Huang, J.; Liu, Q.; Zhao, L.; Ai, N.; Wang, X.; Shao, Y.; Chen, K. Promotional Role of $BaCO_3$ on the Chromium-Tolerance of $La_{0.6}Sr_{0.4}Co_{0.2}Fe_{0.8}O_{3-\delta}$ Cathodes of Solid Oxide Fuel Cells. *Appl. Catal., B* **2023**, *321*, 122080.

101 Huang, J.; Liang, F.; Zhao, S.; Zhao, L.; Ai, N.; Jiang, S. P.; Chen, K. Heterogeneous Catalyst Coating for Boosting the Activity and Chromium Tolerance of Cathodes for Solid Oxide Fuel Cells. *Adv. Funct. Mater.* **2024**, *34* (26), 2310402.

102 Pei, K.; Zhou, Y.; Xu, K.; He, Z.; Chen, Y.; Zhang, W.; Chen, Y. Enhanced Cr-Tolerance of an SOFC Cathode by an Efficient Electro-Catalyst Coating. *Nano Energy* **2020**, *72*, 104704.

103 Niu, Y.; Zhou, Y.; Lv, W.; Chen, Y.; Zhang, Y.; Zhang, W.; Liu, M. Enhancing Oxygen Reduction Activity and Cr Tolerance of Solid Oxide Fuel Cell Cathodes by a Multiphase Catalyst Coating. *Adv. Funct. Mater.* **2021**, *31* (19), 2100034.

104 Wang, Z.; Zhao, S.; Guo, X.; Li, J.; Hu, Q.; Feng, Y.; Sun, H. Inhibition of Chromium Poisoning in $La_{0.6}Sr_{0.4}Co_{0.2}Fe_{0.8}O_{3-\delta}$ Cathode via Simple Electroless Silver Plating for Solid Oxide Fuel Cells. *Int. J. Hydrogen Energy* **2022**, *47* (21), 11250–11260.

105 Chen, Y.; Yoo, S.; Li, X.; Ding, D.; Pei, K.; Chen, D.; Liu, M. An Effective Strategy to Enhancing Tolerance to Contaminants Poisoning of Solid Oxide Fuel Cell Cathodes. *Nano Energy* **2018**, *47*, 474–480.

106 Chen, D.; Mewafy, B.; Paloukis, F.; Zhong, L.; Papaefthimiou, V.; Dintzer, T.; Zafeiratos, S. Revising the Role of Chromium on the Surface of Perovskite Electrodes: Poison or Promoter for the Solid Oxide Electrolysis Cell Performance? *J. Catal.* **2020**, *381*, 520–529.

107 Yuan, M.; Gao, Y.; Liu, L.; Gao, J.; Wang, Z.; Li, Y.; Wei, B. High Entropy Double Perovskite Cathodes with Enhanced Activity and Operational Stability for Solid Oxide Fuel Cells. *J. Eur. Ceram. Soc.* **2024**, *44* (5), 3267–3276.

108 Wei, B., Schroeder, M., & Martin, M. Surface cation segregation and chromium deposition on the double-perovskite oxide $PrBaCo_2O_{5+\delta}$. *ACS Appl. Mater. Interfaces, 2018, 10*(10), 8621-8629.

109 Li, J.; Li, J.; Yan, D.; Pu, J.; Chi, B.; Jian, L. Promoted Cr-Poisoning Tolerance of $La_2NiO_{4+\delta}$-Coated $PrBa_{0.5}Sr_{0.5}Co_{1.5}Fe_{0.5}O_{5+\delta}$ Cathode for Intermediate-Temperature Solid Oxide Fuel Cells. *Electrochim. Acta* **2018**, *270*, 294–301.

110 Shi, H., Qu, J., Tan, W., & Zhu, Y. Chemical Stability Challenges and Mechanistic Insights of SOFC Cathodes. *Energy & Fuels,* **2025**, 39(36), 17177-17191.

111 Peng, C.; Mabaleha, S. S.; Kwong, P.; Zheng, Y.; Xu, X. Recent Advances in Perovskite Air Electrode Materials for Protonic Solid Oxide Electrochemical Cells. *Energy Environ. Sci.* **2025**, *18*, 4555–4595

112 Guo, M.; Li, Z.; Tang, L.; Li, J.; Wang, Z.; Wang, B.; Yue, Z. Chromium Deposition and Poisoning of the Proton-Conducting $BaZr_{0.1}Ce_{0.7}Y_{0.1}Yb_{0.1}O_{3-\delta}$ Electrolyte of Protonic Ceramic Cells. *J. Mater. Chem. A* **2025**, *13*, 1234–1245.

113 Shaigan, N.; Qu, W.; Ivey, D. G.; Chen, W. A Review of Recent Progress in Coatings, Surface Modifications and Alloy Developments for Solid Oxide Fuel Cell Ferritic Stainless Steel Interconnects. *J. Power Sources* **2010**, *195* (6), 1529–1542.

114 Chen, K.; Ai, N.; O'Donnell, K. M.; Jiang, S. P. Highly Chromium Contaminant Tolerant BaO Infiltrated $La_{0.6}Sr_{0.4}Co_{0.2}Fe_{0.8}O_{3-\delta}$ Cathodes for Solid Oxide Fuel Cells. *Phys. Chem. Chem. Phys.* **2015**, *17* (7), 4870–4874.

115 Wei, B., Chen, K., Wang, C. C., Lü, Z., & Jiang, S. P. Cr deposition on porous $La_{0.6}Sr_{0.4}Co_{0.2}Fe_{0.8}O_{3-\delta}$ electrodes of solid oxide cells under open circuit condition. *Solid State Ionics*, 2015, *281*, 29-37.

116 Ni, N.; Wang, C. C.; Skinner, S. J. Synergistic Effects of Temperature and Polarization on Cr Poisoning of $La_{0.6}Sr_{0.4}Co_{0.2}Fe_{0.8}O_{3-\delta}$ Solid Oxide Fuel Cell Cathodes. *J. Mater. Chem. A* **2019**, *7* (15), 9253–9262.

117 Zhen, Y.; Jiang, S. P. Characterization and Performance of (La, Ba)(Co, Fe)O_3 Cathode for Solid Oxide Fuel Cells with Iron–Chromium Metallic Interconnect. *J. Power Sources* **2008**, *180* (2), 695–703.

118 Li, Z.; Guan, B.; Xia, F.; Nie, J.; Li, W.; Ma, L.; Liu, X. High-Entropy Perovskite as a High-Performing Chromium-Tolerant Cathode for Solid Oxide Fuel Cells. *ACS Appl. Mater. Interfaces* **2022**, *14* (21), 24363–24373.

119 Xiong, C.; Qiu, P.; Zhang, W.; Pu, J. Influence of Practical Operating Temperature on the Cr Poisoning for LSCF-GDC Cathode. *Ceram. Int.* **2022**, *48* (22), 33999–34004.

120 da Conceição, L.; Dessemond, L.; Djurado, E.; Souza, M. M. Thin Films of $La_{0.7}Sr_{0.3}MnO_{3-\delta}$ Dip-Coated on Fe–Cr Alloys for SOFC Metallic Interconnect. *Int. J. Hydrogen Energy* **2013**, *38* (35), 15335–15347.

121 Hassan, M. H., Rehman, S. U., Batool, S. Y., Song, R. H., Lim, T. H., Hong, J. E., ... & Lee, S. B. Nanoengineering of a Commercial-Scale Cathode Undergoing Highly Active Oxygen Dissociation via a Synergistic Effect of $Sm_{0.5}Sr_{0.5}CoO_3/Ce_{0.8}Sm_{0.2}O_2$ Composite Catalyst

Infiltration for High-Performance Solid Oxide Fuel Cells. *ACS Appl. Energy Mater.* **2024**, 7 (19) 8622-8634.

122 Zhu, J. H.; Ghezel-Ayagh, H. Cathode-Side Electrical Contact and Contact Materials for Solid Oxide Fuel Cell Stacking: A Review. *Int. J. Hydrogen Energy* **2017**, *42* (38), 24278–24300.

123 Richter, J.; Holtappels, P.; Graule, T.; Nakamura, T.; Gauckler, L. J. Materials Design for Perovskite SOFC Cathodes. *Monatsh. Chem.* **2009**, *140* (9), 985–999.

124 Rembelski, D.; Viricelle, J. P.; Combemale, L.; Rieu, M. Characterization and Comparison of Different Cathode Materials for SC-SOFC: LSM, BSCF, SSC, and LSCF. *Fuel Cells* **2012**, *12* (2), 256–264.

125 Shen, F.; Lu, K. Perovskite-Type $La_{0.6}Sr_{0.4}Co_{0.2}Fe_{0.8}O_{3-\delta}$, $Ba_{0.5}Sr_{0.5}Co_{0.2}Fe_{0.8}O_3$, and $Sm_{0.5}Sr_{0.5}Co_{0.2}Fe_{0.8}O_3$ Cathode Materials and Their Chromium Poisoning for Solid Oxide Fuel Cells. *Electrochim. Acta* **2016**, *211*, 445–452.

126 Agun, L.; Rahman, H. A.; Ahmad, S.; Muchtar, A. Durability and Stability of LSCF Composite Cathode for Intermediate-Low Temperature Solid Oxide Fuel Cells (IT-LT SOFC): Short Review. *Adv. Mater. Res.* **2014**, *893*, 732–737.

127 Mah, J. C.; Muchtar, A.; Somalu, M. R.; Ghazali, M. J. Metallic Interconnects for Solid Oxide Fuel Cells: A Review on Protective Coating and Deposition Techniques. *Int. J. Hydrogen Energy* **2017**, *42* (14), 9219–9229.

128 Duan, N.; Gao, M.; Hua, B.; Li, M.; Chi, B.; Li, J.; Luo, J. L. Exploring $Ni(Mn_{1/3}Cr_{2/3})_2O_4$ Spinel-Based Electrodes for Solid Oxide Cells. *J. Mater. Chem. A* **2020**, *8* (7), 3988–3998.

129 Mao, J.; Wang, E.; Dang, H. Magnetron Sputtered Bilayer Composite $(Mn, Co)_3O_4$ Coating to Improve Oxidation Resistance and Suppress Elements Diffusion for Interconnects of Solid Oxide Fuel Cell. *Appl. Surf. Sci.* **2025**, *691*, 162660.

130 Mao, J.; Wang, E.; Dang, H.; Ouyang, M.; Hu, H.; Wang, H.; Ren, D. Reactive Magnetron Sputtered $(Mn, Co)_3O_4$ Spinel Coatings for Superior Element Diffusion Suppression and

Conductivity in Ferritic Stainless-Steel Interconnects of Solid Oxide Fuel Cells. *Surf. Coat. Technol.* **2025**, *498*, 131829.

131 Molin, S.; Sabato, A. G.; Bindi, M.; Leone, P.; Cempura, G.; Salvo, M.; Smeacetto, F. Microstructural and Electrical Characterization of Mn-Co Spinel Protective Coatings for Solid Oxide Cell Interconnects. *J. Eur. Ceram. Soc.* **2017**, *37* (15), 4781–4791.

132 Ranjbar-Nouri, Z., Soltanieh, M., & Rastegari, S. Applying the protective $CuMn_2O_4$ spinel coating on AISI-430 ferritic stainless steel used as solid oxide fuel cell interconnects. *Surf. Coat. Technol.* **2018**, *334*, 365-372.

133 Zhu, Z.; Darl-Uzu, C.; Pal, U.; Gopalan, S.; Hussain, A. M.; Dale, N.; Basu, S. Comparison of Cu–Mn and Mn–Co Spinel Coatings for Solid Oxide Fuel Cell Interconnects. *Int. J. Hydrogen Energy* **2022**, *47* (87), 36953–36963.

134 Joshi, S.; Petric, A. Nickel Substituted $CuMn_2O_4$ Spinel Coatings for Solid Oxide Fuel Cell Interconnects. *Int. J. Hydrogen Energy* **2017**, *42* (8), 5584–5589.

135 Wang, J.; Pei, Z.; Zhou, N. Rational Design of Nanostructured Porous and Advanced Getter Materials for Vacuum Insulation Panels. *Nanomaterials* **2025**, *15* (7), 532.

136 Dai, M.; Li, F.; Fang, S.; He, D.; Lu, J.; Zhang, Y.; Luo, Y. Advances in Nanostructured Electrodes for Solid Oxide Cells by Infiltration or Exsolution. *Materials* **2025**, *18* (8), 1802.

137 Heo, S. J.; Hong, J.; Aphale, A.; Hu, B.; Singh, P. Chromium Poisoning of $La_{1-x}Sr_xMnO_{3\pm\delta}$ Cathodes and Electrochemical Validation of Chromium Getters in Intermediate-Temperature Solid Oxide Fuel Cells. *J. Electrochem. Soc.* **2019**, *166* (13), F990–F998.

138 Uddin, M. A., Banas, C. J., Liang, C., Pasaogullari, U., Recknagle, K. P., Koeppel, B. J., & Singh, P. Design and optimization of chromium getter for SOFC systems through computational modeling. *ECS Trans.* **2017**, *78* (1), 1063.

139 Uddin, M. A.; Aphale, A.; Hu, B.; Heo, S. J.; Pasaogullari, U.; Singh, P. Electrochemical Validation of In-Cell Chromium Getters to Mitigate Chromium Poisoning in SOFC Stack. *J. Electrochem. Soc.* **2017**, *164* (13), F1342–F1350.

140 Aphale, A.; Uddin, M. A.; Hu, B.; Heo, S. J.; Hong, J.; Singh, P. Synthesis and Stability of $Sr_xNi_yO_z$ Chromium Getter for Solid Oxide Fuel Cells. *J. Electrochem. Soc.* **2018**, *165* (9), F635–F643.

141 Chou, Y. S., Choi, J. P., Stevenson, J. W., Liang, C., Hu, B., Rodriguez, W., & Singh, P. Performance and microstructure of a novel Cr-getter material with LSCF-based cells in a generic stack test fixture. *ECS Trans.* **2017**, *78* (1), 1047.

142 Liang, C., Hu, B., Aphale, A., Venkataraman, M., Mahapatra, M. K., & Singh, P. Mitigation of chromium assisted degradation of LSM cathode in SOFC. *ECS Trans.* 2017, *75*(28), 57.

143 Hong, J.; Heo, S. J.; Aphale, A. N.; Hu, B.; Singh, P. H_2O Absorption Assisted Sr-Segregation in Strontium Nickel Oxide Based Chromium Getter and Encapsulation with $SrCO_3$. *J. Electrochem. Soc.* **2019**, *166* (2), F59–F66.

144 Hong, J.; Aphale, A. N.; Heo, S. J.; Hu, B.; Reisert, M.; Belko, S.; Singh, P. Strontium Manganese Oxide Getter for Capturing Airborne Cr and S Contaminants in High-Temperature Electrochemical Systems. *ACS Appl. Mater. Interfaces* **2019**, *11* (38), 34878–34888.

145 Zhu, Z.; Sugimoto, M.; Pal, U.; Gopalan, S.; Basu, S. Electrochemical Cleaning: An In-Situ Method to Reverse Chromium Poisoning in Solid Oxide Fuel Cell Cathodes. *J. Power Sources* **2020**, *471*, 228474.

146 Han, X.; Ling, Y.; Yang, Y.; Wu, Y.; Gao, Y.; Wei, B.; Lv, Z. Utilizing High Entropy Effects for Developing Chromium-Tolerance Cobalt-Free Cathode for Solid Oxide Fuel Cells. *Adv. Funct. Mater.* **2023**, *33* (43), 2304728.

147 Develos-Bagarinao, K.; Ishiyama, T.; Kishimoto, H.; Shimada, H.; Yamaji, K. Nanoengineering of Cathode Layers for Solid Oxide Fuel Cells to Achieve Superior Power Densities. *Nat. Commun.* **2021**, *12* (1), 3979.

148 Bang, S.; Lee, J.; Kim, J. G.; Kim, J.; Choi, M.; Chen, Y.; Lee, W. Heterostructured Electrodes for Cr-Tolerant Solid Oxide Fuel Cells. *J. Mater. Chem. A* **2024**, *12* (36), 24103–24113.

149 Chen, Y.; Yoo, S.; Pei, K.; Chen, D.; Zhang, L.; deGlee, B.; Liu, M. An In Situ Formed, Dual-Phase Cathode with a Highly Active Catalyst Coating for Protonic Ceramic Fuel Cells. *Adv. Funct. Mater.* **2018**, *28* (5), 1704907.

150 Huang, J.; Liu, Q.; Zhao, L.; Ai, N.; Wang, X.; Shao, Y.; Chen, K. Promotional Role of $BaCO_3$ on the Chromium-Tolerance of $La_{0.6}Sr_{0.4}Co_{0.2}Fe_{0.8}O_{3-\delta}$ Cathodes of Solid Oxide Fuel Cells. *Appl. Catal. B: Environ.* **2023**, *321*, 122080.

151 Pei, K.; Zhou, Y.; Xu, K.; He, Z.; Chen, Y.; Zhang, W.; Chen, Y. Enhanced Cr-Tolerance of an SOFC Cathode by an Efficient Electro-Catalyst Coating. *Nano Energy* **2020**, *72*, 104704.

152 Kalu, A.; Li, X.; Zhou, L.; Liu, S.; Chen, S.; Li, Q.; Li, W. Strategies to Counter Cr Poisoning on Air Electrodes of Solid Oxide Cells. *Int. J. Hydrogen Energy* **2025**, *101*, 85–104.

153 Lahrichi, A.; El Issmaeli, Y.; Kalanur, S. S.; Pollet, B. G. Advancements, Strategies, and Prospects of Solid Oxide Electrolysis Cells (SOECs): Towards Enhanced Performance and Large-Scale Sustainable Hydrogen Production. *J. Energy Chem.* **2024**, *94*, 688–715.

154 Liu, X., Li, X., Chi, B., Pu, J., & Xiong, C. In Situ Electrochemical Recovery: Sediment Transformation under Chromium Poisoning in Reversible Solid Oxide Cells with $La_{0.6}Sr_{0.4}Co_{0.2}Fe_{0.8}O_{3-\delta}$ Based Oxygen Electrodes. *ACS Appl. Mater. Interfaces,* **2024**, *16* (34), 44889-44899.

155 Zhu, Z.; Pal, U.; Gopalan, S.; Hussain, A. M.; Dong, S.; Dale, N.; Basu, S. Alternating-Current Electrophoretic Deposition of Spinel Coatings on Porous Metallic Substrates for Solid Oxide Fuel Cell Applications. *JOM* **2021**, *73* (9), 2764–2770.

156 Cai, Z.; Kubicek, M.; Fleig, J.; Yildiz, B. Chemical Heterogeneities on $La_{0.6}Sr_{0.4}CoO_{3-\delta}$ Thin Films: Correlations to Cathode Surface Activity and Stability. *Chem. Mater.* **2012**, *24* (6), 1116–1127.

157 Horita, T. Chromium Poisoning for Prolonged Lifetime of Electrodes in Solid Oxide Fuel Cells—Review. *Ceram. Int.* **2021**, *47* (6), 7293–7306.

158 Hilpert, K.; Das, D.; Miller, M.; Peck, D. H.; Weiss, R. Chromium Vapor Species over Solid Oxide Fuel Cell Interconnect Materials and Their Potential for Degradation Processes. *J. Electrochem. Soc.* **1996**, *143* (11), 3642–3649.

159 Zhen, Y. D.; Tok, A. I. Y.; Jiang, S. P.; Boey, F. Y. C. La(Ni, Fe)O_3 as a Cathode Material with High Tolerance to Chromium Poisoning for Solid Oxide Fuel Cells. *J. Power Sources* **2007**, *170* (1), 61–66.

160 Seo, H. G.; Staerz, A.; Dimitrakopoulos, G.; Kim, D.; Yildiz, B.; Tuller, H. L. Degradation and Recovery of Solid Oxide Fuel Cell Performance by Control of Cathode Surface Acidity: Case Study Impact of Cr Followed by Ca Infiltration. *J. Power Sources* **2023**, *558*, 232589.

161 Zhao, Z.; Liu, L.; Zhang, X.; Wu, W.; Tu, B.; Cui, D.; Cheng, M. High- and Low-Temperature Behaviors of $La_{0.6}Sr_{0.4}Co_{0.2}Fe_{0.8}O_{3-\delta}$ Cathode Operating under CO_2/H_2O-Containing Atmosphere. *Int. J. Hydrogen Energy* **2013**, *38* (35), 15361–15370.

162 Duan, C.; Hook, D.; Chen, Y.; Tong, J.; O'Hayre, R. Zr and Y Co-Doped Perovskite as a Stable, High Performance Cathode for Solid Oxide Fuel Cells Operating below 500 °C. *Energy Environ. Sci.* **2017**, *10* (1), 176–182.

163 Guo, M., Li, Z., Tang, L., Li, J., Wang, Z., Wang, B., & Yue, Z. Chromium deposition and poisoning of the proton-conducting $BaZr_{0.1}Ce_{0.7}Y_{0.1}Yb_{0.1}O_{3-\delta}$ electrolyte of protonic ceramic cells. *J. Mater. Chem. A.* 2025.

164 Iwahara, H. High temperature proton conducting oxides and their applications to solid electrolyte fuel cells and steam electrolyzer for hydrogen production. *Solid State Ionics*, 1988, *28*, 573-578.

165 Winterhoff, G.; Neitzel-Grieshammer, S. A Review of Proton Migration and Interaction Energies in Doped Barium Zirconate. *Solid State Ionics* **2023**, *397*, 116231.

166 Zhao, L.; Ding, D.; Zhang, L.; Gui, L.; Wang, Z.; Wan, Y.; He, B. The Effect of Cr Deposition and Poisoning on $BaZr_{0.1}Ce_{0.7}Y_{0.2}O_{3-\delta}$ Proton Conducting Electrolyte. *Int. J. Hydrogen Energy* **2014**, *39* (32), 18379–18384.

167 Wang, R.; Sun, Z.; Choi, J. P.; Basu, S. N.; Stevenson, J. W.; Tucker, M. C. Ferritic Stainless Steel Interconnects for Protonic Ceramic Electrochemical Cell Stacks: Oxidation Behavior and Protective Coatings. *Int. J. Hydrogen Energy* **2019**, *44* (47), 25297–25309.

168 Wei, Z.; Li, Z.; Wang, Z.; Zhao, Y.; Wang, J.; Chai, J. A Free-Cobalt Barium Ferrite Cathode with Improved Resistance against CO_2 and Water Vapor for Protonic Ceramic Fuel Cells. *Int. J. Hydrogen Energy* **2022**, *47* (27), 13490–13501.

169 Lv, X.; Chen, H.; Zhou, W.; Li, S. D.; Cheng, F.; Shao, Z. $SrCo_{0.4}Fe_{0.4}Zr_{0.1}Y_{0.1}O_{3-\delta}$, a New CO_2 Tolerant Cathode for Proton-Conducting Solid Oxide Fuel Cells. *Renew. Energy* **2022**, *185*, 8–16.

170 Sozal, M. S. I.; Tang, W.; Das, S.; Li, W.; Durygin, A.; Drozd, V.; Cheng, Z. Electrical, Thermal, and H_2O and CO_2 Poisoning Behaviors of $PrNi_{0.5}Co_{0.5}O_{3-\delta}$ Electrode for Intermediate Temperature Protonic Ceramic Electrochemical Cells. *Int. J. Hydrogen Energy* **2022**, *47* (51), 21817–21827.

171 Xu, Y.; Xu, X.; Bi, L. A High-Entropy Spinel Ceramic Oxide as the Cathode for Proton-Conducting Solid Oxide Fuel Cells. *J. Adv. Ceram.* **2022**, *11* (5), 794–804.

172 Zhang, H., Xu, K., He, F., Zhou, Y., Sasaki, K., Zhao, B., & Chen, Y. Surface regulating of a double-perovskite electrode for protonic ceramic fuel cells to enhance oxygen reduction activity and contaminants poisoning tolerance. *Adv. Energy Mater.* **2022**, *12*(26), 2200761.